CHEMICAL EQUILIBRIA OF RARE EARTH OXIDES IN GLOW DISCHARGE MASS SPECTROMETRY

By

YUAN MEI

A DISSERTATION PRESENTED TO THE GRADUATE SCHOOL
OF THE UNIVERSITY OF FLORIDA IN PARTIAL FULFILLMENT
OF THE REQUIREMENTS FOR THE DEGREE OF
DOCTOR OF PHILOSOPHY

UNIVERSITY OF FLORIDA

1992

UNIVERSITY OF FLORIDA LIBRARIES

to my parents

ACKNOWLEDGEMENTS

My deepest gratitude and respect go to my advisor, Dr. Willard W. Harrison, for his guidance, patience, and encouragement over the years of my graduate career. From his high academic standard and rich knowledge, I have benefitted both professionally and culturally.

I also wish to thank the faculty and staff of the Chemistry Department at the University of Florida. The expertise and support that I have received from both the machine shop and the electronics shop in completing this research work are greatly appreciated. My sincere thanks also goes to Evelyn Butler, Susan Ciccarone, Jeanne Karably, Beverly Lisk, and Wanda Douglas. Without their help, the many business routines involved in this research could not have been done smoothly.

The colleagues and friends whom I have worked with side by side through these years, Christopher Barshick, Jeffrey Klingler, Philip Ratliff, and Susan Ohorodnik, are especially acknowledged. Their friendliness and sense of humor have, in many ways, made it a lot easier and more interesting for me to adjust to the American culture. I particularly wish to thank Phil and Sue for taking the time to proof-read this manuscript.

Finally, I want to express my love and gratitude for my family whose constant love and understanding have been a great support for me in pursuing my graduate career. Without them, this work could not have been possible.

This research has been supported by a grant from the U.S. Department of Energy.

Yuan Mei

University of Florida
Gainesville, Florida

March 27, 1992

TABLE OF CONTENTS

page

ACKNOWLEDGEMENTS iii

ABSTRACT vii

CHAPTERS

1 GLOW DISCHARGE MASS SPECTROMETRY 1

Background 1
Glow Discharge Fundamental Processes 2
General Description 2
Sputter Atomization 5
Excitation/Ionization 20
Analytical Applications 24
Instrumentation 28
Mass Spectrometer System 28
Mass Spectrometer/Atomic Absorption 36

2 RARE EARTH ELEMENTS IN
GLOW DISCHARGE MASS SPECTROMETRY 39

Background 39
REE Analysis Techniques and Limitations 39
Rare Earths in GDMS 47
Non-conducting Samples in GD Sources 47
Sample Preparation 49
Plasma Equilibria of REE 51

3 RARE EARTH OXIDE EQUILIBRIA IN DIRECT CURRENT
GLOW DISCHARGE MASS SPECTROMETRY 67

Elimination of Oxidant Contamination 67
Introduction 67
Cryogenic Condensation--Physical Elimination 68
Getter Reagents--Chemical Elimination 75

Analytical Applications 93
Conclusions 109

Addition of Reactive Gases 110
Introduction 110
Experimental Procedures 111
Effect of Getter Concentration on La-LaO Equilibria . . 112
Effect of Water Concentration on La-LaO Equilibria . . 120
Conclusions 130

4 RARE EARTH OXIDE EQUILIBRIA IN PULSED DIRECT CURRENT GLOW DISCHARGE MASS SPECTROMETRY . . . 132

Background 132
Pulsed DC Discharge 132
Pulsed Glow Discharge of Rare Earth Oxides 134
Redox Equilibria on Cathode Surface 140
Water Signal as a Function of Pulse Period 143
La^+/LaO^+ as a Function of Pulse Period 146
Plasma "Reagent" Introduction through Pulsed Discharge . . . 151
Instrumental Setup 153
Reagent Provision 158
Effect on La^+/LaO^+ 162
Plasma "Reagent" Introduction through Gas Injection 166
Experimental 167
Ar Injection 171
H_2 Injection 173
$H_2{}^{16}O$ Injection 178
$H_2{}^{18}O$ Injection 184
Conclusions 195

5 CONCLUSIONS AND FUTURE STUDIES 196

REFERENCES 201

BIOGRAPHICAL SKETCH 210

Abstract of Dissertation Presented to the Graduate School
of the University of Florida in Partial Fulfillment of the
Requirements for the Degree of Philosophy

CHEMICAL EQUILIBRIA OF RARE EARTH OXIDES IN
GLOW DISCHARGE MASS SPECTROMETRY

By

YUAN MEI

MAY, 1992

Chairman: Willard W. Harrison
Major Department: Chemistry

This research centers around method development and fundamental exploration of the rare earth elements (REE) in glow discharge mass spectrometry (GDMS). The capability of GDMS to analyze directly solids materials (such as geological samples) eliminates the sample dissolution and preconcentration steps required by many other methods that are currently used for REE analysis. The simplicity in both sample preparation and instrumental operation makes GDMS a promising analytical technique for the field of earth science.

Initial studies were dedicated to improving the detection sensitivity of GDMS in analyzing the REE. This was accomplished by eliminating water contamination, a factor that was found to prevent the conversion of the rare earth oxides to their atomic form in the glow discharge plasma. Methods experimented

for water elimination included the uses of both a cryogenic cooling device (physical elimination) and getter reagents (chemical elimination). When used to determine the REE concentrations in a standard rock sample, the chemical elimination approach yielded comparable results to that obtained by other analytical methods.

Further studies focused on probing the chemical reactions involving the REE and other plasma constituents in the glow discharge. It is proposed that the availability of the atomic REE in the glow discharge, which is essential to attaining good analytical sensitivity, is strongly influenced by the oxidant and reductant contents in the plasma. Species that contain oxygen (e.g., water) tend to shift the redox equilibria of REE toward the formation of their oxides, whereas species that compete for oxygen (e.g., getter reagents) help reduce the oxidant content in the plasma, and hence shift the REE redox equilibria toward the formation of the REE atoms. Factors that govern the reaction processes of the REE equilibria were investigated by means of plasma reagent introduction and time-resolved discharge operation. Results indicate that while redox equilibria between the elemental REE and their monoxides exist both on the cathode surface and in the gas phase, interactions occurring in the gas phase are probably the main paths for this equilibration in the glow discharge.

CHAPTER 1
GLOW DISCHARGE MASS SPECTROMETRY

Background

Glow discharge mass spectrometry (GDMS) is an elemental analysis technique designed especially for direct application to solid samples. As the amount of research dedicated to plasma source mass spectrometry continued to increase over the past decade, GDMS gained significant popularity in the field of elemental analytical chemistry. In GDMS, atomization, excitation, and/or ionization of the sample material are enabled by the physical processes inherent to glow discharge operation. Mass spectrometric sampling of the plasma provides qualitative and quantitative determination of ions that represent the sample composition.

The greatest advantage of GDMS over solution-based techniques is its simplicity in handing solid samples, especially those that are resistant to solvent dissolution such as many geological materials. The continuing success of GDMS in analyzing conductors (e.g., pure metals and alloys) has led to the exploration of this technique for the analysis of nonconducting substances. The goal of the work reported in this dissertation is to develop a GDMS analytical method for earth materials and to understand better the fundamental processes of the glow discharge.

Glow Discharge Fundamental Processes

General Description

The glow discharge is one type of gaseous discharge, a phenomenon where an electric current flows through a gaseous medium [1]. In order to maintain a gaseous discharge, a fraction of the gas particles must be ionized and form a current when accelerated by the existing electric field. A glow discharge can be initiated and maintained either by a direct current (DC) or a radio frequency (rf) power supply. A schematic of a DC glow discharge is illustrated in Figure 1, in which a low pressure (0.1 - 10.0 Torr) argon gas is ionized due to the high voltage (500 - 1000 V) applied to the cathode [2]. The glow discharge is also a type of plasma, which is a partially ionized gas consisting of approximately equal concentrations of positive and negative charges plus large numbers of neutral species. According to its physical properties, the GD plasma can be divided into many "zones," whose general aspects have been reviewed extensively [3,4]. The discussion here will only focus on processes that are important for analytical applications of the glow discharge. Processes that are of analytical significance are mainly confined to what are called the cathode dark space and the negative glow regions as shown in Figure 2. The regions are so named according to the luminosity caused by the radiative relaxation of electronically excited species [5]. As shown in Figure 2, the area close to the cathode is the cathode dark space, which shows relatively little emission from electron-atom collisions because of the high energy of the accelerated electrons. Further from the cathode is the luminous negative glow region where excitation

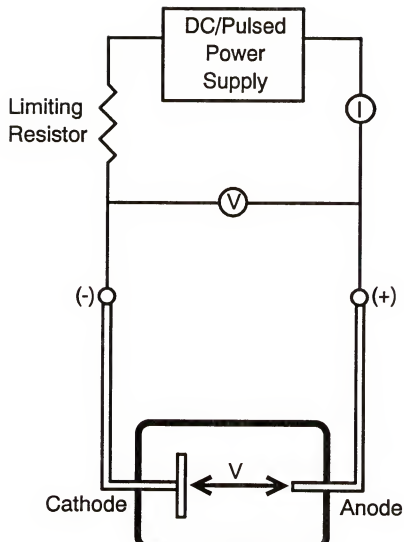

Figure 1 Schematic diagram of a glow discharge circuit.

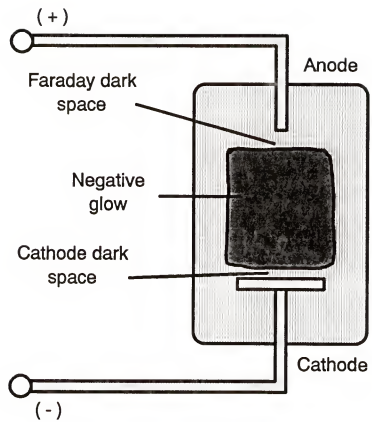

Figure 2 Schematic diagram of the primary regions in the glow discharge.

of atoms is caused by lower energy electrons that have been slowed by inelastic collisions. These two regions are of concern to us because events occurring here cause the formation of atoms, ions, and photons that make the glow discharge useful for analytical chemistry. The major processes involved in these areas are illustrated in Figure 3 in a highly simplified fashion. It can be seen that two important processes occur in distinct regions of the discharge: sputter atomization and excitation/ionization. Both processes will be described in details in the following text.

Sputter Atomization

Cathodic sputtering is the phenomenon that makes a glow discharge useful in analytical spectrometry, because it provides the means of obtaining directly from the sample an atomic population for analytical detection [6]. This atomization process is inherent to the operation of the glow discharge [4, 7]. In the steady state, positive ions of the discharge gas species (in this case, Ar^+) are accelerated toward the cathode. Prior to colliding with the cathode, the ions recombine with Auger electrons released from the surface to become energetic neutral atoms that impact the cathode [8]. Depending on its energy and impact angle, the incoming atom transfers its momentum and kinetic energy to the solid target. If the transferred energy is in excess of the target's binding energy, the bombardment will result in a dislodging of target atoms and eventually the release of these atoms into the gas phase [9]. The sputtered particle flux leaves the cathode surface mainly as ground state neutral atoms [10,11]. Some secondary

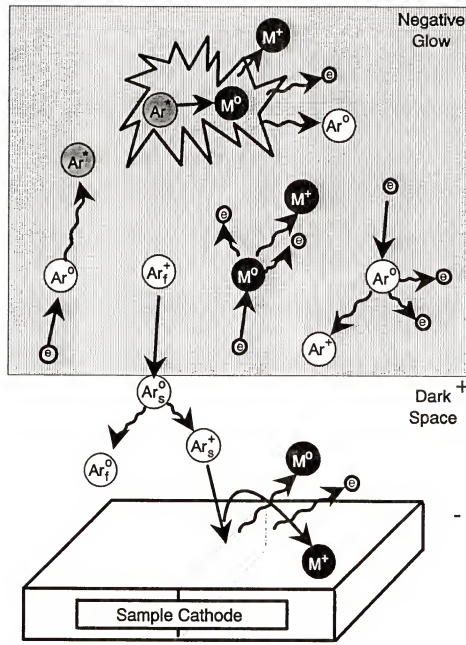

Figure 3 Illustration of fundamental processes in the glow discharge plasma. M° is sputtered atom; M^{+} is atomic ion; f stands for fast; s stands for slow.

ions and electrons are also released during this process. The secondary ions are immediately returned to the sample surface by the electric field at the cathode.

The effectiveness of cathodic sputtering, i.e., how many atoms of a certain target can be removed during a sputtering process, is measured by a parameter called the sputter yield (Y). The sputter yield is defined as the number of sputtered atoms per primary ion colliding with the solid surface [6]:

$$Y = \frac{9.6 \times 10^4 W}{M \cdot i^+ \cdot t} \qquad (1\text{-}1)$$

where W is the weight loss of the cathode as a result of sputtering (in grams), M is the atomic weight, i^+ is the ion current (in amperes), and t is the sputtering time (in seconds). The ion current is related to the total current, i, by

$$i^+ = \frac{i}{1 + \gamma} \qquad (1\text{-}2)$$

where γ is the number of secondary electrons released by one ion. Discussion concerning the γ factor for the noble gas ions can be found in the literature [7].

Because of the difficulty in practically separating the sputter atomization and excitation/ionization steps in the glow discharge, quantitative studies to determine the experimental factors that influence sputtering are mostly done using a collimated high-energy ion beam (the basis for secondary ion mass spectrometry) [12]. The sputter yield is found to be dependent mainly on the following factors: type of incident ions, the bombarding angle and energy of the incident ion, and the nature of the target material [8,9,13].

Type of incident ions

Noble gases are most frequently used as the glow discharge fill gas, for they provide high sputter yields, and their inert nature minimizes chemical reactions with the sample material. Using low-energy ion beam sputtering (under 1 keV), Bay and coworkers have proposed an energy transfer model to explain the dependency of certain material's sputter efficiency on the mass of the bombarding ion [14]. The maximum sputter yield of a target is proportional to the energy transfer factor γ, expressed as:

$$\gamma = \frac{4M_1 M_2}{(M_1 + M_2)^2} \tag{1-3}$$

where M_1 and M_2 are the masses of the incident ion and the target atom respectively. The maximum energy transfer occurs, and hence the maximum sputter yield is obtained when $M_1 = M_2$. This is why Ar was found to be the best choice for copper sputtering and probably for most medium atomic weight elements [13,15]. Wehner and coworkers have measured the sputter yields of a series of elements using 400 eV He^+, Ne^+, Ar^+, Kr^+, and Xe^+ ion beams, shown in Figure 4 [16,17]. It can be seen that as the mass of the bombarding ion increases in the order of $He^+ < Ne^+ < Ar^+ < Kr^+ < Xe^+$, the sputter yields of elements with higher masses increase. This theory will be used in Chapter 3 to explain results obtained from studies using alternative gas addition.

Incident ion energy

By means of high vacuum beam studies, the minimum kinetic energy required to dislodge an atom from its matrix is determined to be approximately

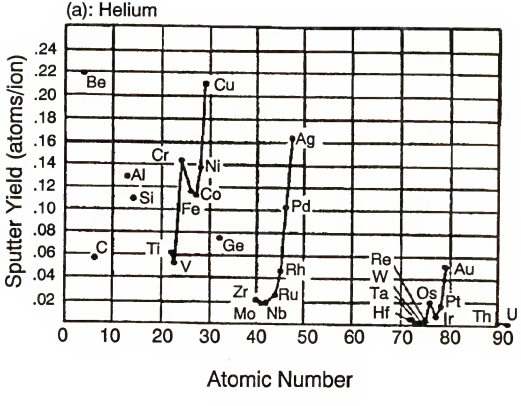

Figure 4 Sputter yield of multiple elements under 400 eV ion bombardment. a) by He; b) by Ne; c) by Ar; d) by Kr; e) by Xe [16,17].

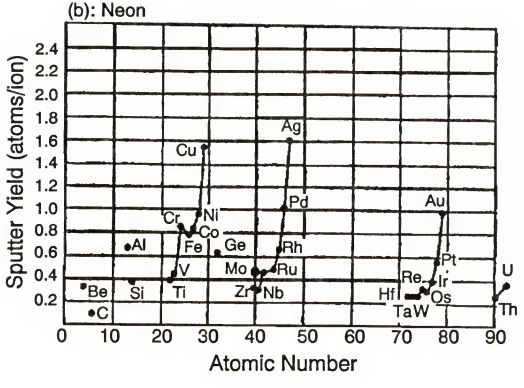

Figure 4--continued.

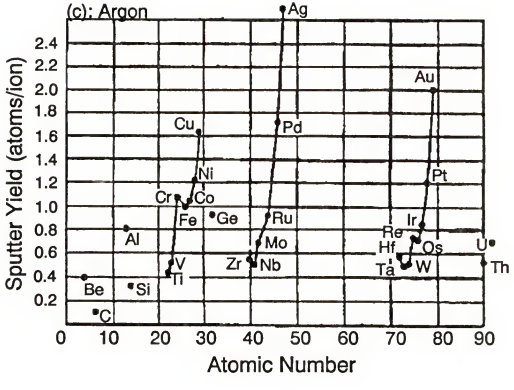

Figure 4--continued.

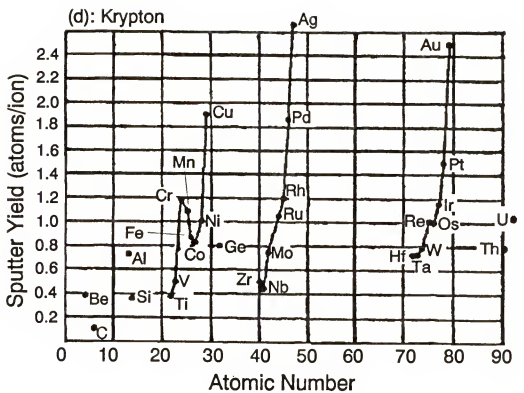

Figure 4--continued.

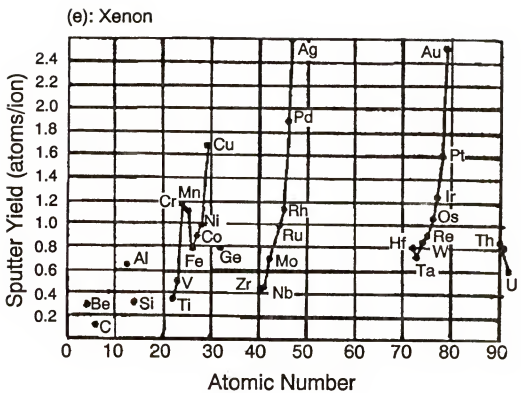

Figure 4--continued.

four times the material's heat of sublimation [8]. This threshold energy is characteristic for a specific gas-target combination. Above the threshold, the sputter yield rises first exponentially and then linearly with ion energy, and reaches a float maximum or plateau at ~ 1 keV depending on the gas. In the glow discharge environment, energy of the bombarding ion is not easily acquired because of the energy loss caused by the many collisions an ion undergoes as it passes through the cathode dark space region. Several authors have addressed this issue and their results can be found in the literature [18,19]. A method has been used in this laboratory to calculate the average energy of the incident ion arriving at the cathode under typical glow discharge conditions [15,20]. The calculation was based on the pressure and the cathode fall potential of the discharge, and an ion energy range of 100 eV to 575 eV (corresponding to 400 - 2000 VDC) was established as the typical value for the bombarding ion. Therefore, most of the sputter yields obtained by low energy beam studies (under 1 keV) can be related to the glow discharge experiments.

Target material

As also revealed by Figure 4, under the same ion bombardment conditions, elements of the periodic table do not have identical sputter yields. These data show that the sputter yield increases in any one period of the periodic table. This results in uneven sputtering rates of different elements from multi-component or alloy samples, called preferential sputtering [21-23]. At first glance, this effect may make it difficult to obtain atom populations in the gas phase proportional to their bulk concentrations. Fortunately, the glow discharge processes passively

correct for preferential sputtering, because the resulting enrichment of the surface with species having smaller sputter yields leads to the eventual equilibrium system. Therefore, after the initial period during which the equilibrium is established, the gas phase atomic population becomes proportional to that of the solid sample [24].

Molecular sputtering

The ejection of molecular species during the sputtering process is known as molecular sputtering. While sputtering a target composed of several elements with a high energy Xe^+ beam, Jensen and Veje observed radiation from BH, CH, and MgO [25,26]. A combination of absorption and emission spectroscopy was also used by Stirling and Westwood, who concluded, from measurements on both metals and insulators, that a significant fraction of the sputtered particles was "molecular" [27-30]. Using electron impact in a plasma, Oechsner and Gerhard observed Cu, Cu_2, and Cu_3 species sputtered from a copper target by 1 keV Ar^+; the relative intensities of the signals were 1, 0.1, and 0.01, respectively [31]. They also developed a recombination theory to account for this observation, which stated that molecular sputtering was caused by the agglomeration of two or more atoms ejected from one binary collision cascade in the target [32]. In a more recent study using secondary neutral mass spectrometry, the atomic combination model was further confirmed by cluster formations from a series of NiW and NiMo alloys under Ar^+ bombardment [33]. It was explained that "direct" ejection of molecules from an inorganic crystal target (as opposed to fragmentation of large organic molecules by fast atom bombardment) was only possible for such high

interatomic bond strengths as in oxidic systems, a conclusion that was reinstated by other researchers who used laser ionization and subsequent time-of-flight mass spectrometry to investigate metallic cluster emission under ion bombardment [34].

Of particular interest to this work is the molecular sputtering as a result of ion bombardment on oxide targets. Both atomic (Nb) and monoxide (NbO) species have been observed when a Nb_2O_5 target was sputtered by an Ar^+ beam [35]. Discussions concerning the monoxide formation during the oxide sputtering will be given in detail in Chapter 2 in combination with an introduction to the rare earth species.

Reactive sputtering

Sputtering produced wholly or in part by ions of a chemically active gas that react with the ejected material is known as reactive sputtering (or chemical sputtering) [29]. Both decrease and increase of the sputter yield have been observed during sputtering of elements with reactive ions as well as sputtering in a residual gas containing reactive atoms [36]. Reactive sputtering has been used as a thin film preparation technique for many years, where the reactive gases are intentional reactants and are usually controllable in amount. In other situations such as the glow discharge, these chemically reactive gases are considered impurities and therefore reactive sputtering induced by these species is undesirable. Because of its direct relevance to studies described in this dissertation, sputtering in a reactive atmosphere deserves further discussion.

When sputtering a metal target with non-reactive ions in a reactive atmosphere, certain surface compounds may form due to reactions between the target material and the reactive gas. Such formations have been observed to influence the sputter yield of the target material. In an uncontrolled way this occurred in nearly all early sputtering measurements that were made in poor vacuum conditions and has been a major concern in all well-defined sputtering yield measurements. Systematic investigations in a well-defined residual gas atmosphere have been conducted with high vacuum beam sputtering. An example is given in Figure 5 [37,38], where the sputter yield of Ti in various gas environments is shown as a function of the ion arrival rate ratio between the reactive ions and Ar ions ($n_{ra.}/n_{Ar}$, where ra. stands for reactive gas). The sputter yields were measured by recording the time needed for sputtering through a thin Ti film with 11 keV Ar ions in a residual gas containing various amounts of N_2, O_2, or H_2 molecules. It can be seen in Figure 5 that at distinct ratios of $n_{ra.}/n_{Ar}$, the sputter yield of Ti decreases sharply, dropping to 50 - 70% of its original value. The proposed rationale is that if the arrival rate for reactive atoms ($n_{ra.}$) is higher than the sputtering rate (proportional to n_{Ar}), a stable compound phase can be formed at the target surface that may extend over many monolayers due to diffusion, causing the change in sputter yields [39]. Similar results have been obtained in a more recent study by which the effects of reactant gas pressure on sputter yields of several transition metals were determined [40]. As shown in Figure 6, for all tested metals the sputter yield under oxygen is decreased mainly within a small pressure range, and the magnitude of decrease is proportional to

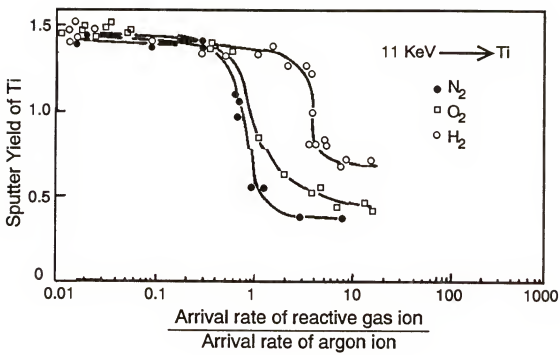

Figure 5 Effect of reactive gases on the sputter yield of Ti by 11 KeV Ar [37].

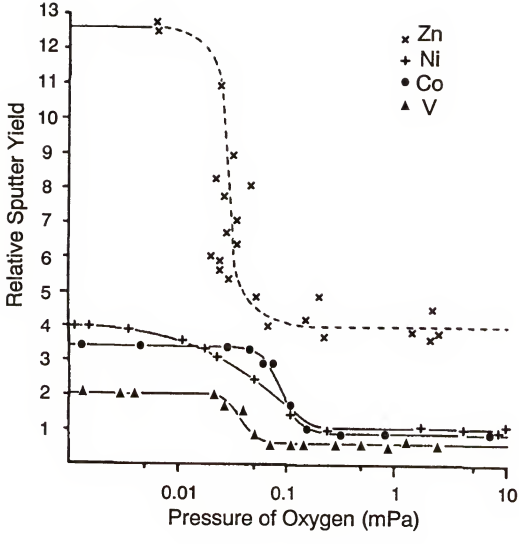

Figure 6 Effect of O_2 pressure on sputter yields of Zn, Ni, Co, and V [40].

the reactivity of that metal. The authors suggested that before the point where the sharp decrease occurred, the target was primarily metallic in nature; after that point, the surface was coated with an oxidized layer that caused reduced sputter yield.

Although the glow discharge sputtering system is different from the high vacuum beam sputtering in many ways, the reactive sputtering phenomenon can also be expected in the glow discharge environment given a sufficient reactive gas pressure. It is worth pointing out that unlike the high vacuum system in which the previous experiments were carried out, the glow discharge is a collision-rich and reaction-rich plasma, where the interactions between the reactant gases and the target material may not be limited to the sample surface, but may also occur in the gas phase. A more complicated plasma environment, in terms of the types of reactants and products, is expected when a significant percentage of gaseous impurities is present in the glow discharge. The reactive sputtering theory introduced here will be elaborated upon in Chapters 1 and 2, where studies of such GD plasmas will be discussed.

Excitation/Ionization

Once species from the sample cathode are sputtered into the plasma, they can be excited and ionized when sufficient energy has been transferred to them. Figure 7 depicts the negative glow region, a collision-rich environment where electrons of the discharge species are promoted to higher energy levels and even removed, resulting in excitation and ionization. Such processes are not only necessary for the maintenance of a stable discharge, but they are also crucial to

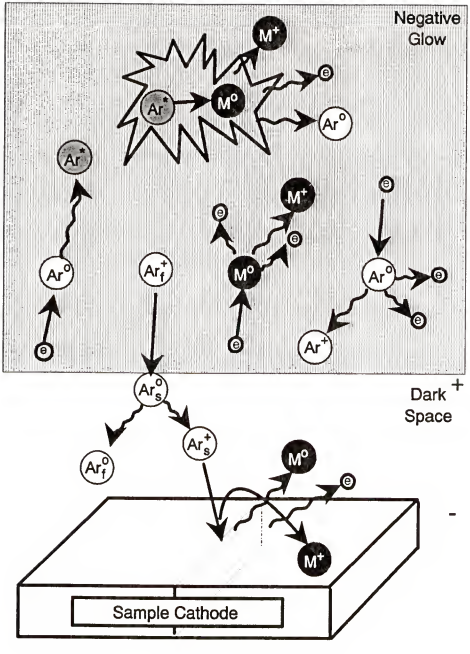

Figure 7 Illustration of fundamental processes in the glow discharge plasma.

the analytical utility and plasma chemistry of the discharge [41]. The three principal types of collisions in the negative glow are: (1) collisions involving discharge electrons, (2) collisions involving excited discharge species and (3) collisions involving discharge ions (Figure 8). Within this frame, the two processes that directly cause the ionization of the sputtered species are electron ionization and Penning ionization. In the glow discharge, electron ionization, is accomplished through electrons accelerated across the cathode fall or the secondary electrons possessing energy in excess of the ionization potential of the target species. Expressed by Equation 1-4, this process is believed to be an

$$X + e^- \rightarrow X^+ + 2e^- \qquad (1\text{-}4)$$

important source of ionization for the discharge gas medium [3]. If the energy of the electron that collides with the target species is below the target atom's ionization energy but above its lowest excitation energy, such a collision will result in electronic excitation of the target species. This process can be probed by optical spectroscopy, for the relaxation of the excited species to the ground state emits photons that are characteristic of that species [43]. Ionization of a ground state atom or molecule can also occur by a collision with an excited atom whose total energy is equal to or greater than the first ionization energy of the neutral species. When the excited atom is at a metastable energy level from which a radiative transition to the ground state is forbidden, this ionization process is known as Penning ionization [44], as shown by Equation 1-5:

$$Ar^* + X \rightarrow Ar + X^+ + e^- \qquad (1\text{-}5)$$

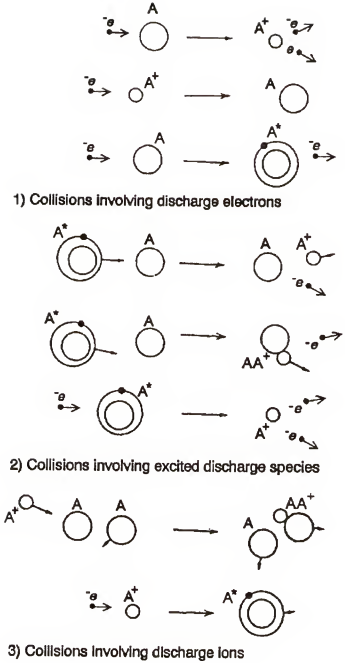

Figure 8 Types of excitation and ionization mechanisms in the glow discharge [42].

The low-lying metastable energy levels of the noble gas atoms are listed in Table 1-1. The relative importance of the electron and Penning ionization mechanisms in rf glow discharges has been discussed in several papers by Coburn and coworkers [44-48]. A series of experiments has been conducted using a laser or quenching agent to depopulate the Ar metastable atoms in the discharge and to study the induced effect on Penning ionization [15,49-51]. It has been proposed that Penning ionization is responsible for 40 - 80 % of the ionization in the glow discharge [51]. When using Ar as the discharge gas, many elements and their monoxides can be Penning ionized. Other routes besides electron and Penning ionizations might also contribute to the ionization of sputtered species [52], and these so-called "secondary ionization mechanisms" are listed in Table 1-2.

Analytical Applications

Glow discharges have been used for many years as atom generators for both optical spectroscopic methods [53-59] and mass spectrometry. As GDMS becomes more competitive with other established elemental methodologies, this originally academic centered technique has received growing interest and acceptance that have led to numerous types of successful analytical applications.

The general fields of GDMS applications can be found in a number of review articles published in recent years [42,52,60-68]. As stated earlier, GDMS is a trace elemental analysis technique that allows direct characterization of solid materials. Because the sample to be analyzed serves as the glow discharge cathode, many of the problems associated with solution based techniques can be avoided, e.g., incomplete dissolution, solvent contamination, and dilution of the

Table 1-1. Low-lying Metastable Energy Levels of Noble Gas Atoms

Gas Atom	Metastable Energy (eV)	Ionization Energy (eV)
He	19.8, 20.7	21.56
Ne	16.6, 16.7	21.56
Ar	11.5, 11.7	15.76
Kr	9.9, 10.5	14.00
Xe	8.3, 9.4	12.13

Source: Ref [52].

Table 1-2. Secondary Ionization Mechanisms in the Glow discharge

A. 1.	Nonsymmetric Charge Transfer:
	$A^+ + M^\circ = M^+ + A^\circ$
2.	Symmetric (Resonance) Charge Transfer:
	$B^+_{fast} + B^\circ_{slow} = B^+_{slow} + B^\circ_{fast}$
3.	Dissociative Charge Transfer:
	$A^+ + MO = M^+ + O + A^\circ$
B.	Associative Ionization:
	$A^*_m + M = AM^+ + e^-$
C.	Photoionization:
	$M^* + h\nu = M^+ + e^-$

Source: Ref.[52].

trace components during dissolution. GDMS has been widely applied to the analysis of metals, alloys, and high purity materials, offering both superior detection sensitivities and broad coverage of elements [69-72]. Applications range from high purity metals characterization [73] to semiconductor analysis [74], and to depth profiling of Si doped wafers [75]. Quantitative analysis of such difficult elements as B, C, Si, P, and S in NBS standard steel samples have also yielded good results [76]. For quantitative analysis, two calibration methods are commonly used in GDMS.

Internal standard

The internal standard method is mainly used for semiquantitative analysis. When the species to be quantified are first identified from a survey, the next analytical step is to acquire spectra from samples with known and unknown concentrations. Comparison of the sensitivity (signal intensity/concentration) observed for a reference element (ref) allows estimation of the concentration of an analyte (anal) through a ratio of signal intensities, expressed as:

$$C_{anal} = \frac{I_{anal} \times C_{ref}}{I_{ref}} \qquad (1\text{-}6)$$

where C stands for concentrations and I stands for ion signal intensities. The internal standard can be either spiked into the sample or selected as the least interfered isotope of an element with known concentration in the sample.

Relative sensitivity factors (RSF)

Because of the difficulty in obtaining solids standards for calibration, this alternative calibration method was developed to take into consideration the many

variables that can affect the observed ion signal intensity between different samples and separate analysis runs on a given instrument. Originally developed for spark source mass spectrometry [77], this method has been successfully adapted to GDMS [78-80]. The relative sensitivity factor is defined as [81]:

$$RSF = \frac{I_{anal} \times C_{ref}}{I_{ref} \times C_{anal}} \qquad (1\text{-}7)$$

where I_{anal} and I_{ref} are the signal intensities of the analyte and the reference peaks respectively; C_{anal} and C_{ref} are the corresponding concentrations. The reference element serves as an internal normalization factor to compensate for differences in instrument tuning, detector sensitivity, and other parameters that affect the ion signal intensity. Using the RSF, the unknown analyte's concentration can be determined by Equation 1-8:

$$C_{anal} = \frac{1}{RSF} \times \frac{I_{anal} \times C_{ref}}{I_{ref}} \qquad (1\text{-}8)$$

Isotopic adjustments, not shown in these equations, are necessary in detailed concentration calculations. An important advantage with RSF is that the RSF values do not vary appreciably among different matrices, avoiding the requirement of matching standards that are difficult to obtain [81].

Instrumentation

Mass Spectrometer System

The mass spectrometer system used in this work is an updated version of the original quadrupole GDMS system constructed by Bentz, Bruhn, and Harrison

[82]. Shown in Figure 9, the mass spectrometer consists of a Balzers Plasma Monitor system (Balzers; Leichtenstein) equipped with an ion source designed by King *et. al* [83] and controlled by a modified THQ (Finnigan MAT; Bremen, FRG) electronics module. The entire hardware can be divided into five segments: (1) ion source assembly, (2) vacuum support, (3) ion optics, (4) mass analyzer, and (5) ion detection and data acquisition. Detailed descriptions of all the major components can be found in a previous dissertation [83], and therefore will not be elaborated exhaustively here. General introductions of the five segments will be given with emphases focused on modifications made particularly for this work.

Ion source

The original ion source consists of the a direct insertion probe, discharge chamber, and sample introduction assembly as shown in Figure 10. The ion source was developed to facilitate sample introduction, minimize vacuum interruption, and optimize analytical performance. The "true" ion source, the discharge chamber, is a 316 stainless steel Ultra-Torr tee (Cajon; Macedonia, OH) modified to house the sample cathode. In its original design, shown in Figure 11, the two coaxial ports of the tee have been machined to accept glass windows. The wall of the tee opposite to the sample introduction port was equipped with a removable ion exit orifice plate made from drilling a 0.5 mm orifice in the center of a tantalum sheet. The ion source modified for this work is illustrated in Figure 12, where one of the window ports was re-machined to fit a "tunnel" made from a stainless steel bellows. The other end of the "tunnel" is connected to a demountable flange that allows for coupling of another insertion device into the

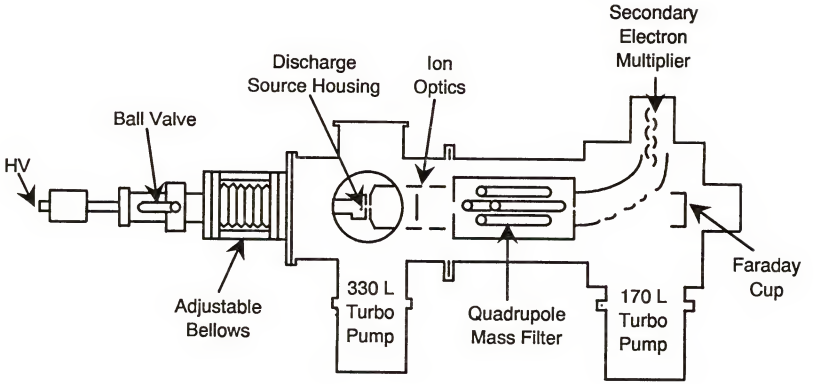

Figure 9 Glow discharge quadrupole mass spectrometer.

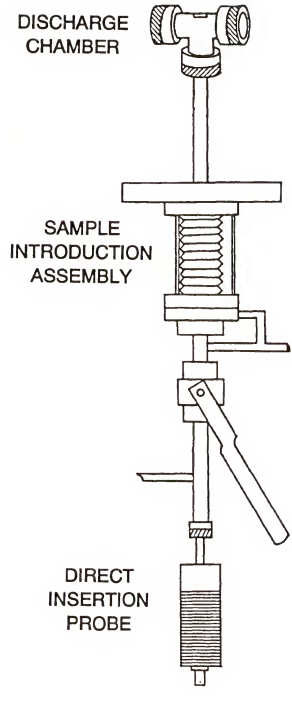

Figure 10 Glow discharge mass spectrometer sample introduction assembly.

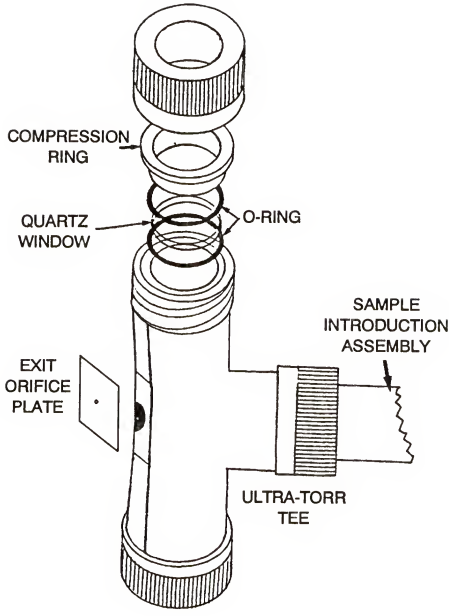

Figure 11 Diagram of the glow discharge chamber.

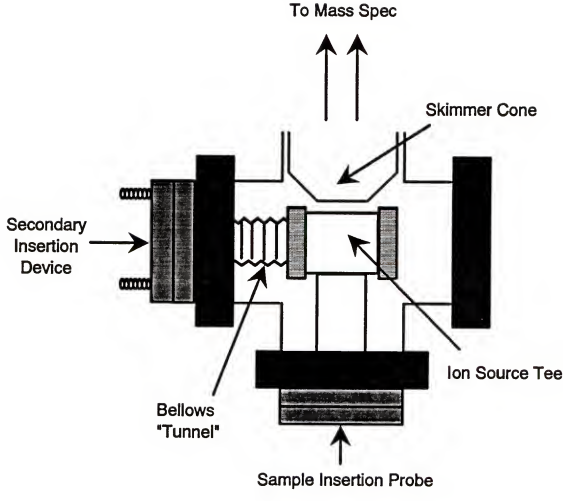

Figure 12 Modified glow discharge chamber.

discharge chamber. This modification created additional accessibility to the discharge volume, which the original design lacked, for conducting plasma manipulation studies. The sample introduction assemblies remain the same as used in the original design [83].

Vacuum support

To maintain the 10^{-4} Torr vacuum required by the mass spectrometer while the discharge is operated at near one Torr, differential pumping in three stages is used. The first stage is the discharge chamber, containing approximately one Torr argon with a 0.5 mm ion exit orifice. The orifice opens to a second chamber, maintained at about 10^{-4} Torr and pumped by a 300 Ls^{-1} turbomolecular pump. The mass analyzer region is evacuated by a 170 Ls^{-1} turbomolecular pump attaining a normal operating pressure of approximately 10^{-6} Torr.

Ion optics/mass analyzer

As shown in Figure 13, the ion optic assembly consists of five primary components: (1) the skimmer cone, (2) the first lens, (3) the second lens (equipped with a 5 mm diameter neutral beam stop), (4) the third lens, and (5) the quadrupole housing. The entire assembly serves two purposes: first, as a Bessel box electrostatic energy analyzer and second, to block noise caused by neutral atoms and photons with the center beam stop. Ion transmission of up to 40 % of the total ion beam has been reported with this assembly [84]. The mass analyzer employed in this system is the QMA 150 (Balzers; Leichtenstein) consisting of four cylindrical rods each of 200 mm length and 4 mm radius.

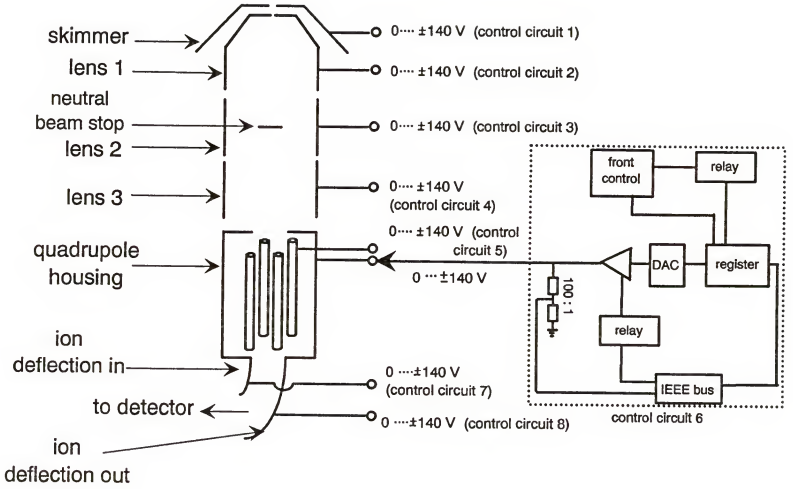

Figure 13. Illustration of ion optics in the quadrupole glow discharge mass spectrometer.

Ion detection and data acquisition

Two types of detectors are employed in this system; they are an on-axis Faraday cup and a 17-stage discrete dynode secondary electron multiplier (SEM) (Balzers; Leichtenstein) mounted 90° off-axis with respect to the quads. The SEM can be monitored either by analog or digital electronics, allowing for different sensitivities. When operated in the digital mode by using a pulse preamplifier (Balzers; Leichenstein), the SEM signal can be converted to TTL pulses to be collected by a multichannel analyzer (MCA) (Tracor-Northern; Middleton, WI). The MCA is equipped with an IEEE bus port that permits communication with the HP 9816 (Hewlett-Packard; Palo Alto, CA) micro computer system used to control the QMA scanning.

When operating in the DC mode, a Heizinger HNCS 2500-1500 ump power supply (Heizinger, Rosenheim, Germany) was used to provide high voltage to the cathode. Typical discharge parameters were 1000 volts with approximately 3.0 mA current in a one Torr high purity Ar environment.

Mass Spectrometer/Atomic Absorption

Pioneered by Russell and Walsh [85], the combination of sputter atomization and atomic absorption (AA) detection has been used for the analysis of metallic samples for many years [28,86-88]. This is possible because the overwhelming majority of the sputtered species is neutral atoms. Atomic absorption spectroscopy has also been used to assist the mass spectrometric probing of the plasma chemistry in the glow discharge [89]. While information obtained by the MS pertains mainly to the ion signals, AA offers a means to

monitor the ground state atomic population. By relating the two measurements *in situ*, we hope to gain insight on some fundamental processes of the plasma.

Atomic absorption measurements were conducted using the instrumental set-up illustrated in Figure 14 [15]. The mass spectrometer used in these studies was another quadrupole mass spectrometer in this laboratory, different from the one described in the previous section. The difference relevant to this work is mainly in the discharge source design. Instead of being a tee housed inside a higher vacuum environment, the ion source on this instrument is a stainless steel six-way cross that allows optical probing of the plasma *in situ* with mass spectrometric operation. All MS/AA work presented in this dissertation was carried out on this instrument, whose description can be found elsewhere [90].

In the MS/AA experimental set-up (Figure 14), light from a commercial neon (or argon) filled hollow cathode lamp (HCL) was focused down to 3 mm in diameter immediately in front of the ion exit orifice. The beam was focused into a 0.5 M Ebert spectrometer (Jarrell-Ash, Waltham, MA), and its intensity detected by a photomultiplier tube (Hamamatsu R956, Bridgewater, NJ) and a photometer (Model # 110, Pacific Instruments, Concord, NJ) after traversing the negative glow region of the discharge. The HCL output was modulated by a mechanical chopper (Model 300, Scitec Instruments Ltd., Hampshire, UK), and the detected signal fed into a photon counter. The transmitted light intensities, after background subtraction, were acquired directly from the digital display of the photon counter and each final number was an average of at least ten readings. The atomic absorbance was then calculated based on the detected transmittance.

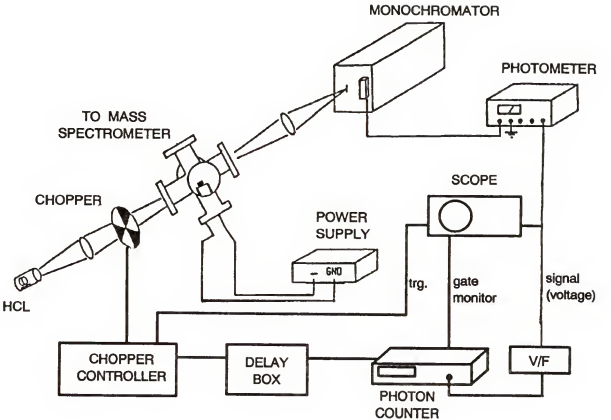

Figure 14 Block diagram of *in situ* MS/AA set-up.

CHAPTER 2
RARE EARTH ELEMENTS IN GLOW DISCHARGE MASS SPECTROMETRY

Background

The rare earth elements (REE or lanthanides) consist of a group of 14 naturally occurring elements (from lanthanum to lutetium) that exhibit remarkably similar chemical and physical properties [91]. The REE play an important role in the study of the earth's geological evolution and the manufacture of superconductors, super-magnets, and cathode-ray tubes. The determination of lanthanides in geological samples is one of the most difficult and complicated tasks for analytical chemistry because of the similarity in their chemical behavior, as well as the often complex geological matrix in which they are found [92].

REE Analysis Techniques and Limitations

The analytical techniques that are currently used for the REE analysis in geological materials include neutron activation analysis (NAA) [93,94], X-ray fluorescence spectroscopy (XRF) [95-98], thermal ionization [99,100] and spark source mass spectrometry [101,102], inductively coupled plasma (ICP) optical spectroscopy [103-106], and mass spectrometry, etc. [107-111]. The following discussion will focus on sample treatment steps required by each method. Specific experimental procedures concerning each method can be found in the corresponding references listed above.

Neutron activation analysis

Nuclear activation analytical methods are all based on the transmutation of stable nuclei into radioactive, metastable states that then decay, emitting characteristic radiation. Most of the nuclear activation methods currently in use involve neutron irradiation, followed by γ- or β-ray spectrometry of the induced activity, called neutron activation analysis. NAA is one of the traditional and most sensitive techniques for the determination of REE. Sub-μg/g detection limits are obtained on a routine analysis basis, and nanogram level detection limits have also been achieved with certain elements. In most cases, to ensure successful determination of extremely low concentration (nanogram level) REE in various natural samples, appropriate chemical separation procedures must be carried out to increase the sensitivity and reduce interferences. Procedures for separating the REE as a group from other interfering elements are based on classical hydroxide-fluoride or hydroxide-oxalate precipitation cycles with carriers (e.g., Ca). These procedures may be applied either before or after the irradiation of the sample (which usually lasts from several hours to a day) including the steps listed in Table 2-1 [92]. Separation of scandium is an important part of the scheme, because its isotopes have strong γ-ray peaks that may interfere with the REE peaks. The separation procedure is usually repeated two to three times, since only about 50 -80 % of the Sc is separated each time. Other separation methods include sample digestion with acids followed by eluting the solution through a cation or anion exchange column. Such extensive sample treatment steps not only prolong the analysis time, but may also introduce potential interferences to

Table 2-1. A Common Separation Procedure For the REE in NAA

(1) Fusion of an irradiated sample in a nickel or zirconium crucible with sodium peroxide and hydroxide in the presence of REE carriers.
(2) Dissolution of the fusion cake with water or dilute acid.
(3) Addition of sodium hydroxide or ammonia to precipitate REE hydroxide.
(4) Separation of iron by extraction with diisopropyl ether from hydrochloric acid medium.
(5) Separation of scandium by dimethyl ether extraction in the presence of ammonium thiocyanate.

Source: ref.[92]

the analytes in some cases. These two factors, in combination with the requirement of properly shielding the instrument for safety, are considered common traits of this highly sensitive method.

X-ray fluorescence spectroscopy

XRF is a useful and versatile method for the determination of REE in a variety of materials. Typical applications are analyses of REE in rocks, minerals, ores, and process solutions. Similar to other instrumental methods, XRF is subject to spectral and other modes of interferences, which makes a chemical separation step necessary in order to achieve good analytical results. With the availability of stable modern X-ray spectrometers, the accuracy of XRF analysis now depends primarily on the sample preparation techniques. Different procedures have been proposed for preliminary chemical enrichments and separations of trace elements from the original sample for use with XRF analysis, e.g., precipitation, solvent extraction, and ion exchange. In addition, for the final determination of analytes by XRF, it is preferable that samples be in the solid state after the concentration step, making a re-solidifying step necessary. Forming glass disks by fusion (for non-REE elements) is a frequently used method of sample preparation for subsequent analysis by XRF, where the removal or prevention of excessive stress has been identified as the key to success. To alleviate the stress, the fusion melt often needs to be annealed in the mold at 500 °C for over an hour with subsequent cooling to less than 350 °C in approximately another hour. While offering good detection limits (sub μg/g) and excellent accuracy (as good as ±0.5%), sample preparation procedures required by

XRF tend to lengthen the overall analysis time. Sholkovitz recently reported using XRF to determine the REE concentrations in marine sediments and geological rock materials in which the dissolution step alone lasted over 12 hours [98].

Thermal ionization and spark source mass spectrometry

The distinct advantage of using mass spectrometry for REE analysis in the geological matrix is the ability to determine simultaneously a wide range of elements. Because the MS detection of elements is based on the elements' mass to charge ratio rather than their optical properties, fewer interferences are encountered than in the cases of NAA and XRF. The early application of spark source mass spectrometry (SSMS) to the geological field was pioneered by Taylor [112,113]. Although certain success has been achieved in improving the precision and accuracy of this technique in trace elemental analysis [101], compared with the later developed ICP techniques, SS mass spectrometer remains complicated to operate while the analytical results are often sporadic.

Since the early publications on this technique, thermal ionization mass spectrometry (TIMS) combined with isotope dilution technique has been considered the most precise method for REE analysis in rocks and minerals [114]. Picogram quantities of REE have been determined in meteoritic materials using this technique [99]. A recent study has reported using freon to suppress isobaric interferences by oxide ions during a multielement REE analysis [100], which has made it possible to perform isotopic dilution analyses on much smaller samples than normally required. However, similar to what is often encountered

in the other REE analytical methods, extensive sample treatment steps are also required by TIMS, and a representative case is shown in Figure 15 [99].

Inductively coupled plasma spectrometry (AE and MS)

The development of ICP as an analytical source both for atomic emission and mass spectrometry was prompted partly by its potential in the field of earth sciences [111,115]. The ability to provide rapid multielemental information about the sample combined with the relative simplicity and low cost of the instrument has made ICPAES a very popular technique since its early introduction to geological sciences [116]. At a reasonably higher instrumental cost, ICPMS offers even better detection sensitivity, simpler spectra, and information on isotopic abundances for geological samples. Hence, ICPMS is accepted increasingly as the choice of trace elemental analysis for many types of geological materials.

Because of the large diversity of sample forms presented by the geological materials, a major aspect of ICP researches has involved the development of sample preparation schemes. Aqueous samples or samples that are easily converted to solution forms usually present fewer difficulties when applied to ICP techniques, although sometimes preconcentration and separation steps are still required to achieve accurate, reliable, and sensitive results. A thorough review of sample preconcentration and separation methods used with both ICPAES and ICPMS has been provided by Barnes *et al.* [117]. Pretreatment for samples originally in solid form is more complicated than for solution samples and hence presents a more challenging problem for geological applications. The traditional method of handling samples such as rocks involves a multi-acid digestion of the

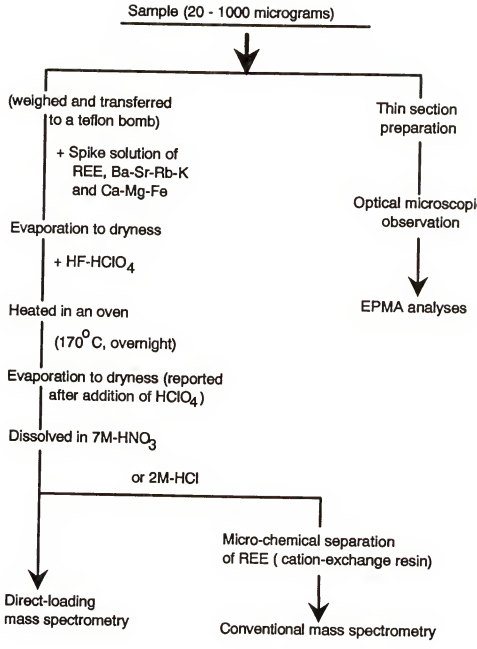
Sample (20 - 1000 micrograms)
(weighed and transferred to a teflon bomb)
+ Spike solution of REE, Ba-Sr-Rb-K and Ca-Mg-Fe
Evaporation to dryness
+ HF-HClO4
Heated in an oven
(170°C, overnight)
Evaporation to dryness (reported after addition of HClO4)
Dissolved in 7M-HNO3
or 2M-HCl
Direct-loading mass spectrometry
Micro-chemical separation of REE (cation-exchange resin)
Conventional mass spectrometry
Thin section preparation
Optical microscopic observation
EPMA analyses

Figure 15 Typical sample pretreatment procedures for REE analysis using TIMS [99].

sample with hydrofluoric, nitric, and perchloric acids. If the REE are contained in mineral phases that are resistant to acid attack and therefore difficult to digest, a fusion method must be used, followed by further dissolution and sometimes ion-exchange separations. In recent years, several new types of sample introduction methods have been established to avoid complete dissolution of the solids. Among them slurry nebulization has received much attention both for ICPAES and ICPMS [118,119]. Certain modification of the ICP nebulization system is needed for the introduction of slurry samples. In the study reported by Javis *et al.* [119], the ground solid powders were directly added into two milliliters of tetrasodium pyrophosphate with zirconia beads, followed by a 15-hour period of constant shaking to form a homogeneous slurry for the ICP nebulization. Although the sample can be left unattended during this step, the 15-hour mixing time lengthens the entire sample turn-around time. Another "direct" solids analysis method designed to suit ICP application is the combination of laser ablation for atomization and ICP for ionization. Imai [120] has applied this technique successfully to determine 42 major and minor elements in twelve original rocks and mineral inclusions. The drawback of this approach is the added cost of the laser system and the difficulty in instrumental operation. Compared with the previously discussed techniques for REE analysis, solids sample preparation is still a time-consuming endeavor where further improvement is desired, despite the reduced instrumental time required by ICPMS to carry out complete multielemental analyses.

Rare Earths in GDMS

As discussed in Chapter 1, the GD sputtering process generates an atomic population directly from the solid phase, which eliminates the sample dissolution steps required by almost all of the previously discussed techniques. The separations of all elements contained in the sample from the matrix and from each other are accomplished on the atomic scale, which is most ideal for elemental analysis. This apparent advantage of GD atomization has initiated our interest in applying GDMS for the analysis of REE in geological materials. So far, research in this area has been limited compared with the amount of studies devoted to GD plasma characterization of metals and alloys.

Non-conducting Samples in GD Sources

The majority of the REE in earth materials exist in the ionic form, and hence is not electrically conducting. Although GD analytical methods are most suitable for bulk conductors, non-conducting materials can also be analyzed using two operation modes of the power supply: direct current (DC) and radio frequency (rf). In the traditional DC mode, the sample must be made conducting by mixing the ground, non-conducting powder with a conducting binder (e.g., Cu or Ag); the mixture is then pressed to form a cathode pellet. This method, combined with optical emission detection, was first documented by Massmann for the determination of 12 elements [121]. In more recent years, Brenner *et al.* have reported using a GDAES system to determine both major and minor elements in a variety of solid geological materials and related non-conductors [122].

Winchester and Marcus have developed a method for analyzing Fe(III) and Al(III) oxides in an NBS geological reference material using GDAAS [123]. The detection limit was reported in the low parts-per-million (ppm) range with the analytical accuracy of 8 %. Another publication by Marcus *et al.* reported using GDAAS to determine platinum and rhodium concentrations in automotive catalyst materials [124]. An improved relative error of 2-3 % was achieved on this aluminum based catalyst. It has also been reported that matrix dependence of the calibration can be minimized when the analyte is finely dispersed (grain size $< 60\,\mu$m) and blended with an excess of fine copper powder [125]. A relatively new approach is using the electrical power operated at radio frequencies to sustain the glow discharge of non-conducting materials. This method does not require the matrix mixing step and therefore further simplifies the sample preparation procedure. Although the original research in this area was initiated in the 1970s by Coburn [44-46], it was not until recently that its analytical utilities were further explored. Rf powered GD sources have been combined with AES to analyze glasses and ceramics, two of the most solvent resistant and hence difficult substances for analytical chemistry [126,127]. Compared with investigations carried out in GDAES, publications on using GDMS for non-conductor analyses have been relatively limited over the past decade. Robinson and Hall have reported using the commercial GDMS VG 9000 to determine the concentration of uranium oxide in nuclear materials [128]. In a related study conducted by Harrison *et al.*, the hollow cathode plume was applied to the elemental analysis of geological materials by atomic emission [129], in which

standard clay samples were mixed with a conducting matrix and pressed to form the cathode. Harrison and coworkers have also addressed the problem of molecular interferences when using GDMS to analyze oxides in geological matrices [130].

It was the goal of this work to further the development of GDMS application in the field of earth science and to explore the fundamental mechanisms involved in this process. In order to do so, some of the plasma characteristics involving geological samples, particularly the rare earths, needed to be considered. Among them, factors that contribute to the chemical environment in the ion source including preparation of the sample cathode must first be explained.

Sample Preparation

The cathode preparation procedure described here was used throughout the work presented in this dissertation. The selected analyte, in most cases lanthanum oxide La_2O_3 (AG, Fisher Scientific Company), was mixed with one of the following conducting matrices: silver, carbon, tungsten, tantalum, or titanium. The highest available purity of each was used, with a grain size of 75 μm or smaller. In most cases, a mixture of 10 % analyte - 90 % matrix was prepared with each of the conducting binders. After thoroughly mixing the powders on a Wig-L-Bug (Model 3110B, Crescent Dental Manufacturing, Co., Chicago, IL), the sample mixture was pressed with a custom designed die, shown in Figure 16, into a 4 mm diameter disk. The typical compressing pressure applied was 800 - 1000 psi. The compressed disk was then mounted into a copper (or brass) cup to be fixed on the cathode probe tip. The probe was inserted into the ion source for

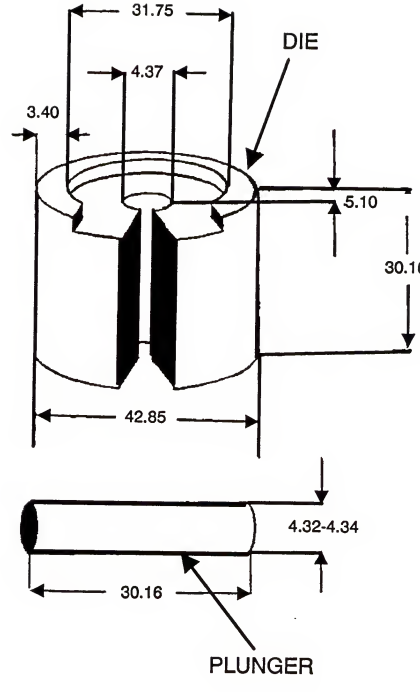

Unit is mm

Figure 16 Diagram of die assembly for compressing disk cathodes.

the glow discharge operation. Shielding the probe tip with a Macor cap limited discharge access to the pressed disk.

Plasma Equilibria of REE

The fundamental processes of a rare earth oxide in the glow discharge also follow the sputter atomization and subsequent plasma ionization pattern as described in Chapter 1. But because of the distinct difference between an oxide and a metallic sample and the different ways by which each sample is prepared in GDMS, the glow discharge plasma formed about an oxide sample possesses some unique features that need to be addressed. The uniqueness of the GD forming about an oxide sample exists mainly in two aspects: (1) mode of sputtering and (2) chemical environment of the plasma. The former is caused by the different bond strength of an oxide from a pure metal, resulting in different patterns of bond dissociation upon argon bombardment. The increased amounts of gaseous species brought into the discharge by the oxide sample (especially the oxygen content) result in a more chemically reactive plasma than that of a pure metal. These two aspects, regarded as two interacting equilibrium systems, will be discussed separately in the following text.

Sputter equilibria

In Chapter 1 the sputtering process of the glow discharge has been discussed using mainly a bulk metal as the model target. The effect of Ar^+ bombardment on an oxide substrate differs from that on a metallic substrate, as briefly mentioned in the "molecular sputtering" section. Coburn and coworkers have studied neutral species that are rf sputtered from several oxide targets and

noticed the ejection of both M atoms and MO molecules [131]. A proportional relationship was established between the ratio of $MO^+/(MO^+ + M^+)$ and the M-O bond energy of the oxide (Figure 17). Here the REE representative Pr yields one of the highest $MO^+/(MO^+ + M^+)$ ratios (0.5) because of the high Pr-O bond strength (7.8 eV). Although the molecular sputtering mechanism in the glow discharge is not fully understood because of difficulties in separating the sputtering and ionization steps, oxide sputtering has been investigated in other related areas for many years. Some sputtering models developed in secondary neutral mass spectrometry (SNMS) will be used here to explain indirectly the molecular sputtering phenomenon observed in GDMS.

It needs to be pointed out that significant differences exist in the sputtering conditions and ion source vacuums between SNMS and GDMS [132]. In SNMS, a directional beam of accelerated ions (mostly inert gas) is used to bombard the target situated in a 10^{-4} - 10^{-9} Torr high vacuum environment. In GDMS however, sputtering projectiles collide onto the sample surface from almost all directions, and the much higher source pressure (0.1 - 10 Torr) causes further collisions among the sputtered neutrals and other species in the gas phase, resulting in re-deposition and various gas phase reactions. Ionization modes are also different between the two methods. While electron ionization occurring in a separable step after sputtering is the major mechanism in SNMS, the GD plasma incorporates a combination of many ionization paths that cannot be practically separated from the sputtering process. In this sense, ions detected in GDMS do not necessarily reflect the species' neutral forms in which they are sputtered off the sample

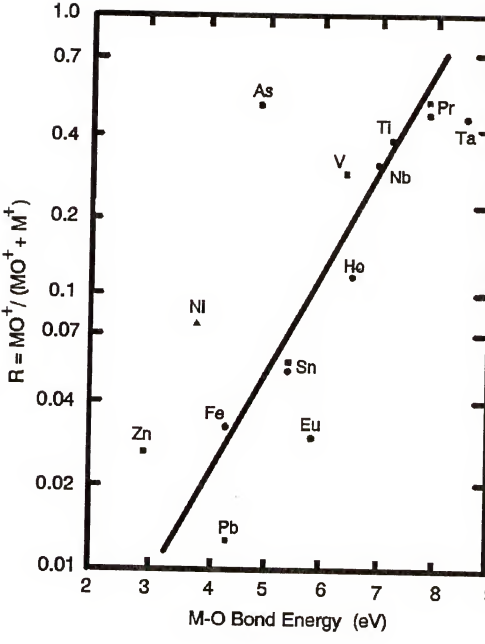

Figure 17 Ion signal ratio $MO^+/(MO^+ + M^+)$ as a function of M-O bond energy in sputtering oxides with rf discharge [131].

surface. For example, if the detected M^+/MO^+ ratio is *x*, it does not necessarily mean that the M/MO neutral ratio as they are sputtered off the cathode surface is also *x*. Whereas in SNMS, the two ratios resemble each other much more closely because there are fewer interactions among species in the gas phase due to the much lower pressure. By the same token, if the energy of the ion projectiles used in a SNMS experiment is similar to that in GDMS, the GD sputtering can be modeled after results obtained by SNMS. Sputtered neutral population measured by SNMS ion signals may be considered representative of those neutral population obtained in the equivalent GD sputtering step.

In a study carried out by Oechsner *et al.*, the sputtering pattern of Ta_2O_5 by Ar^+ ions at energies below 1 keV was monitored by SNMS [133]. The detected intensity ratio of TaO^+/Ta^+ as a function of the Ar^+ ion energy of 50 - 900 eV is presented in Figure 18. This ion signal ratio closely represents the sputtered neutral ratio of TaO/Ta. Because the average Ar^+ bombarding energy in the glow discharge falls within the neighborhood of 300 - 500 eV [90], the sputtered neutral ratio of TaO/Ta in the glow discharge should be in the range of 1.0 - 1.5, according to Figure 18. Applying this estimation to the rare earth La_2O_3 (La-O has a similar bond energy as Ta-O), we can expect the sputtered LaO/La ratio to be also in the neighborhood of 1.0 - 1.5 under our normal GD conditions. In another related SNMS study reported by Oechsner *et al.*, the oxidized surface of Ce was bombarded with Ar^+ at an energy of 4 keV and an angle of 45° [134]. A CeO^+/Ce^+ ratio of 5.15 was discovered to be indicative of the neutral concentration ratio for CeO/Ce. The reason that the monoxide concentration was

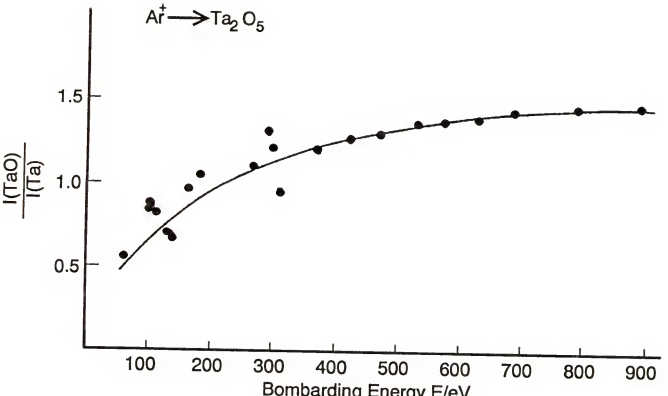

Figure 18 Ratio of sputtered neutral I(TaO)/I(Ta) as a function of the bombarding projectile Ar^+ energy [133].

dominantly higher in this case was because there was a 4 X 10^{-5} Torr oxygen pressure applied above the sample surface, which may have caused partial oxidation of the sputtered Ce atoms. A theory for the neutral molecule ejection by the sputtering processes was proposed and mathematically modeled by Gerhard [135]. He suggested that the insufficient energy transfer between atoms of distinctly different masses (such as encountered in a metal oxide) was the main cause for molecular sputtering. For instance, when an argon ion bombards a Ta_2O_5 substrate, kinetic energy is dissipated into the Ta-O bond lattice. Because a Ta atom is much heavier than an O atom, during the energy cascade through the oxide, the kinetic energy transfer from a Ta atom to a neighboring O atom in the surface layer is very small. Consequently, the Ta-O bond is not dissociated and both atoms can leave the surface together with the same velocity, resulting in the ejection of a TaO molecule. Due to the large mass differences between REE and the O atom, a similar situation is expected during the sputtering of rare earth oxides. This means that a significant fraction of the sputtered neutral flux may be comprised of rare earth monoxide molecules.

Another characteristic phenomenon of using an ion beam to sputter an oxide target is the preferential sputtering of O atoms in the oxide sample, which leads to an altered surface stoichiometry of the target. Using Auger electron spectroscopy (AES) and low- energy ion scattering (ISS), the surface composition of a Ta_2O_5 target was monitored following Ar^+ and Ne^+ bombardment at different energies. [136,137]. It was found that as a result of the 1 keV Ar^+ bombardment, the surface Ta/O ratio was near unity, which was significantly higher than that

(2/5) in the original compound (Figure 19). They believed this was caused by the preferential sputtering of O atoms over Ta atoms during the initial period of sputtering. Umezama and Reilley studied the effect of argon ion bombardment on metal complexes and oxides by X-ray photoelectron spectroscopy [138]. They also found significant oxygen depletion from the sample surface as a result of a 0.5 - 2 keV Ar^+ sputtering. For example, the La/O ratio has decreased from the original 1/2.75 in the $LaCoO_3$ sample to the final 1/1.82 after argon bombardment. Whether such surface stoichiometry changes also occur in GD sputtering is more difficult to monitor because of the severe surface re-deposition; what is relevant about these results to the GD study is that the amount of atomic oxygen released during the oxide sputtering is at least comparable to that of the metal if not more. Additional preferential sputtering investigations of oxides have been documented in other publications with similar observations [139,140].

Based on the previous discussions, we can conclude that during the GD sputtering process of an oxide (e.g., La_2O_3), both La and O atoms as well as LaO molecules are expected to be ejected from the sample surface. Certain equilibria governed mainly by the La-O bond strength, the bombarding energy of Ar^+, and the mass ratio of La/O are established among the sputtered concentrations of the three species. Under typical discharge conditions, i.e., 1000 - 1500 V, the amounts of sputtered LaO and La neutrals are expected to be comparable.

Reaction equilibria

The essence of the last section (sputter equilibria) was to draw an analogy between GD and high vacuum beam sputtering of the oxide sample in order to

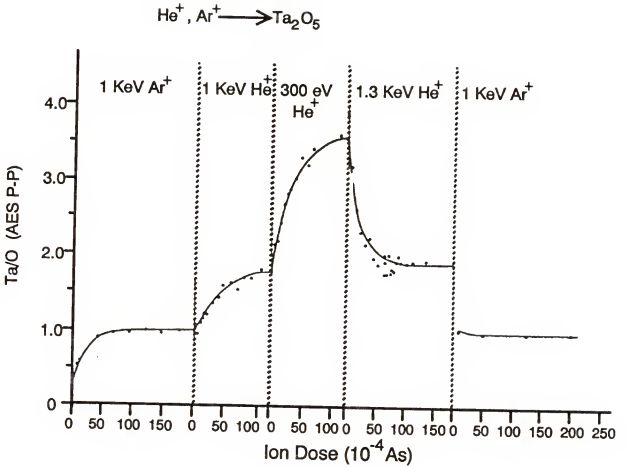

Figure 19 Surface stoichiometry ratio of Ta/O after Ar^+ and He^+ bombardment as a function of the ion dose [136].

obtain insight about the rare earth sputtering mechanism in the GD. This section emphasizes the uniqueness of GD in that its much higher source pressure creates another equilibria system in the plasma beyond the sputtering step: the reaction equilibria. In order for a chemical reaction to occur in the gas phase, it is necessary that: (1) there are sufficient reactants and (2) the reactants have the opportunity to interact. Both requirements can be fulfilled in a GD plasma, in which many chemical species (including the discharge supporting gas, sputtered sample species, and gaseous contaminants) act as the reactants. The small mean free path (about 0.01 cm) of the fill gas in a one Torr GD source ensures collisions among the plasma species that may lead to both wanted and unwanted chemical reactions.

An example of wanted plasma reactions may be Penning ionization of the sputtered analyte species by collision with argon metastable atoms. The first ionization energies of the REE and the bond strengths of the REE monoxides are tabulated in Table 2-2. It can be seen that first ionization energies of all the REE are below the energy level of the argon metastable atom, hence Penning ionization is considered a major mechanism for the formation of REE ions. Because the summation of the M-O bond energy and the ionization energy of M exceeds the energy level of the argon metastable atom, a collision between most of the REE monoxides (except for YbO) and an argon metastable atom will not result in dissociative ionization of that monoxide, that is:

$$Ar^{*} + MO \neq M^{+} + Ar^{\circ} + e^{-} \qquad (2\text{-}1)$$

Table 2-2. Ionization Energies of Rare Earth Elements and Ionization Energies and Bond Strengths of Rare Earth Monoxides

Element	Ionization Energy (eV)[a]	Monoxide	Ionization Energy (eV)[b]	M-O Bond Energy (eV)[b]
La	5.28	LaO	4.9	8.3
Ce	5.47	CeO	4.9	8.3
Pr	5.42	PrO	4.9	7.8
Nd	5.49	NdO	5.0	7.3
Pm	5.55	PmO	-	7.0
Sm	5.63	SmO	-	6.0
Eu	5.67	EuO	-	4.9
Co	6.14	GdO	-	7.4
Tb	5.85	TbO	-	7.3
Dy	5.93	DyO	-	6.3
Ho	6.02	HoO	-	6.4
Er	6.10	ErO	-	6.3
Tm	6.18	TmO	-	5.8
Yb	6.25	YbO	-	4.4
Lu	5.43	LuO	-	7.2

Source: a). CRC Handbook of Chemistry and Physics, 66th Edition, 1985-1986.
b). Ref [147].

Also listed in Table 2-2 are ionization energies for LaO, CeO, PrO, and NdO molecules, which are significantly lower than the argon metastable energy level. Therefore, the REE monoxides are subject to Penning ionization as a result of collision with the argon metastable atoms, i.e.:

$$Ar^{*} + MO = MO^{+} + Ar^{o} + e^{-} \qquad (2\text{-}2)$$

Unwanted plasma reactions result in interferences, one example being the formation of metal argides in the glow discharge [141]. In the case of bulk metals, most gaseous impurities can be eliminated by pumping the ion source extensively and leading to limited occurrence of unwanted plasma reactions. Due to the disk compressing step in sample preparation, powdered samples such as the rare earths can trap a large amount of gaseous contaminants inside the disc cathode and bring them into the discharge housing. Unlike gaseous molecules adsorbed on the bulk metal surface, these contaminants enveloped inside the cathode cannot be removed from the ion source just by pumping. They will, however, be released during the discharge operation due either to cathode heating or Ar^{+} sputtering. This concept is illustrated in Figure 20 in which the analyte oxide (La_2O_3) is mixed in a conducting matrix M with a 10 % concentration. During the discharge operation, the co-releasing of gas molecules (O_2, H_2O, CO_2, etc.) with the sputtered M atoms enriches the plasma with chemically reactive species. The presence of water contamination in the GD formed by a 10%La_2O_3/90%Ag sample, was detected at significantly high concentrations as shown in Figure 21. Figure 21a and b were acquired at 10 and 70 minutes after the discharge was turned on respectively. While pre-sputtering

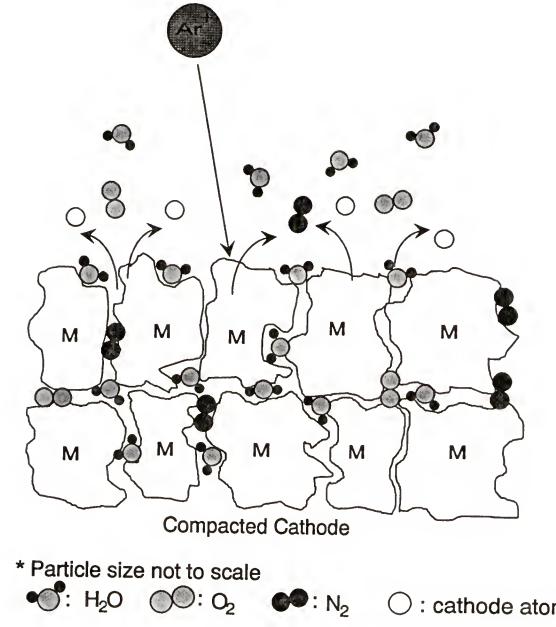

Figure 20 Illustration of gaseous contaminants trapped within a compressed cathode disk.

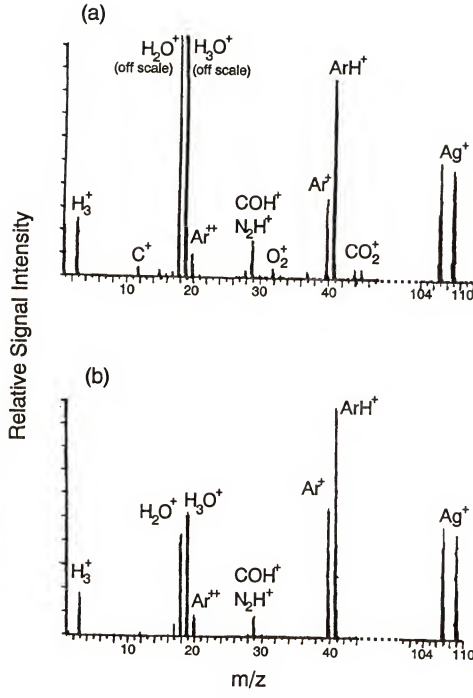

Figure 21 Mass spectra of gaseous species in the plasma of a 10%La_2O_3/90%Ag sample; (a) obtained 10 min after discharge initiation; (b) 60 min after (a).

a bulk sample over 30 minutes usually suffices to reduce water contamination to a minimal level, it can be seen here that extensively sputtering the compressed disk cathode could only reduce the water signals (H_2O^+ and H_3O^+) to a smaller level, but could not eliminate them completely from the discharge. This is because water, oxygen, and other gaseous impurities are being released constantly into the discharge from within the compressed cathode. These reactive impurities present in the discharge may be involved in various chemical reactions with the analyte species, hence altering both the existing form and concentration of the analyte species. Of all possible reactions among the analyte REE and other plasma species, redox reactions controlling the distribution of M and MO are most important to the elemental analysis capability of GDMS. This concept can be expressed by Equation 2-3:

$$MO \underset{\text{oxygen donor}}{\overset{\text{oxygen scavenger}}{\rightleftharpoons}} O + M \qquad (2\text{-}3)$$

The interactions among M, MO, and other oxygen-influential species comprise the reaction equilibria that determine the M^+ and MO^+ signals as detected by the mass spectrometer.

Combining the sputter equilibria and reaction equilibria of a rare earth oxide, e.g., La_2O_3, the basic glow discharge processes of La_2O_3 can be portrayed by Figure 22. La_2O_3 will be sputtered off the cathode surface in the forms of O and La atoms and LaO molecules as a result of Ar^+ bombardment. Gaseous contaminants trapped in the sample are also released into the plasma during this process. Redox equilibria involving all oxygen-sensitive species will be

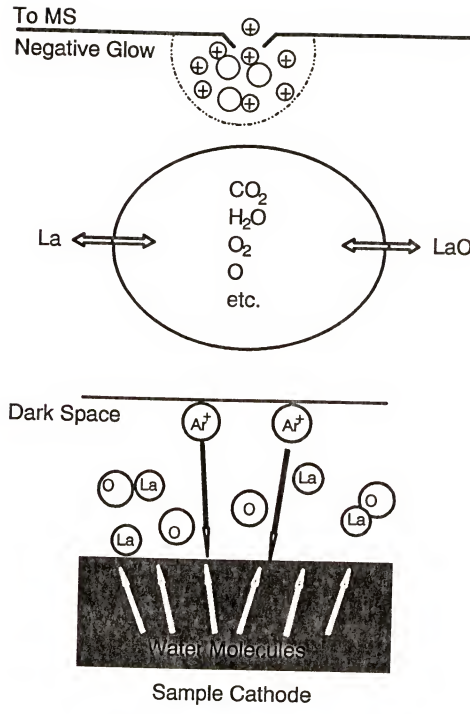

Figure 22 Illustration of the La-LaO equilibria in the glow discharge plasma.

established in the plasma that may ultimately determine the availability of the La analyte, and hence the analytical sensitivity of the method. The main body of the remaining text will be divided into two aspects centering around this equilibria system: (1) to develop a GDMS method for REE analysis in geological matrices, and (2) to explore the fundamental processes of the M-MO equilibration in the glow discharge.

CHAPTER 3
RARE EARTH OXIDE EQUILIBRIA IN DIRECT CURRENT GLOW DISCHARGE MASS SPECTROMETRY

Elimination of Oxidant Contamination

Introduction

The rare earth oxide equilibria introduced in Chapter 2 are the basis for all the plasma manipulation studies carried out in this work. As illustrated in Figure 22, many gaseous contaminants (especially water) are co-released with the analyte species from the compacted sample into the plasma during discharge operation. Studies have shown that water, when present in the plasma even in trace amounts, will depopulate argon metastable atoms resulting in inefficient ionization [142]. While the reduced ionization problem is universal for all GD analyses, water presents additional problems to REE analysis, i.e., the severe oxidation of the analyte atom. The oxidation effect is depicted by Equation (2-3), in which excessive oxygen containing species will cause the reaction equilibria to shift toward the formation of MO rather than M. In order to enhance the elemental population, ways of shifting the La-LaO equilibria to the formation of La are desired. According to equilibrium theory, this can be achieved by either reducing the concentration of the oxidant or increasing the concentration of the reductant. Because a significant fraction of the oxidants present in the discharge is water, the removal of water molecules from the plasma becomes the focus of

contaminant elimination. Two methods of water elimination have been explored in this work: (1) physically removing water by cryogenic condensation, and (2) chemically removing water by redox reactions. The comparison of those methods is the main theme of this chapter.

Cryogenic Condensation--Physical Elimination

Removal of water

Application of cryogenic methods to GDMS is not new; a cryogenically cooled ion source is a standard feature of the commercial VG 9000 glow discharge mass spectrometer and is used in routine analyses to reduce the water interference [143]. However, limited studies have been done to monitor closely the effect of cryogenic cooling on plasma chemistry. As part of the study of plasma chemistry, the effect of cryogenic cooling on plasma processes of La_2O_3 was investigated.

In this study, an in-house custom designed stainless steel coil was made, allowing liquid nitrogen to circulate around the sample cathode (Figure 23). The coil, made from a ⅛ inch o.d. stainless steel tubing with a total surface area of ca. 2.5 cm^2, was placed coaxially around the cathode probe. Liquid nitrogen can be drawn through the stainless steel coils to avoid ice locks and ensure sufficiently low temperature on the coil surface.

The first goal was to study the efficiency of water elimination effected by rapidly cooling the coils. The sample disk, made from a 10% La_2O_3 and 90% Ag mixture as described in Chapter 2, was used as the discharge cathode. After pumping the cathode for over an hour to allow out-gassing in the ion source, the

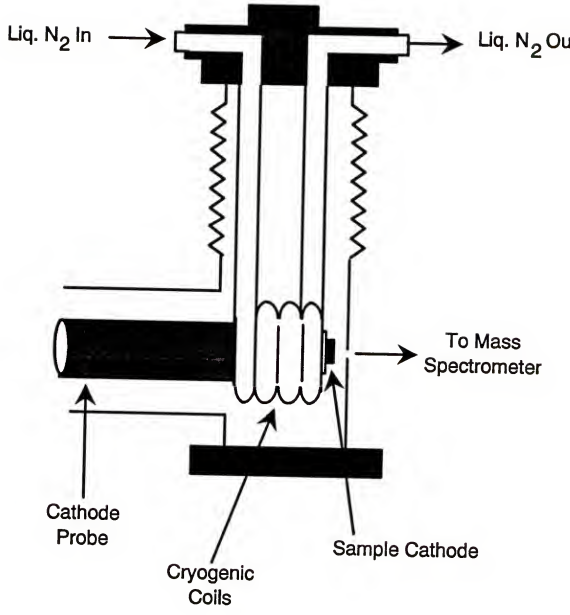

Figure 23 Illustration of the cryogenic cooling coil arrangement in the discharge chamber.

discharge was turned on and maintained at a constant 1000 V. A pre-sputtering period of 10-20 minutes was usually required to allow the discharge to stabilize, during which ion signals were too sporadic to be monitored. Shown in Figure 24 are the ion signal intensities of Ar^+, H_2O^+, and N_2H^+ versus sputtering time (timing started at the end of pre-sputtering). All three ion signals stayed relatively stable within the first 3 minutes of measurement. Liquid nitrogen was then added into and drawn through the cooling coils at the time indicated in the graph. As shown in Figure 24, following a time delay of about 30 seconds, the H_2O^+ and N_2H^+ signals started to decrease rapidly, whereas the Ar^+ signal showed an increase. The N_2H^+ and H_2O^+ signals dropped to below the detection limit after the last data point shown in the graph (because zero intensity can not be adapted to log-scale). The decrease in water signal during the first five minutes following the introduction of liquid nitrogen was about three orders of magnitude. The addition of liquid nitrogen clearly caused a significant concentration decrease in the species with a freezing point higher than the liquid nitrogen temperature.

Analyte ion signal

Following the addition of liquid nitrogen, the LaO^+ signal also demonstrated a rapid decrease (by a factor of fifty in Figure 25), whereas the La^+ signal increased to a peak value and then leveled off. The rapid cooling of the coils has resulted in the immediate depletion of water and other oxygen carriers in the plasma, preventing them from participating in the redox equilibria between La and LaO. The analytical significance of such signal changes can be realized by calculating a signal ratio, $R = La^+/(La^+ + LaO^+) \times 100$ %. The increase in the R

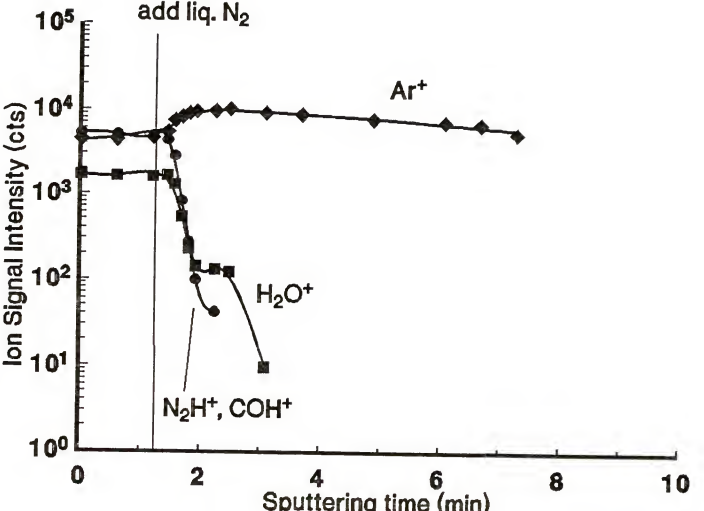

Figure 24 Effects on gaseous species signals by cryogenically cooling the ion source.

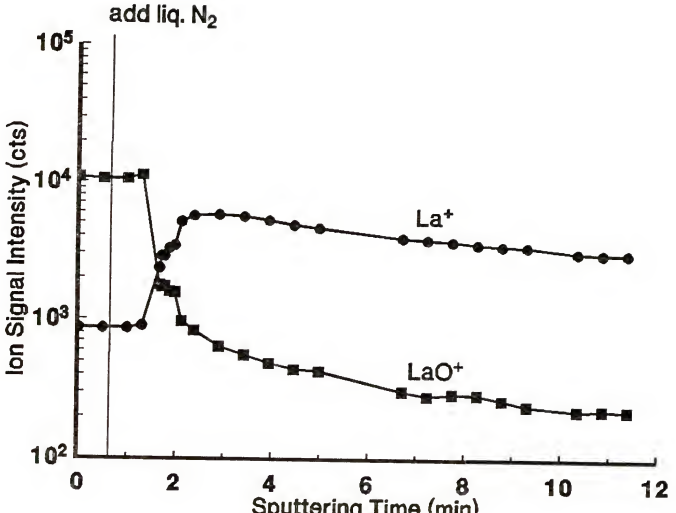

Figure 25 Effect of cryogenic cooling on the analyte signals.

value, as a result of liquid nitrogen addition, can be seen in Figure 26. Results from two disks prepared in the same manner are shown to have good reproducibility. This means that by using liquid nitrogen to remove water from the plasma reaction system, over 90 % of the analyte ions are in the atomic form, which is beneficial for elemental analysis.

Analyte atom concentration

The increase of the R value observed in Figure 26 may be attributed to one of the following two causes or a combination of both depending upon whether the La-LaO system is equilibrated mainly in the atomic state or the ionic state. First, if the La-LaO equilibria mainly involve neutral species, the removal of water may have prevented ground level La atoms from being consumed in reactions with water, hence resulting in a substantial increase in the La atomic and subsequent La^+ populations in the plasma. Second, if the La-LaO equilibration occurred primarily in the ionic state, then a large increase in the La^+ signal could be observed upon removal of water even without a substantial increase in the ground level La concentration. To differentiate these two, it was necessary to measure the atomic La population *in situ* as the ion signals were monitored by the mass spectrometer. The instrumental set-up has been described in Chapter 2.

Experiments were conducted with a sample mixture consisting of 85% Ag and 15% La_2O_3 by weight, both with and without the use of liquid nitrogen separately. The reason for increasing the La_2O_3 portion in the mixture was to provide sufficient La atoms to ensure enough AA sensitivity. First without using liquid nitrogen, the ion signals of La^+ and LaO^+ and the atomic absorbance of La^o

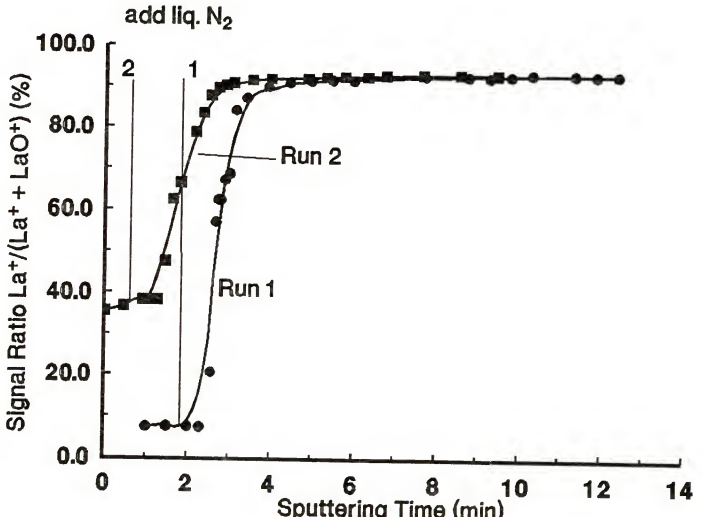

Figure 26 Effect of cryogenic cooling on the $La^+/(La^+ + LaO^+)$ ratio.

were recorded as a function of sputtering time, and plotted in Figure 27. All three signals showed an initial increase with sputtering time, possibly due to the "sputter-cleaning" of the sample surface. In the last 70 minutes of the experiment, the La° absorbance and the ion signals increased slightly at an equal rate, yielding a stable La^+/LaO^+ ratio. Next, the experiments were repeated and liquid nitrogen was applied in the same manner as described in the previous section to remove water from the discharge. The effect of the cryo-cooling step on the absorbance of La° is shown in Figure 28 as well as the *in situ* La^+ and LaO^+ signals. Clearly, upon adding liquid nitrogen and in turn removing water, the absorbance of La° was enhanced by a comparable magnitude as was the La^+ signal, whereas the LaO^+ signal decreased drastically. The La° absorbance increased proportionally to the La^+ signal, indicating that the increased La^+ signal was more likely a result of the enhanced La atomic population in the plasma rather than a phenomenon occurring in the ionic state only. It is believed that the removal of water from the system was the main cause for shifting the La-LaO equilibria toward a higher La concentration.

Getter Reagents--Chemical Elimination

Introduction

As opposed to condensing physically water from the discharge by using cryogenic coil, an alternative means of water removal is through chemical reactions between water and getter reagents.

Getter reagents, having high affinities toward oxygen, have been used in high vacuum techniques to eliminate gaseous contaminants [144]. They are most

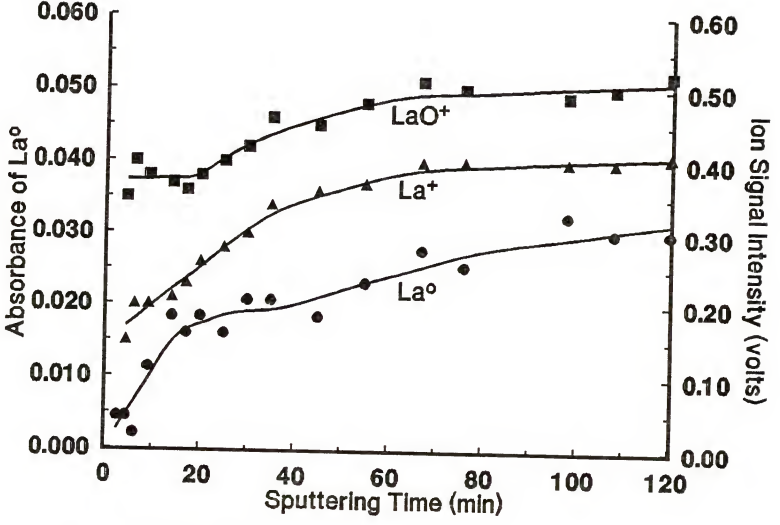

Figure 27 La^+ and LaO^+ signals La° atomic absorbance as a function of the sputtering time.

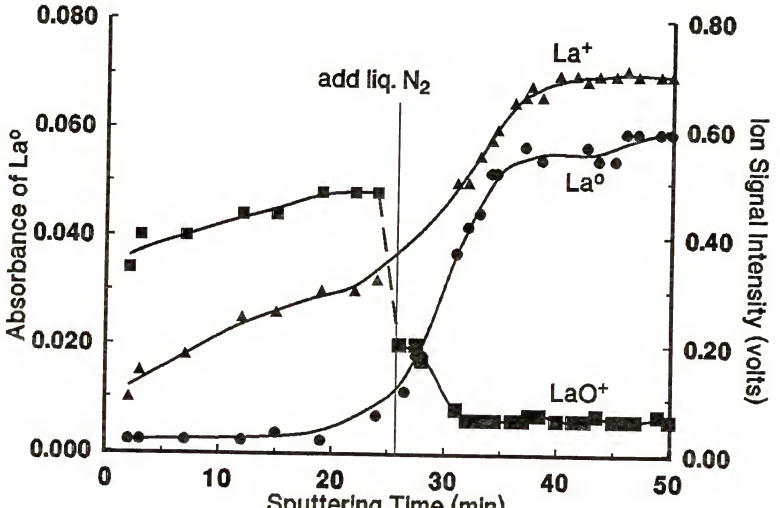

Figure 28 Effect of cryogenic cooling on La^+ and LaO^+ signals and La° absorbance.

effective when introduced in the reactive atomic form, often accomplished by thermal evaporation [145] or sputter introduction [146] into the environment to be gettered. By incorporating an effective getter material into a glow discharge cathode as a host matrix, the sputter action of the discharge itself will create a steady-state population of getter atoms in the plasma. In this way, the reactive getter atoms are available to scavenge undesirable components from the discharge simultaneously as the analyte is sputtered into the discharge for analytical purposes.

The selection of a getter material as a potential host matrix for GDMS requires several considerations. For such a sensitive technique as GDMS, the material must be available in a rather pure form so as to contribute few impurities. It should also be amenable to compaction with the analytical sample to form stable electrodes. Ideally, the getter would be mono-isotopic to minimize spectral interferences with analytical elements. In addition, it should not contribute significant poly-atomic species, either in the sputter step itself or by interactions in the plasma. For the purpose of this study, we have compared a series of materials, ranging from those with no reputed getter characteristics to those of high getter action.

Several metal powders with varying degrees of gettering ability were chosen to be sample host matrices: silver, carbon, tungsten, tantalum, and titanium. The highest available purity of each was used, with a grain size of 150 μm or smaller. The analyte for all the studies was La_2O_3. A mixture consisting of

10% La_2O_3 - 90% matrix was prepared with each of the matrices. Sample discs were prepared in the fashion described in Chapter 2.

Evaluation of performance

The first goal was to evaluate the matrices mixed with the tenaciously bound metal oxide, La_2O_3, in terms of the host matrix's ability to convert the oxide (LaO) to the atom (La). The ion signal ratio $R = La^+/(La^+ + LaO^+) \times 100\%$ was again used for comparison purposes. The effectiveness of all the materials increased with discharge running time, as illustrated by the R vs. discharge time plot in Figure 29. Initially, there was little evidence of the atomic ion compared with the molecular ion, but the R value increased with time as the plasma was cleared of residual water vapor. A sharp contrast in getter effectiveness is evident among the five materials. Tungsten, tantalum, and titanium, which are all known getter reagents, produced a large R value (comparable to that obtained in the cryogenic studies) with different degrees of efficiency. Graphite eventually did reach a reasonably large R, but only after an extensive period of time. However, spectra taken with a graphite matrix often suffer from numerous hydrocarbon contributions that are potential interferences. In this sense, it is not a good choice for host matrix. Silver, as anticipated, exhibited little getter activity and served as a reference point for a nonreactive sputtered matrix. The change in R was believed to be a result of chemical processes in the plasma. Specifically, getter reagents sputtered into the plasma compete with La for the available oxygen.

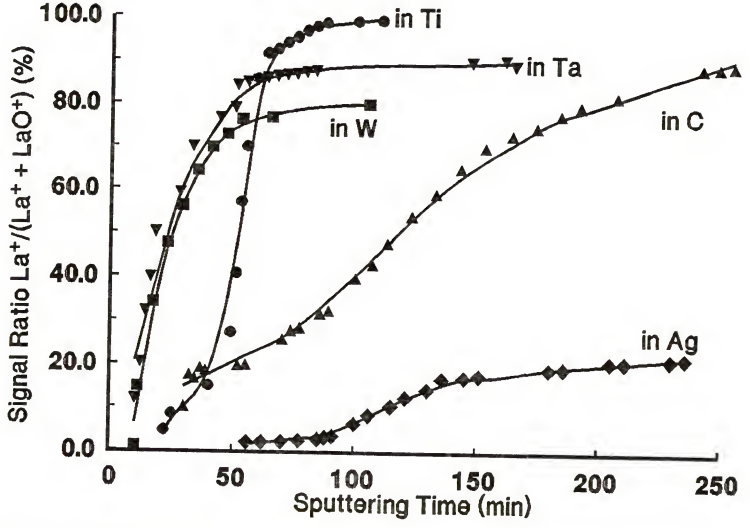

Figure 29 R as a function of sputtering time for various sample matrices.

Mode of gettering action

Mass spectrometric studies. As shown in Figure 9 in Chapter 2, mass spectra taken from a Ag matrix disk were dominated by the ion peaks at m/z 18 (H_2O^+), 19(H_3O^+) and 29(COH^+ and/or N_2H^+). These signals were high and did not vary significantly with sputtering time. However, if the sample matrix was a getter, signals of the gaseous species were greatly reduced after extensive sputtering. Note in Figure 30 that with time the water peaks were eventually removed and an ion signal for the Ti matrix appeared. This means that getters have created a plasma relatively free of gaseous interferences. These mass spectra also indicate that the oxygen content in a Ti discharge is more efficiently removed than in a Ag discharge. Therefore, sputtered La atoms have a lower probability of reacting with oxygen species, greatly reducing the LaO^+ population.

The reduction of gaseous contaminants in a gettering discharge is considered a result of the reactions between the sputtered getter particles and the gases. In the early stage of sputtering, mass spectral observations revealed such reaction products such as TiO^+, $Ti(OH)_2^+$, $Ti(OH)_3^+$ and $Ti(OH)_3(H_2O)^+$. Accompanied by an increase in R, these species were found to decrease with sputtering time (Figure 31). The spectra shifted from being dominated by the oxide ions to a clear dominance by the atomic La^+ ion. Early in the discharge operation, the getter served primarily to remove the large quantities of water vapor desorbing from the compacted sample and the source walls. Oxygen sputtered from the lanthanum oxide sample was produced at a more or less steady-state.

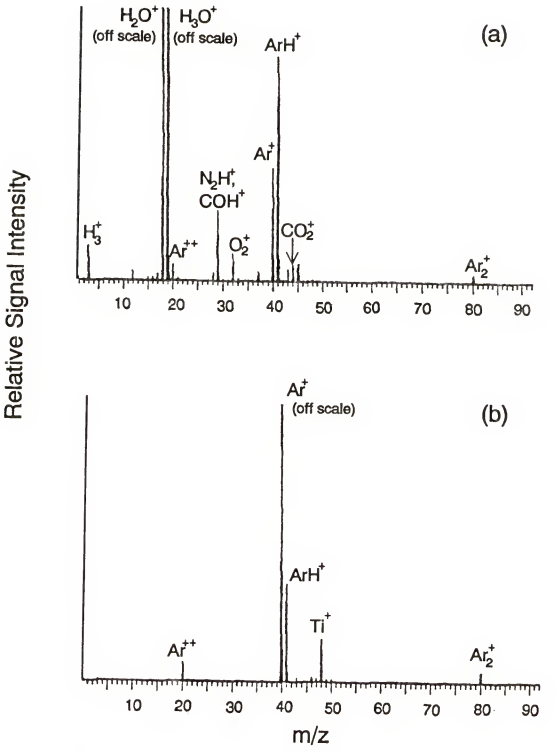

Figure 30 Mass spectra for a 10%La_2O_3/90%Ti sample. (a) 10 min after discharge initiation; (b) 60 min after (a).

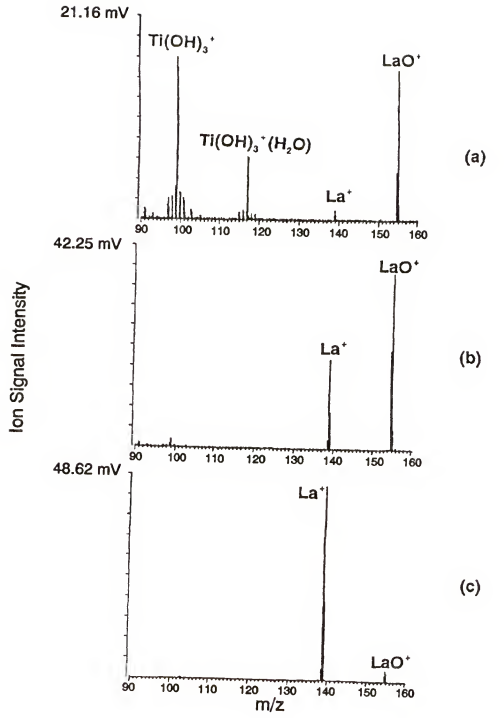

Figure 31 Mass spectra of La^+ and LaO^+ signals and Ti/water clusters. (a) 10 min after discharge initiation; (b) 30 min after (a); (c) 30 min after (b).

The large TiO^+ formed initially, changing to a much smaller, steady-state TiO^+ with time, indicated that the contribution of oxygen from the intrinsic water vapor was much larger than from the sputtered oxygen. Figure 32 illustrates the effect of a Ti getter on reactive plasma gases, as well as on the important ion signal ratio of the $La^+/(La^+ + LaO^+)$.

The selected matrix materials exhibit different degrees of efficiency in creating a large atomic La^+ population, reflecting their differing abilities to dissociate sputtered LaO and/or to prevent oxygen-carriers from reacting with La. This action may be a function of a number of factors associated with the host metals, e.g., M-O bonding energy, oxidation reaction rate, and sputtering rate of the host matrix. In the case of Ti powder, a very effective getter, the metal particles were all covered with an oxide coating that must be removed before effective getter action could occur. A surface cleaning step (activation) was necessary and was accomplished by pre-sputtering, during which the air-oxidized surface of Ti was sputter-removed, leaving a fresh, reactive Ti layer exposed. The effect of Ti is illustrated by the decrease of TiO^+/Ti^+ with time in Figure 32. It is evident that the sharp drop in the water signal began only when a clean Ti surface was generated.

Generally speaking, if Ti competes with La for available oxygen, the concentration of Ti in the plasma should have an effect on the relationship between R and sputtering time. To examine this theory, three mixtures were studied containing decreasing proportions of the Ti getter: 10%La_2O_3/90%Ti, 20%La_2O_3/80%Ti and 50%La_2O_3/50%Ti. As anticipated, Figure 33 shows an

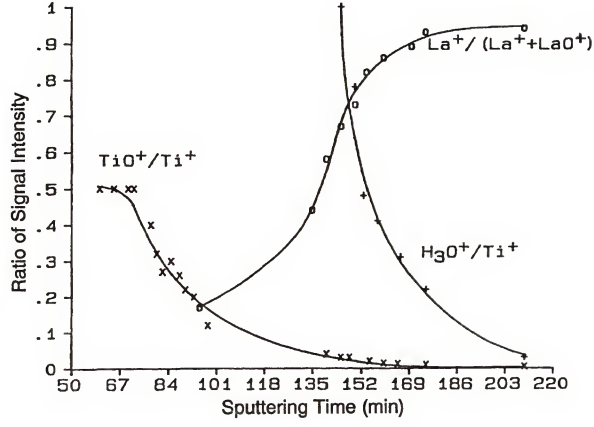

Figure 32 Signal ratios of Ti^+/Ti^+, H_3O^+/Ti^+, and $La^+/(La^+ + LaO^+)$ as a function of sputtering time.

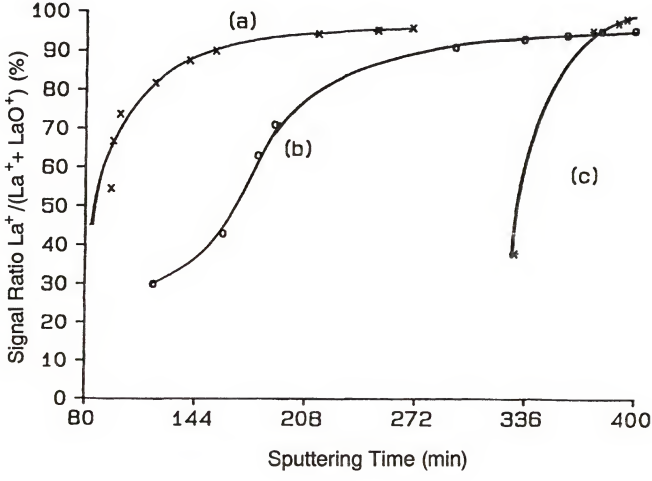

Figure 33 R as a function of sputtering time for three samples: (a) 10%La_2O_3/90%Ti; (b) 20%La_2O_3/80%Ti; (c) 50%La_2O_3/50%Ti.

increase in the sputtering time required to maximize R as the concentration of Ti in the electrode (and in the plasma) decreases.

Atomic absorption studies To investigate further the gettering mechanism in the glow discharge and to compare it with that of the cryogenic method, atomic absorption measurements of ground level La° population were carried out *in situ* with mass spectrometric detection of ion signals using getters as sample matrices. Again, the purpose was to distinguish whether plasma interactions mainly involve ground level reactants or ionic level reactants. The La^+ and LaO^+ signals and the absorbance of La° are plotted against the sputtering time in Figure 34. The correlation between the La^+ signal and the La° absorbance (i.e., both increase at a similar speed with time) is similar to the observation made using the cryogenic method.

The same experimental setup was used to monitor the population of Ti atoms in the discharge as a function of the sputtering time. It was stated earlier that when the ion signal of the getter species was maximized in the discharge, the discharge was considered "reducing" in nature. This can be evidenced if the concentration of getter atoms is also maximized under the same conditions. To investigate this by atomic absorption measurements, a Ti hollow cathode lamp (HCL) was used as the light source instead of the La HCL in the same MS/AA set-up. As shown in Figure 35, the absorbance of Ti° (λ=365.4 nm) increased with sputtering time in a similar fashion as that of La° in Figure 34. Because the atomic absorption instrument only allows single element detection at a time, the absorbance of both La° and Ti° atoms in one discharge can not be monitored

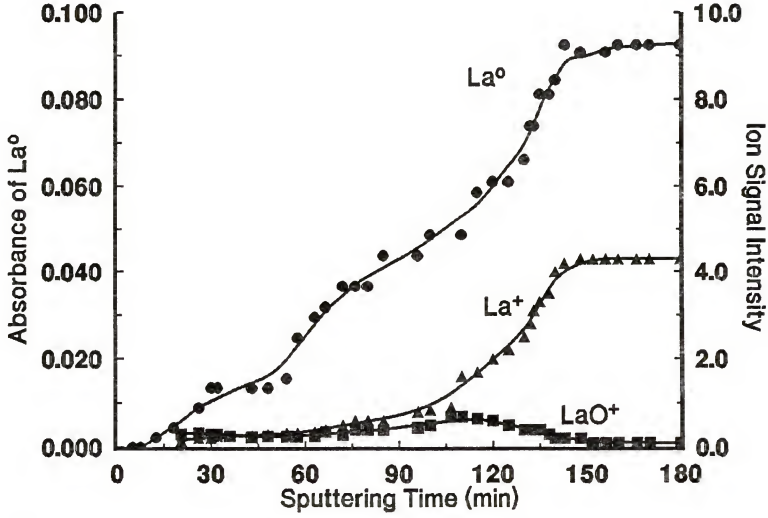

Figure 34 Absorbance of La° and La^{+} signal as functions of sputtering time for a La_2O_3/Tl sample.

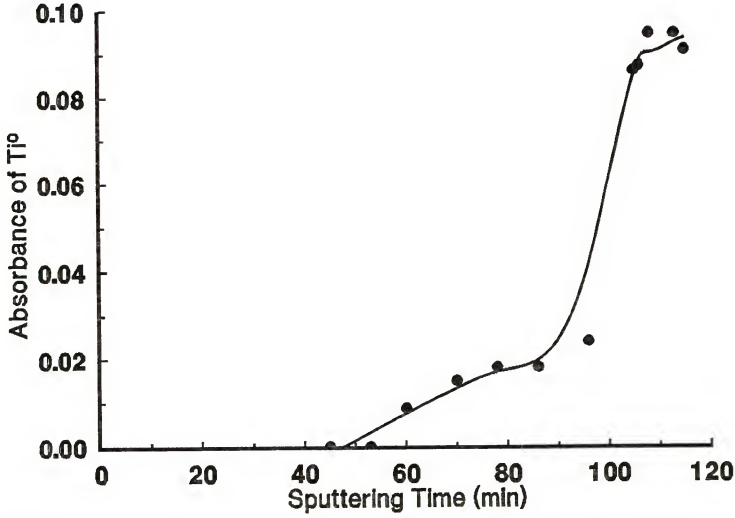

Figure 35 Absorption of Ti° as a function of the sputtering time.

simultaneously. The fact that they had to be measured with different samples may have resulted in the different lengths of sputtering time needed for the absorbance increase to occur. Nevertheless, these results support the theory that the removal of water contamination by getter materials is a self-sustaining process: water concentration is decreased by sputtered getter atoms, leading to a better sputter yield for more getter atoms, which in turn, results in a faster and more thorough removal of water. As the plasma is transformed from being oxidizing to reducing in nature, more La atoms are free from oxidation to form LaO, resulting in an enhanced La^+ and the subsequent R value.

Further discussion

It was introduced in the "sputter equilibria" section in Chapter 2 that in the energy range of glow discharge sputtering, tenacious oxides such as La_2O_3 should be sputtered off in the form of both LaO and La neutrals with comparable amounts. If these sputtered species are directly ionized without further deformation, the R value is expected to be close to 50 %. However, when using getter matrices, an ultimate R value of 98% has been obtained with Ti, indicating that a large number of sputtered LaO molecules must have undergone a reduction process prior to or during ionization. Atomic absorption data obtained on both La° and Ti° atoms seem to support the theory that the reduction process of LaO occurs in the atomic state, i.e., prior to ionization. Possible reactions leading to the dissociation of LaO molecules may include collisions with argon ions and with argon metastable atoms (without simultaneous ionization). In the reducing atmosphere created by getters, released oxygen particles have less

opportunity to recombine with La atoms than in a plasma without getters. In addition, a gettering plasma is relatively free of contaminant gas species that can quench argon metastable atoms. The result is an enhancement of argon metastable atoms available to ionize the free La atoms, yielding higher ion signals of the analyte.

Based on the foregoing assumptions, a matrix metal offering high sputter yield and strong bonding tendency toward oxygen is desirable for obtaining a large monatomic population of the analyte. The M-O bonding strengths [147] and sputter yield [16] values for the five matrices used in this study are listed in Table 3-1. The different gettering abilities exhibited by these metals appear to be a manifestation of factors listed in Table 3-1. For example, Ag (a non-getter) has a very high sputter yield, but its weak bond strength with oxygen hinders it from effectively removing oxygen from the system. Therefore, a Ag discharge remains more oxidizing in nature even after extensive sputtering. Carbon has a high bonding energy with oxygen, but due to its very small sputter yield, it does not rank high in our gettering function evaluation. The slow rise and yet relatively high plateau value of R in a carbon matrix (Figure 29) suggest that the optimization of La^+ signal in a carbon-containing discharge may be a kinetically slow process but still thermodynamically favored, which would be expected based on the strong C-O bond. The best getter reagents, Ti and Ta, have a combination of relatively strong M-O bonds and good sputter yields. Although the La-O bond is stronger than the Ti-O bond (8.30eV vs. 6.90eV), the higher concentration of Ti in the plasma may make Ti more competitive for oxygen. In addition, reaction

Table 3-1. Comparison of Oxide Bond Strength and Sputter Yield of Sample Matrices

Elements	M-O Bond Energy (eV)[a]	Sputter Yield (atoms/ion)[b]
Ti	6.92	0.42
Ta	8.36	0.45
W	6.73	0.50
C	11.18	0.10
Ag	2.33	2.70

Source: a) Ref [147].
b) Ref [16].

kinetics (speed) between Ti and O may be more favorable than that between La and O.

Analytical Applications

The significance of eliminating oxidant interferences in analyzing real world geological materials was investigated by determining REE concentrations in a sedimentary rock standard, SCo-1, obtained from the US Geological Survey (USGS). Emphasis was placed on comparing four situations: (1) using a non-getter matrix only, (2) using a non-getter matrix and cryogenic cooling, (3) using a getter matrix, and (4) incorporating cryo-cooling with the use of a getter matrix.

Experimental procedures

The sample, obtained in a powdered form, was mixed homogeneously in separate Ag and Ta matrices with a percentage of 5.8% and 5.4%, respectively. Before compress-forming the cathodes, the mixtures were kept dry in an vacuum oven at 115 °C overnight. Once the discharge was free from the initial arcing, the discharge voltage was set constant at 1250 volts; the current and ion signals of major species were monitored by the analog detector. Counting mode data acquisition was started as the gaseous signals dropped to minimal levels. When the cryo-cooling was applied, data acquisition was usually started at five minutes after the addition of liquid nitrogen into the coils. For both mixtures, two disks were prepared and at least two runs were conducted on each disk with 40 scans completed in each run. In all experiments, ^{140}Ce in the SCo-1 sample was used as an "internal standard" for calculating the remaining REE concentrations.

Ag matrix only

Indicated in the previous sections, gaseous contaminants in a Ag discharge are usually present at high concentrations, thus prohibiting the reduction of the rare earths. Figure 36 is a mass spectrum obtained for the low mass range of the Ag plasma using the Faraday detector. The fact that these gaseous contaminants are clearly shown in the mass spectrum on this scale indicates their high concentrations in the plasma. The corresponding mass spectrum for a higher mass range (from m/z = 135 to 180) is shown in Figure 37a+b, where peaks are identified mostly as the REE monoxides ions and polyatomic ions formed from Ag and several existing gas species. Since nearly 50% of the rare earth oxides were not converted to their atomic forms, little quantitation could be performed on these data.

Ag matrix with cryogenic cooling

Previous experiments have shown that the degree of gaseous contamination could be alleviated by applying liquid nitrogen into the steel coils surrounding the discharge. The reduction of LaO molecules to La atoms can thus be enhanced. Whether the cryo-cooling method used with our instrument could improve the quantitative analysis of the REE was examined in this study. With the use of liquid nitrogen, the gas impurity contents were reduced to a much smaller degree as shown in Figure 38. Consequently, in the REE mass range, the M^+/MO^+ ratios were enhanced by almost a factor of five (Figure 39). Polyatomic interferences formed between gaseous molecules and the matrix Ag atoms were still present, with those containing oxygen and hydrogen at lower levels. The

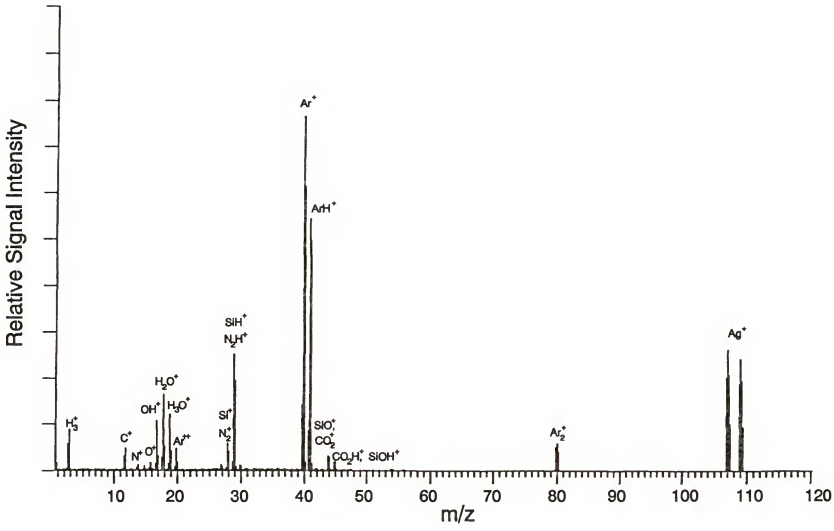

Figure 36 Mass spectrum of gaseous impurities for a SCO-1/Ag sample.

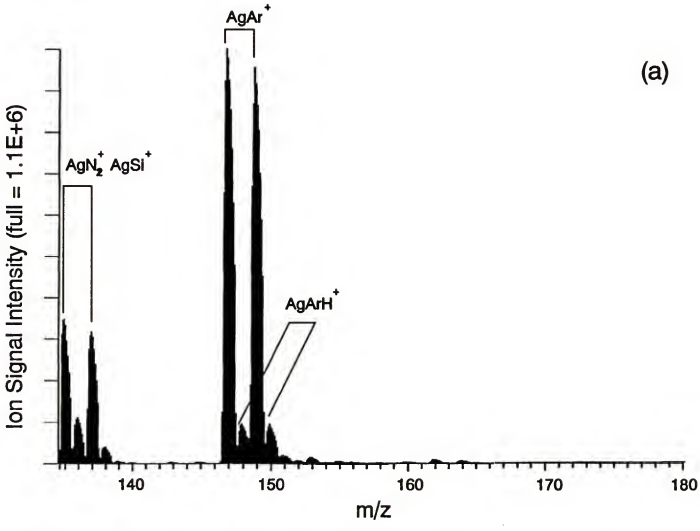

Figure 38 Mass spectra ranging from m/z=1 to 120 for an SCO-1/Ag sample with cryogenic cooling.

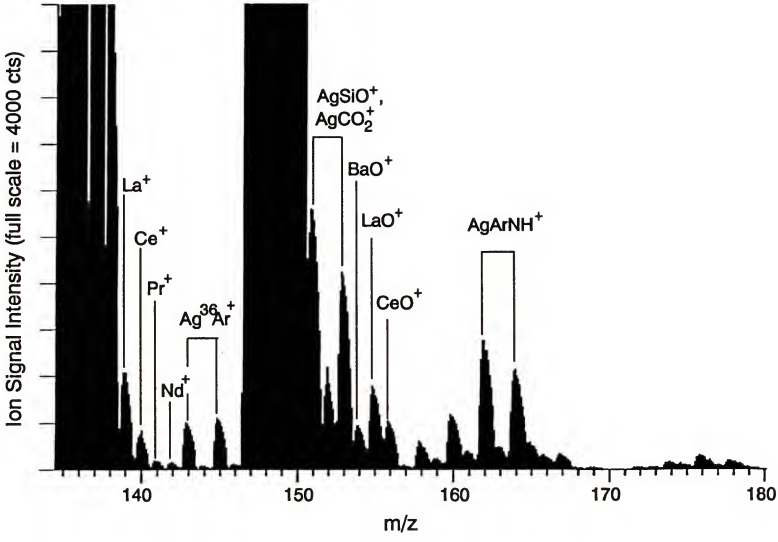

Figure 37--continued.

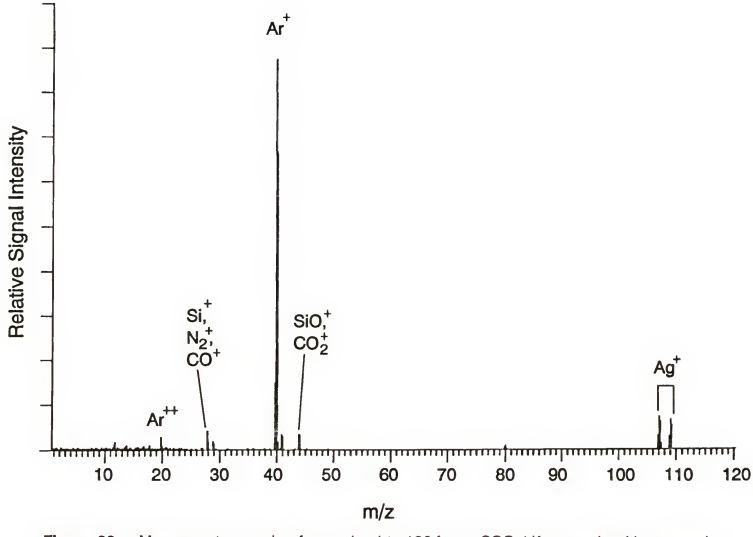

Figure 38 Mass spectra ranging from m/z=1 to 120 for an SCO-1/Ag sample with cryogenic cooling.

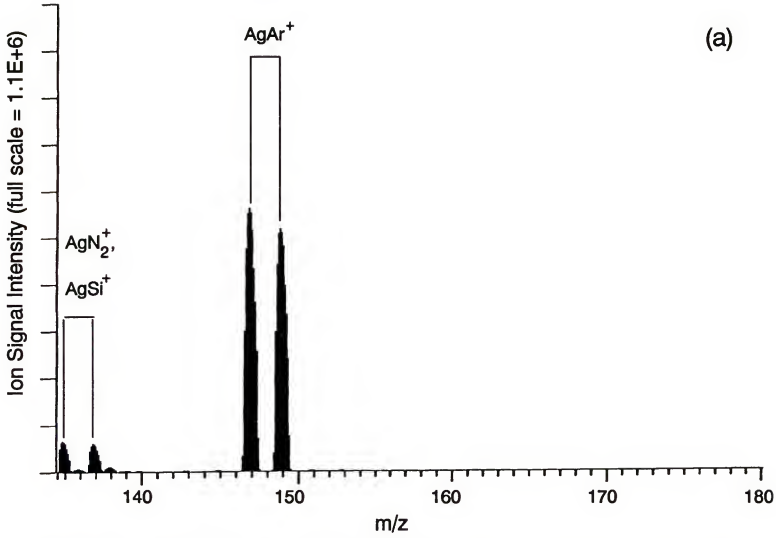

Figure 39 Mass spectra ranging from m/z=135 to 180 for an SCO-1/Ag sample with cryogenic cooling. (a) full intensity scale is 1.1E+6 counts; (b) full scale is 4000 counts.

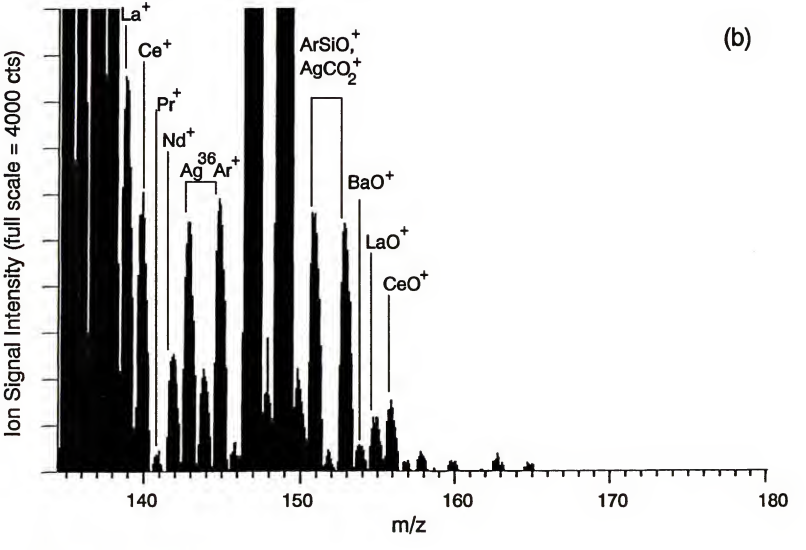

Figure 39--continued.

molecular interferences on many nominal m/z ratios makes it difficult to find an un-interfered isotope for some REE (e.g., both isotopes of Eu are superimposed by $AgCO_2$ and the monoisotopic Ho is overwhelmed by AgArO). For the quantifiable REE, their concentrations were calculated using Equation (1-8) with ^{140}Ce as the "internal reference" peak. The RSF values used in these calculations were obtained by Tong and Harrison [148]. The final results are tabulated in Table 3-2, in comparison with the reported concentration values obtained by several other techniques. Overall, the GDMS results are much higher than the reported values except for Pr. Listed in Table 3-3 are various types of molecular interferences superimposed on many of the REE isotopes. These molecular interferences, apparently still present at high levels compared with the trace elemental concentrations, are considered responsible for the overall positive error. These results suggested that although the cryo-cooling method was successful in removing water-contained oxygen out of the plasma reaction system, the elimination of carbon and nitrogen species or oxygen existing in forms other than water was limited. Therefore, even the minimum degree of gaseous contamination achievable by our cryo-cooling device still presented problems for the quantitation of REE at the parts-per-million (ppm) level (ppb in the gas phase).

Ta matrix

As an oxygen scavenger, Ta was used as the host matrix for the SCo-1 standard. Water and other gaseous impurities were eliminated after extensive sputtering (Figure 40). The corresponding mass spectrum of the REE isotopes is shown in Figure 41a, where the La^+/LaO^+ ratio has reached 5.5. Figure 41b

Table 3-2. Analysis of REE in USGS Standard Rock Sample with GDMS Using Cryogenic Cooling

Element	GDMS Conc. (ppm)	XRF Conc. (ppm)[a]	SSMS Conc. (ppm)[b]	ICPAES Conc. (ppm)[c]
La	-	30.31	29.7	29.7
Gd	internal standard	58.70	63.4	58.5
Pr	4.6 ± 0.5	7.29	7.62	6.8
Nd	36.6 ± 4.9	29.94	27.9	27.5
Sm	13.8 ± 1.9	5.60	5.07	6.08
Eu	-[d]	1.09	1.03	1.12
Tb	2.2 ± 0.7	-	0.64	0.63
Gd	21.4 ± 4.1	4.9	4.00	4.99
Dy	5.7 ± 1.0	4.23	3.79	4.35
Ho	-[e]	-	0.83	0.88
Er	-	2.5	2.39	2.68
Tm	-	-	0.32	<0.4
Lu	-	0.37	0.34	0.41
Yb	-	2.41	2.25	2.86

Source: a) Ref. [98].
b) Ref. [102].
c) Ref. [104].

Note: d) Both isotopes are interfered by $AgCO_2$ or AgSiO.
e) Isotope is interfered by AgArO.

Table 3-3. Molecular Interferences on Elemental REE

Element	Molecular Interference
139-La	107Ag-O_2
143-Nd	107Ag-36Ar
145-Nd	109Ag-36Ar
147-Sm	107Ag-40Ar
145-Sm	109Ag-40Ar
151-Eu	107Ag-SiO, or 107Ag-CO_2
153-Eu	107Ag-SiO, or 107Ag-CO_2
155-Gd	139La-O
156-Gd	140Ce-O
157-Gd	141Pr-O
158-Gd	142Nd-O
160-Gd	144Nd-O
159-Tb	143Nd-O
161-Dy	145Nd-O
162-Dy	146Nd-O
163-Dy	147Sm-O
164-Dy	148Sm-O
165-Ho	149Sm-O
166-Er	150Nd-O, 150Sm-O
167-Er	151Eu-O
168-Er	152Sm-O
170-Er	154Sm-O
169-Tm	153Eu-O
171-Yb	155Gd-O
172-Yb	156Gd-O
173-Yb	157Gd-O
174-Yb	158Gd-O
176-Yb	160Gd-O

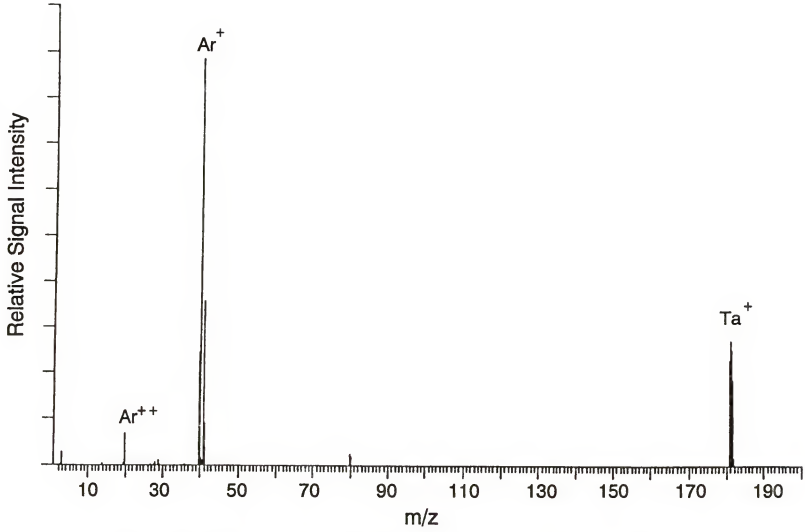

Figure 40 Mass spectrum ranging from m/z=1 to 200 for an SCO-1/Ta sample.

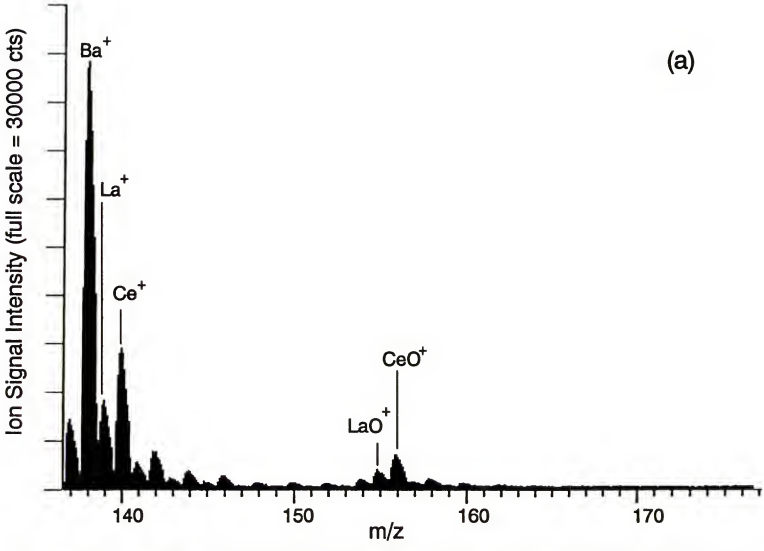

Figure 41 Mass spectra for an SCO-1/Ta sample. (a) mass range is m/z=137 to 177, intensity scale is 30000 counts; (b) mass range is m/z=140 to 177, scale is 2500 counts.

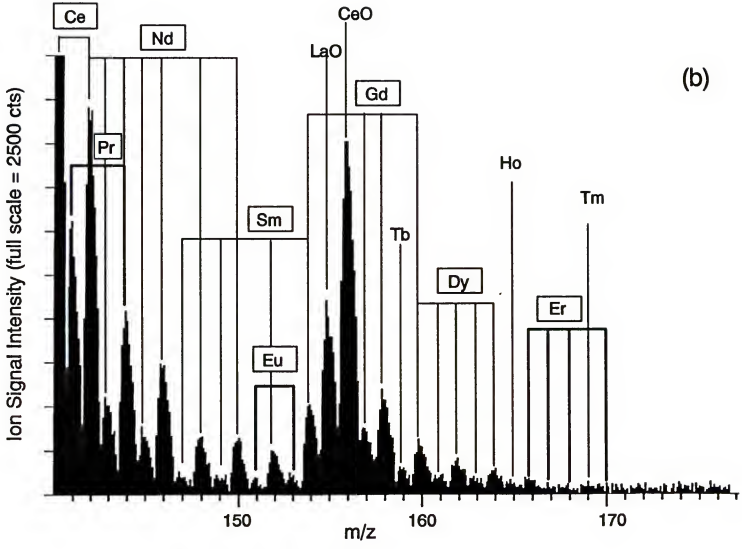

Figure 41--continued.

illustrates the same mass spectrum on an expanded scale for closer identifications of the trace elements. The concentrations of the detectable REE were calculated and tabulated in comparison to the reported values in Table 3-4. The results were improved from those obtained with the Ag matrix. For elements whose reported concentrations were higher than one ppm, the relative error was within 10 %; 50 % for those below one ppm. Gadolinium has the highest percent error (170 %) relative to the reported value. This is probably because all four prominent isotopes of Gd are overlapped by other REE monoxides of much higher concentrations (^{139}LaO, ^{140}CeO, ^{142}NdO, and ^{144}NdO).

Ta matrix with cryogenic cooling

Finally, liquid nitrogen was also applied when using Ta as the sample matrix in hopes that it may reduce the time required to "clean out" the water contamination. Results have shown that although the water signal could be quickly reduced by adding liquid nitrogen in the coils, the cathode still needed to be sputtered for an extended period of time for the analyte signals to stabilize. This is probably because the many nonmetal components in the SCo-1 sample (e.g., Si, C, O, and N) could not be eliminated from the plasma just by lowering the temperature to liquid nitrogen level. Chemical reactions with getter atoms over a certain period of time were still needed to achieve a plasma "clean" enough for quantitative trace analysis. The analytical results obtained in these experiments were comparable to those obtained by the Ta matrix alone.

Overall, the quantitation of REE in geological materials using GDMS can be improved as the gaseous impurities content in the discharge is minimized, by

Table 3-4. Analysis of REE in USGS Standard Rock Sample with GDMS Using Ta as Sample Matrix

Element	GDMS Conc. (ppm)	XRF Conc. (ppm)[a]	SSMS Conc. (ppm)[b]	ICPAES Conc. (ppm)[c]
La	27.6 ± 2.9	30.31	29.7	29.7
Ce	internal standard	58.70	63.4	58.5
Pr	8.3 ± 2.5	7.29	7.62	6.8
Nd	25.1 ± 0.8	29.94	27.9	27.5
Sm	4.9 ± 0.5	5.60	5.07	6.08
Eu	1.4 ± 0.4	1.09	1.03	1.12
Tb	1.0 ± 0.2	-	0.64	0.63
Ce	10.9 ± 0.6	4.9	4.00	4.99
Dy	3.7 ± 0.8	4.23	3.79	4.35
Ho	0.6 ± 0.1	-	0.83	0.84
Er	2.3 ± 0.9	2.5	2.39	2.68
Tm	-	-	0.32	<0.4
Lu	-	0.37	0.34	0.41
Yb	-	2.41	2.25	2.86

Source:
a) Ref. [98].
b) Ref. [102].
c) Ref. [104].

ways of either physical or chemical elimination. With our setup, the getter reagent method appears to offer a more thorough elimination of all major impurities containing O, N, and C than does the cryo-cooling method, and therefore provide better analytical results. Better results can be expected with the cryogenic method if the cooled cell surface could be increased substantially.

Conclusions

In this section, two methods have been examined for the elimination of gaseous contaminants (e.g., water) in the glow discharge of compacted samples, especially those containing the rare earths, e.g., La_2O_3. The cryogenic approach can rapidly condense water molecules out of the glow discharge reaction system, thus hindering the formation of unwanted LaO molecules in the La-LaO equilibria. The same goal can also be achieved by introducing a steady stream of getter reagents into the plasma to remove the oxygen containing species through chemical reactions. Because getter reagents are reactive toward oxygen in any form (not just in water) as well as other gaseous species, they appear to provide a more thorough purification of the discharge. While both methods are successful in achieving a high $La^+/(La^+ + LaO^+)$ ratio when using the oxide in high purity, better results have been obtained when using the getter method to analyze a standard rock sample because all major impurities can be eliminated. It is worth mentioning that due to the lack of instrumental flexibility, the cryogenic coils used in our system have a limited surface area that is quickly saturated by condensed water, making it difficult to maintain a sufficiently low temperature for a long

period of time. The results should have been more acceptable if a better cryogenic device had been used.

Although the degree of efficiency varies, the two methods appear to share the same role in affecting the La-LaO equilibria, i.e., creating a "reducing" atmosphere by eliminating the oxygen carriers. While the liquid nitrogen approach has a straight forward physical condensation mechanism, the chemical interactions between getter reagents and the La-LaO equilibria need further elucidation, which comprises the main theme of the remainder of this dissertation.

Addition of Reactive Gases

Introduction

Studies discussed in the previous section have shown that by using getter reagents as the conducting sample matrix, over 90 % of the sputtered species from the La_2O_3 analyte can eventually be converted to La atoms. It was proposed that this successful reduction of LaO to La was a result of sputtered getter particles removing oxygen from the plasma through chemical reactions. Relating this theory to Equation 2-3, it is equivalent to shifting the La-LaO equilibrium to the formation of La.

To further our understanding of the chemical processes in an oxide plasma, a different approach was taken to affect this proposed equilibria. The idea was to create an argon plasma that has already been equilibrated to obtain a maximized La population, then disturb the system by introducing into the "steady-state" plasma gases or vapors having different redox properties; the La-LaO

equilibrium would be expected to re-equilibrate accordingly; a process that may provide information about the plasma chemistry of the oxide. The experiments were expected to be most informative when a spectrum of gases with distinctly different chemical natures were used as added "reagents" because each may induce a different effect on the La-LaO equilibria. The selected gases included the noble gas neon, the "reducing" hydrogen, and the oxidizing water vapor.

Experimental Procedures

The analyte La_2O_3 was mixed, 10% by weight, separately with three matrices: Ta, Ti, Ag. The mixtures were then pressed to form disk cathodes. A pure Ar discharge was run initially to clean the sample surface and to maximize the La^+/LaO^+ ratio before adding any one of the following auxiliary gases: Ne (99.999%, Spectra Gases Inc.), H_2 (99.95%, Liquid Air Co.), distilled $H_2{}^{16}O$ and $H_2{}^{18}O$ (97 atom% ^{18}O, Sigma Chemical Company). The total discharge pressure was kept at 0.95 torr; the partial pressure of the added gases was set in the range of zero to 0.95 torr for Ne and H_2, and zero to 0.2 torr for the water vapors with remaining partial pressure made up by Ar gas. The discharge was re-equilibrated in pure Ar to its best reproducible stage (in terms of obtaining the same La^+/LaO^+ ratio) before each auxiliary gas addition at a new pressure setting. Signal intensities for both La^+ and LaO^+ ions were monitored prior to and after the addition of the auxiliary gases. In the case of Ne addition, atomic absorption and weight loss studies were also carried out to monitor changes in the sputter yield of the matrix metal. The discharge was typically run at a constant 1000 V. The discharge current varied as the mixing ratio of the discharge gases was changed.

Effect of Getter Concentration on La-LaO Equilibria

Addition of neon

The purpose of using Ne was to cause a concentration change of the sputtered materials in the plasma without varying the discharge voltage. Because of its inert nature, Ne added to an Ar discharge should not directly participate in the redox reactions of the oxide analyte. However, according to the theory discussed in Chapter 1, replacing part of the Ar with a lighter Ne as the sputtering gas will decrease the sputter yield of the sample cathode [149,150]. If the cathode metal reacts with oxygen containing species in the plasma (as proposed to be the case for getter reagents), then a decrease in sputter yield may cause inefficient removal of oxygen from the discharge. This is equivalent to increasing indirectly the oxygen concentration in Equation 2-3, and the La-LaO equilibria will shift accordingly. The main variable introduced here that may influence the La-LaO equilibria is the gas phase concentration of the sputtered matrix metal. If the metal is not involved in the La-LaO equilibria, then reducing its concentration should not affect the equilibria significantly. If the matrix metal does participate in the La-LaO equilibration such as proposed for getter matrices, then the La-LaO equilibria should be affected by its concentration change. By comparing results obtained using both getter and non-getter matrices, we hope to further our understanding of the getter reagents' role in the plasma equilibria.

Neon has been shown to have smaller sputter yields than Ar in the glow discharge due to its lighter atomic weight (Figure 4b-c). Most studies done in terms of comparing sputter yields between Ar and Ne have been individual sputter

yield measurements made separately for both gases. Sputter yields for mixed gases, however, were unavailable in the literature at the time of this work. When mixing the Ar and Ne at different ratios, the discharge current could not be held constant if the discharge voltage is maintained constant. This is because Ne and Ar gases have difference ionization efficiencies, and do not yield the same current values under the same voltage. This means that sputter efficiencies of the two gases mixed by different ratios can not be compared under the same current. Since our goal was not to compare absolute sputter efficiencies of the two gases, but to create a change in the sputtered species concentrations, and then relate such a change to the oxide equilibria, a constant discharge current was not necessary. To monitor the sputter yield change in these experiments, both weight loss and atomic absorption measurements were carried out.

Measuring weight loss after sputtering the sample at a constant current for a given period of time is the traditional way of evaluating sputter yield [6]. It provides information on how much cathode material has been sputtered into the discharge chamber over a time integral. Metals that are highly reactive toward oxygen (e.g., getter reagents) are not suitable for weight loss studies. This is because severe oxidation reactions will occur once the sample is removed from the vacuum chamber into the air, causing errors in the weighings. In this study, weight loss measurements were carried out on a Ag sample instead of the highly reactive Ti; the goal was to examine whether less sample material was sputtered when Ar was replaced by Ne. Figure 42 shows the Ag weight loss normalized to the weight loss obtained from pure Ar sputtering in a series of Ne/Ar mixtures

versus the partial pressure of Ne. There was an apparent decreasing trend in the sample weight loss with the addition of Ne. The sputter weight loss decreased about 60 % for Ag going from pure Ar to pure Ne.

Because sputter weight loss is affected by both the sputtering efficiency and the re-deposition rate of the sputtered material, a reduced weight loss is not necessarily caused by less sputtering per ion bombardment, but also possibly by more re-deposition, especially when the constituents in the gas phase have changed. In other words, the weight loss method only measures the sputter yield over a time integral, but does not provide information on the sputtering efficiency at any particular time incidence. Therefore, the weight loss data in Figure 42 alone was not sufficient to conclude that there were an actual decrease of the sputtered species population in the gas phase. Direct measurement of the sputtered neutral population in the gas phase was necessary, and was carried out by atomic absorption methods. The absorbance of the Ti° was measured for five Ne/Ar mixing ratios, and normalized to the absorbance of Ti° obtained in the pure Ar discharge. The normalized absorbance is plotted against the corresponding Ne partial pressure in Figure 43. The decreasing trend of the Ti° absorbance is in agreement with the sputter weight loss data shown in Figure 42. Results from both experiments suggest that the concentration of the sputtered species in the plasma was reduced when Ar was replaced by Ne. Whether this effect will cause the La-LaO equilibria to shift will be examined in the following experiments.

Possible effects on the oxide signals adding Ne to Ar can be categorized in two ways: (1) "direct effects" including preferential sputtering and/or biased

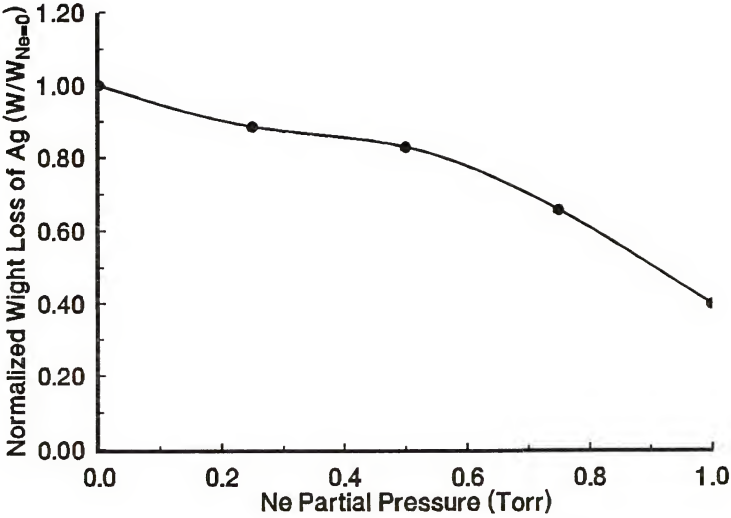

Figure 42 Effect of Ne on the sputtered weight loss of Ag.

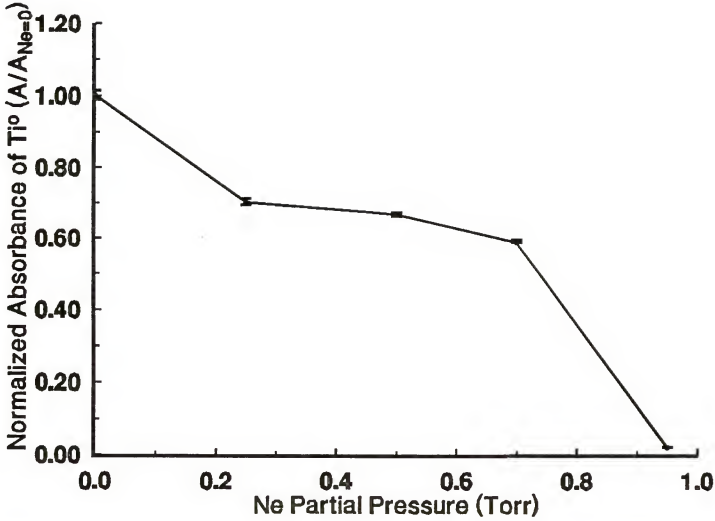

Figure 43 Effect of Ne partial pressure on the absorbance of Ti°.

ionization between La and LaO, and (2) "indirect effects" manifested in changes of the two ion signals as a result of chemically shifting the La-LaO equilibrium. "Indirect effects" can be initiated by the concentration change of the oxygen available in the plasma, and hence by species that react with oxygen such as getters whose sputter yield is influenced by Ne. The "direct effects" should be matrix-independent. The degree of Ne's "direct effects" on the La-LaO equilibria needed to be determined first before any "indirect effects" could be probed. To examine the "direct effects" only, possible causes for "indirect effects" must be ruled out by using a less oxygen-reactive matrix (e.g., Ag).

Neon addition experiments were first conducted on a Ag matrix with 10 % La_2O_3 mixed within. Following the optimization of the La^+/LaO^+ ratio in Ar, Ne gas was bled into the system to replace an equivalent (by pressure) amount of Ar. For each Ne/Ar mixing ratio, the signal ratio La^+/LaO^+ was measured and normalized to the value obtained in pure Ar. Data are plotted as the normalized La^+/LaO^+ ratio versus the corresponding Ne partial pressure (Figure 44). The La^+/LaO^+ ratio shows a small decrease before 75 % of the Ar gas was replaced by Ne, and a larger drop when in pure Ne. The same experiments were conducted with a Ti matrix (Figure 44), which yielded a more pronounced reduction in the La^+/LaO^+ ratio over the same range of pressure change.

The fact that the La^+/LaO^+ ratio remained fairly stable with the Ag matrix suggested that: (1) the sputtered ratio of neutral La/LaO may not have been affected by replacing Ar with Ne until at least 75% of Ar was replaced and, (2) preferential ionization possibly caused by the more energetic Ne metastable

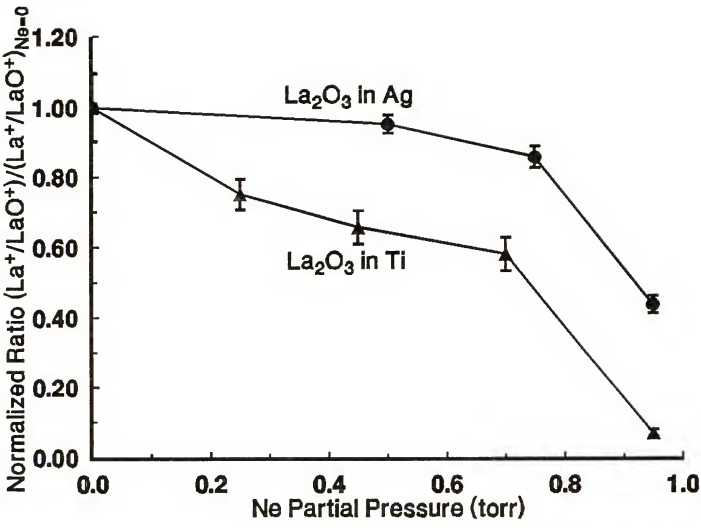

Figure 44 Comparison of effect of Ne on the La^+/LaO^+ ratio between Ag and Ti matrices.

atoms (over Ar metastables) was negligible. Overall, the Ne addition did not seem to have a significant "direct effect" on the oxide signals until the Ar concentration was reduced to only 25 %. "Indirect effects", as demonstrated by the more widely changing La^+/LaO^+ ratio with the Ti matrix, were more pronounced. Furthermore, by comparing Figure 44 with Figure 43, it is apparent that the decreasing rate of the La^+/LaO^+ ratio was in close agreement with that of the Ti° absorbance. This suggests that reducing the supply of Ti into the gas phase was essentially responsible for shifting the La-LaO equilibria towards the formation of LaO.

Addition of hydrogen

The second reagent added, hydrogen, is similar to Ne in that it may significantly reduce the sputter yield from Ar due to the large amount of light mass H^+ and H_3^+ ions carrying the discharge current [151]. Dissimilar to Ne, hydrogen has a more active chemical nature. Considered a reducing agent, hydrogen gas has been used in ICP sources to help eliminate molecular interferences by dissociating strongly bound oxides [152]. Whether such reducing reactions are favorable in the glow discharge, where the thermal energy is much lower than in an ICP source, is of interest. Another dissimilarity between H_2 and Ne is that preferential sputtering of oxygen due to hydrogen bombardment is possible [p116 in 36], which may disturb the La-LaO equilibria through the concentration change of oxygen.

Hydrogen addition experiments were carried out on the La_2O_3/Ti sample, and the normalized La^+/LaO^+ ratio was plotted against the partial pressure of H_2

in Figure 45, in which the La^+/LaO^+ ratio decreased as Ar was partially replaced by H_2. There did not seem to be any reducing reaction occurring between hydrogen and LaO to enhance the La^+ signal (as in ICP). This is probably because the glow discharge has a much lower temperature than the ICP, and therefore a much lower thermodynamic energy, which hinders this redox reaction from happening. The decreasing trend of the La^+/LaO^+ ratio as H_2 was added into Ar may be explained in the same fashion as with the Ne addition. That is, a less reducing environment was created due to reduced concentration of the getter reagents sputtered into the discharge. Moreover, the decrease in the La^+/LaO^+ with the H_2 addition was to a higher degree than with Ne for each mixing ratio tested (Figure 45). This may be attributed to the even smaller sputter efficiency of H^+ than Ne^+, resulting in a larger decrease in the Ti concentration in the gas phase.

Effect of Water Concentration on La-LaO Equilibria

Water, when used as a plasma reagent, has the ability to provide oxygen directly to the left side of Equation 2-3, and is expected to shift the La-LaO equilibrium toward the formation of LaO. Should such a shift occur, mechanisms that may be attributed to the shift include: (1) less dissociation of the sputtered LaO molecules in an oxidizing environment and, (2) formation of LaO through free La reacting with added water either on the sample surface or in the gas phase or both. In order to confirm and differentiate between these two possibilities, isotopically labeled water ($H_2{}^{18}O$) was used as an added gas. Oxidation reactions between free La and added $H_2{}^{18}O$ (including both on the sample surface and in

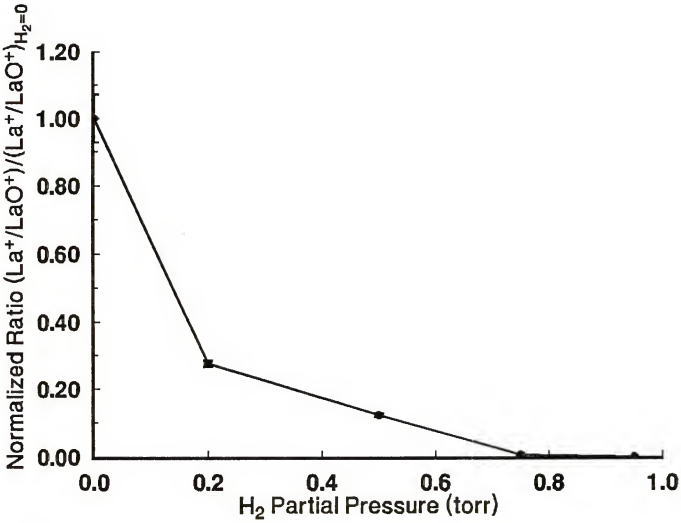

Figure 45 Effect of H_2 partial pressure on the La^+/LaO^+ ratio for a La_2O_3/Ag sample.

the gas phase) could be confirmed if the new species $La^{18}O$, which did not exist in the sample, could be detected by the mass spectrometer. In addition, a better understanding of getter reagents' role in the glow discharge chemistry may also be gained through these experiments. As shown earlier, getter reagents can create discharges much more reducing in nature than do non-getter reagents. Therefore, when water is added into such different plasmas, the induced effects on the plasma species, including La^+ and LaO^+, are expected to be different.

Addition of water-$H_2{}^{16}O$

These experiments were designed to disturb the La-LaO equilibria by providing additional oxygen through water. Principal reactions involving water molecules in the Ar glow discharge have been studied by Lindinger [153] and are demonstrated by the following equations,

$$Ar^+ + H_2O = ArH^+ + OH \quad (3\text{-}1)$$

$$ArH^+ + H_2O = H_3O^+ + Ar \quad (3\text{-}2)$$

$$H_2O^+ + H_2O = H_3O^+ + OH \quad (3\text{-}3)$$

$$Ar^+ + H_2O = H_2O^+ + Ar \quad (3\text{-}4)$$

$$H_3O^+ + e = H_2O + H \quad (3\text{-}5)$$

The oxygen containing fragments from water dissociation may be capable of oxidizing La atoms to form LaO molecules in the discharge. Since the interest here was to promote LaO production rather than dissociating it, the signal ratio of LaO^+/La^+ (rather than La^+/LaO^+) was used for data presentation in this section. Because water was reported to quench the Ar metastable ionization of sputtered species [154], an overall decrease in all ion signals of the sputtered species was

therefore expected. The additional oxygen provided into the discharge from the added water may react with La atoms to form LaO molecules, a process that may occur either on the sample surface or in the gas phase. The LaO production may compensate for some of the loss in the LaO^+ signal caused by reduced Penning ionization. The decrease in the absolute LaO^+ signal was not as large as the La^+ signal, resulting in an increased LaO^+/La^+ ratio with added H_2O partial pressure (Figure 46). With the LaO^+/La^+ ratio obtained from both Ta and Ag discharges, there appeared to be a threshold in the H_2O partial pressure between 0.07 and 0.15 torr where the LaO^+/La^+ ratio increased drastically. The change in the LaO^+/La^+ ratio was so abrupt that the appearance of the plots almost resemble that of a titration curve. This "titration" like phenomenon was more pronounced with the Ta matrix than with Ag.

Although the cause of such curve shapes is not completely clear to us, some hypotheses have been made in an attempt to explain this phenomenon. Because the steepness of the LaO^+/La^+ ratio vs. water concentration curve seemed dependent on the matrix metal, it was reasonable to deduce that the sputter production of the matrix material played an important role in affecting the LaO^+/La^+ ratio. In other words, how the LaO^+/La^+ ratio changed was possibly influenced by how the matrix metal was affected by the added water vapor.

One explanation can be related to the "reactive sputtering" theory introduced in Chapter 1, since the sputtering situation encountered in these experiments resembled what was defined as a "reactive sputtering" environment. It was demonstrated by Brudy and Seidel (Figure 6) that certain metal's sputter

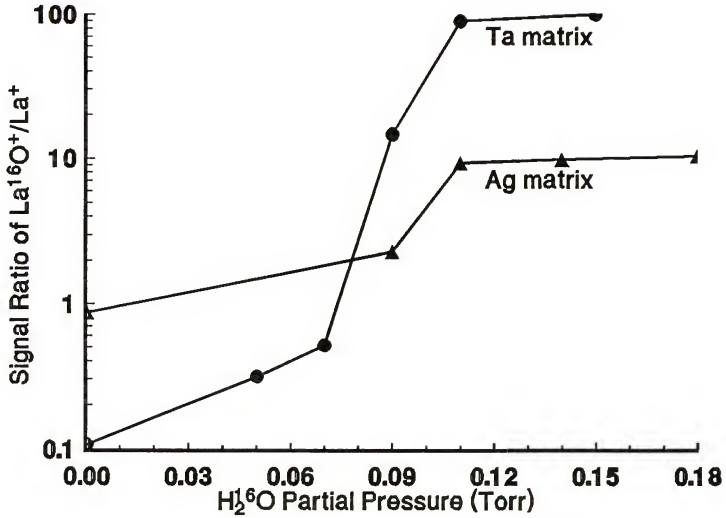

Figure 46 Comparison of water vapor' effect on the $La^{16}O^+/La^+$ ratio between Ta and Ag matrices.

yield can be rapidly reduced by severely oxidizing the metal surface in the presence of reactive gases, also showing a "titration" shaped curve. Similar observations have been made by Ratliff and Harrison in this laboratory when studying water vapor's effect on GDMS signals [155]. This means that in our experiments, once the water concentration exceeded its value at the "equivalence" point of the redox equilibria in the plasma, the cathode surface was quickly covered with excess oxygen, oxidizing the cathode metal as well as reducing its sputter yield. As a result, the reducing environment created by sputtering Ta could no longer be maintained, and the La-LaO system was quickly dominated by the formation of LaO molecules.

It cannot be excluded that similar redox equilibria may also exist in the gas phase. The oxidation of the sputtered Ta atoms in the gas phase may be the main cause for the loss of the reducing plasma, even if the cathode surface was still metallic in nature at this point. With the reactive gas being introduced into the plasma at a constant pressure, it is difficult to distinguish between reactions happening on the cathode surface or in the gas phase. Chemical interactions that occur primarily in the gas phase will be further addressed in Chapter 4. A foundation for these studies is provided by the following experiment.

Addition of water-$H_2{}^{18}O$

The oxygen atom released from regular water ($H_2{}^{16}O$) has the same dominant isotope ^{16}O as the oxygen atoms originating in the La_2O_3 sample. Therefore, the origin of the increased LaO^+ signal upon adding $H_2{}^{16}O$ could not be resolved from the following possible sources: (1) product of recombination

reactions between La and added water or, (2) less dissociation of originally sputtered LaO molecules. To distinguish between these two processes and to provide further evidence of gas phase reactions between sputtered La and added water, ^{18}O-labeled water ($H_2{}^{18}O$) was used as a plasma "reagent" to replace regular water. Upon the addition of $H_2{}^{18}O$, a new species at m/z 157, $La^{18}O^+$, was observed in the spectrum shown in Figure 47b. Not originating from the oxide sample, the new species was considered a reaction product between La and added $H_2{}^{18}O$.

Introducing $H_2{}^{18}O$ into the discharge created a new species, causing the analyte atom La to re-distribute among its three forms: La, $La^{16}O$, and $La^{18}O$. When the concentration of $H_2{}^{18}O$ was changed, the equilibria among the three species were expected to shift accordingly, so that concentrations of La^+, $La^{16}O^+$, and $La^{18}O^+$ would also change. Figure 48 demonstrates the signal profiles of the three lanthanum species as the amount of $H_2{}^{18}O$ was increased. Starting from zero $H^{18}O$ concentration, $La^{18}O$ eventually became the dominant species as more $H_2{}^{18}O$ was bled in the discharge. No data point was shown for the $La^{18}O^+$ signal at zero $H_2{}^{18}O$ concentration because the signal was below detection limit. This suggests that a competitive reaction mechanism was responsible for the re-distribution of La in its two oxide forms. Similar to regular water addition, the "titration" phenomenon was also observed in the plot of $La^{16}O^+/La^+$ versus $H_2{}^{18}O$ partial pressure in Figure 49. The highly reducing discharge created by Ta acted as an "oxygen buffer" until its reducing capacity was saturated by added water, and then the drastic increase in the $La^{18}O^+/La^+$ ratio occurred. Whether the $La^{18}O$

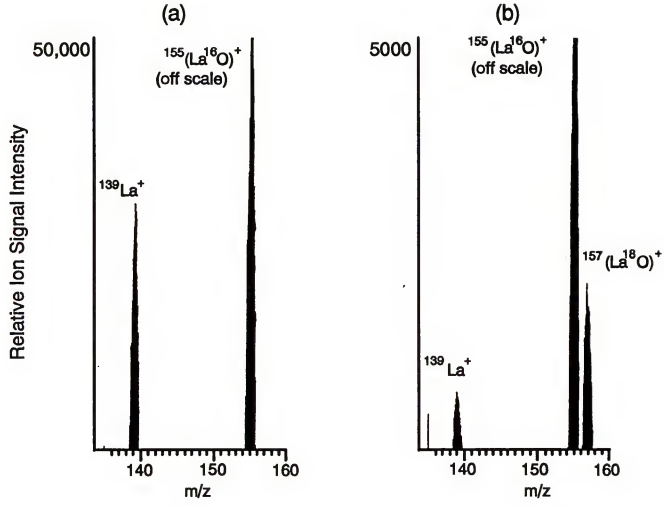

Figure 47 Production of $La^{18}O$ in the glow discharge by adding $H_2{}^{18}O$ vapor. (a) mass spectrum obtained before $H_2{}^{16}O$ addition; (b) mass spectrum obtained after $H_2{}^{16}O$ addition.

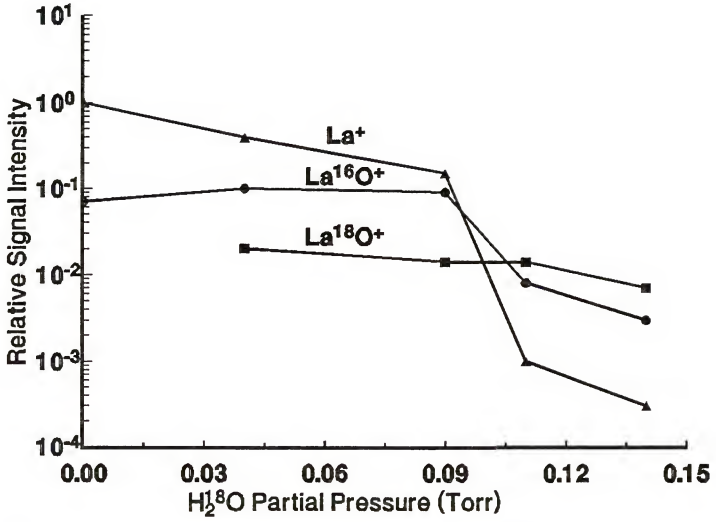

Figure 48 Ion signals of La^{+}, $La^{16}O^{+}$, and $La^{18}O^{+}$ as functions of the $H_2{}^{18}O$ partial pressure.

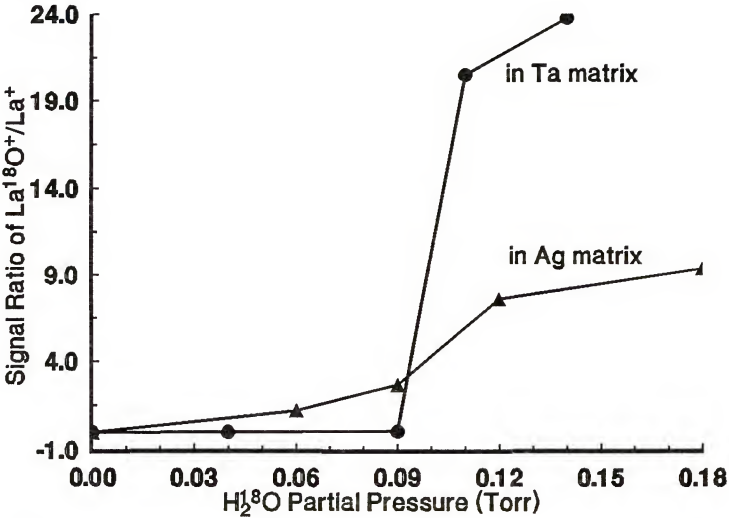

Figure 49 $La^{18}O^+/La^+$ as a function of the $H_2{}^{18}O$ partial pressure with both La_2O_3/Ag and La_2O_3/Ta samples.

molecules were formed primarily by oxidation of the cathode surface or in the gas phase is still debatable, but results from these studies do indicate that the oxidation reaction between La and water does occur in the glow discharge as long as there are sufficient reactants.

Conclusions

The reversibility of the La-LaO redox equilibrium in the glow discharge has been studied by chemically manipulating the plasma chemistry through various gas additions. A discharge that is "reducing" in nature enhances the atomic population of the rare earth oxide analyte. The "reducing" effect of getter reagents in the glow discharge can be weakened when using less sputter-efficient discharge gases. This will result in a decrease in the atomic population of the oxide analyte relative to its monoxide population. The use of isotopically labeled water as a plasma reagent has shown that oxidation reactions between La atoms and oxygen atoms not originated in the sample itself are possible in the glow discharge.

In this study, the gas mixing and introduction processes were carried out in the steady-state mode. This determined that the added gas not only would act as reagents for gas phase reactions, but also would take part in the sputtering process of the discharge. The inability to separate these two steps prevented us from resolving data that might carry information from both sources. For instance, results in this study seemed to indicate that using hydrogen did not help dissociate the oxide, but it was difficult to conclude whether this was due to possible changes in the sputtering mechanism of the oxide caused by H^+, or the

less competitiveness of H_2 to react with oxygen than La. Another example would be the difficulty in resolving oxidation reactions of La on the sample surface from those in the gas phase when using water as the added gas.

In order to focus the study primarily on the gas phase reaction aspect, a pulsed injector was used in the following studies to introduce "plasma reagents" in a transient mode, allowing the La-LaO redox equilibrium to be investigated in a more discriminating and time-resolved fashion.

CHAPTER 4
RARE EARTH OXIDE EQUILIBRIA IN PULSED DIRECT CURRENT GLOW DISCHARGE MASS SPECTROMETRY

Background

Pulsed DC Glow Discharge

A pulsed DC glow discharge is induced by periodically extinguishing the DC voltage applied to the discharge cathode. Pulsed discharges have been used in optical spectroscopy for several applications [156,157]. The investigation of pulsed glow discharge in mass spectrometry was initiated by an important phenomenon observed in emission spectroscopy, i.e., a significant population of neutral species is present in the afterglow that can be used for analytical purposes [158,159]. Klingler *et al.* have shown that pulsed GDMS offers many advantages including reduced cathode heating, increased discharge voltage, and enhanced sample sputter yield and ion signal intensities [160]. They also reported the observation of a series of analytically useful anomalies in the pulsed ion signals (Figure 50). Instead of the anticipated square-wave pattern as demonstrated by the applied voltage, reproducible peaks were observed at the beginning or end of the pulse, depending on the species being detected. The sudden increase in the sputtered species signal after termination of the pulse to form an "afterpeak" was found to be typical for sample components, metal dimers,

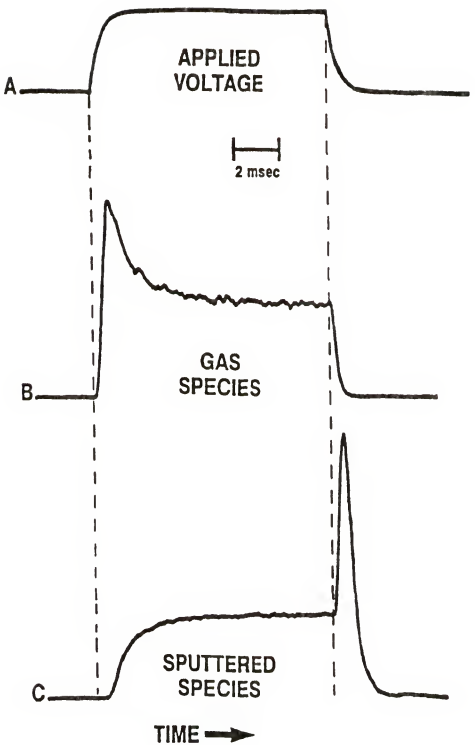

Figure 50 Ion signal profiles in the pulsed discharge. (a) applied voltage; (b) gaseous species; (c) sputtered species [90].

and metal argides [159]. The analytical usefulness and the fundamental theory of these signal anomalies were investigated in depth by Klingler et al. [161].

Pulsed Glow Discharge of Rare Earth Oxides

Pulsed glow discharges were first applied to oxide samples in hopes that signals of the elemental ion and the monoxide ion (e.g., La^+ and LaO^+) might show distinguishably different time profiles, that is, one might demonstrate an afterpeak whereas the other one might not. If such an observation were made, not only could a discriminative La^+/LaO^+ ratio be obtained at different regions of the pulse period, but information about the ionization mechanisms of the two species could also be gained.

Instrumentation

The basic mass spectrometer system has been described in Chapter 1. The coupling of the pulsing device to the discharge power supply and the corresponding data acquisition system are shown in Figure 51. A custom designed pulse generator and delay circuit were housed in one box, constructed by Schmidt at Finnigan MAT, Bremen, Germany. The square-wave function sent out by the pulse generator, with controllable amplitude, frequency, and duty cycle, was used to drive a Kepco OPS3500 operational power supply. The period of the square-wave can be varied between 0.2 ms and 1 second with the "on" duration controllable between 0.2 to 18 ms. Ion signals from the mass spectrometer could be collected in two modes: (1) as a single ion intensity versus time profile by synchronizing the MCA with the pulse trigger signal (shown as the solid line wiring in Figure 51), and (2) as a full mass spectrum of a specified mass range

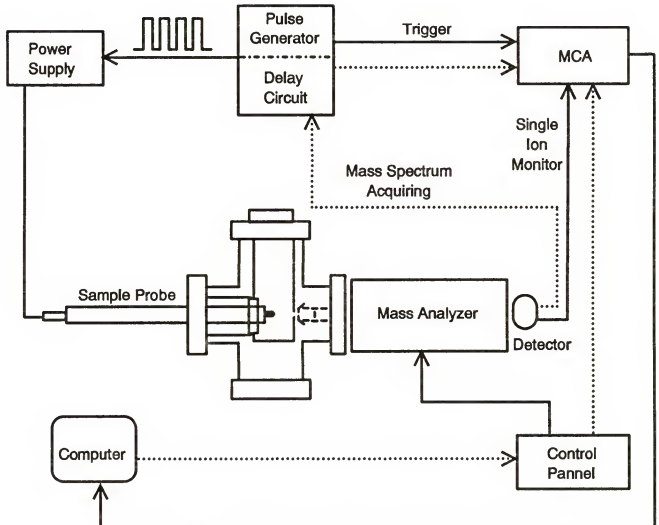

Figure 51 Illustration of pulsed discharge operation.

obtained through a data acquisition gate. The acquisition gate could be placed anywhere along the pulse period with a variable width of 0.2 to 18 ms.

Signal profiles

As a result of the pulsed discharge operation, the signals of both La^+ and LaO^+ showed an afterpeak when the pulse was terminated (Figure 52). According to current theory on afterpeak formation, an afterpeak can be observed only for those species that are Penning ionized in the glow discharge [159]. The fact that an afterpeak was observed for both La^+ (IE = 5.28) and LaO^+ (IE = 4.9) means that both species were ionized primarily through Penning ionization. By visual observation of the two signal profiles in Figure 52, there does not seem to be any significant difference in the shape of the signal through the entire pulse period. For further comparison, the La^+/LaO^+ ratio was calculated from signal intensities obtained through a one ms data gate placed on several positions along the pulse period. The calculated La^+/LaO^+ ratio is plotted as a function of time in Figure 53, where data obtained from two sample matrices are presented. The purpose of using both sample matrices (Ti and Ag) was to create different plasma environments. As a getter reagent, Ti was expected to help create a plasma more reducing in its chemical nature than that of Ag, hence yielding a much larger La population than LaO. The two discharges served as two representative plasma environments in which the La-LaO equilibrium was dominated by different species. Whether the difference in chemical components would cause different responses in the pulsed La^+ and LaO^+ signals was of interest. As shown in Figure 53, the magnitude of the La^+/LaO^+ ratio obtained with the Ti matrix is larger than that with

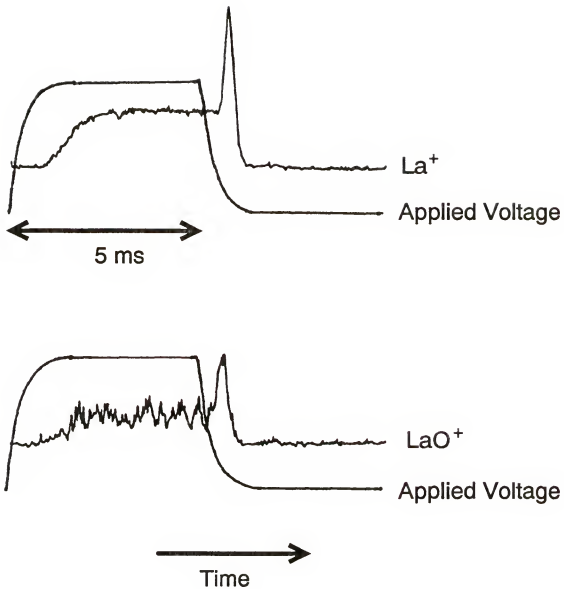

Figure 52 Signal profiles of La^+ and LaO^+ in the pulsed glow discharge.

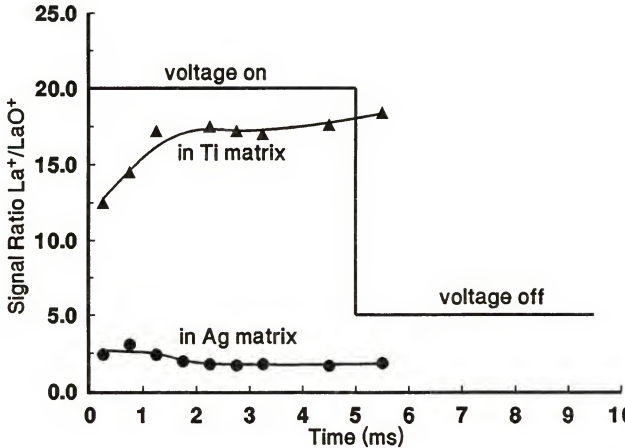

Figure 53 Signal ratio profiles of La^+/LaO^+ for the LaO_3/Ag and La_2O_3/Ti samples during pulsed discharge operation.

the Ag matrix by a factor of seven. This is in general agreement with the observation made with a DC discharge. For the Ag matrix, the La^+/LaO^+ ratio showed a slight decrease with time during the "on" portion of the pulse period. The Ti matrix, however, yielded a La^+/LaO^+ ratio that increased with time in the first 2 ms of the period. No significant difference in the La^+/LaO^+ ratio was observed, in either case, between the "on" region and the afterpeak region, which probably means that mechanisms responsible for the ionization of La and LaO were comparable in these regions (later part of the plateau and the afterpeak).

During the first two ms of the pulse "on" time, species sputtered off the cathode surface tend to have a large amount of gaseous contaminants due to their deposition during the "off" time of the previous pulse cycle. In the case of Ti in Figure 53, this may have caused a temporary lack of gettering action on the sample surface at this point, resulting in a slight shift of the La-LaO equilibrium to the formation of LaO and a lower La^+/LaO^+ ratio. As the discharge became more stable (i.e., beyond 2 ms of the "on" portion), a relatively "clean" surface was generated and a steady state gettering environment was maintained. As a result, the La^+/LaO^+ ratio increased and stayed relatively stable in the remaining portion of the pulse "on" time. Since Ag does not demonstrate an obvious gettering ability, such a phenomenon was not observed with the Ag matrix. In fact, the La^+/LaO^+ ratio was slightly higher in the early stage of the discharge "on" time than during the remainder of the pulse cycle. This was believed to be a result of cathode heating which was enhanced as more electric power was applied to the discharge with longer "on" time. The effect of sample heating was of particular

interest because it is a direct cause for water vaporization, which, as discussed earlier, is an important oxidant in the La-LaO equilibria. Investigation of how the La-LaO equilibria were affected by a heat-induced water concentration change, especially on the cathode surface, was carried out with the experiments discussed in the following section.

Redox Equilibria on Cathode Surface

As mentioned earlier, the first goal of applying pulsed discharges to an oxide sample was to search for possible differences in the afterpeak formations of La^+ and LaO^+. No such differences were observed in the results. However, time-resolved La^+/LaO^+ ratios obtained with two types of discharges showed differences during the early portion of discharge "on" time (Fig 53), a period when the chemical condition of the cathode surface plays an important role in affecting the signals of the sputtered species. This has prompted the second goal of applying pulsed discharges to the oxide sample, i.e., to study how the La-LaO equilibria are affected by the chemical environment of the cathode surface. Here, pulsing the discharge provides a means of changing and monitoring the chemical composition on the cathode surface.

In a DC glow discharge, the cathode surface undergoes a constant equilibration between sputter ablation and re-deposition of the discharge constituents [162]. After the initial step of sputter "cleaning" the sample surface, a process that lasts an average of 10 to 30 minutes depending upon the sample, the chemical composition on the cathode surface can be considered at

equilibrium and remains relatively stable with sputtering time. The amount of gaseous molecules residing on the cathode surface of a DC discharge is also at equilibrium, but their absolute amounts are difficult to obtain. Under such conditions, little information can be obtained on how the chemical constituents affect the La-LaO equilibria on the cathode surface.

Although the absolute amount of gaseous impurities on the cathode surface are difficult to measure, it is possible to induce systematic changes in the concentration of these adsorbed gases by pulsing the discharge. In this way, a relative indication of their amounts can be obtained. This concept can be explained using Figure 54, where four pulsing schemes are shown to have the same "on" time but different "off" time for each pulse cycle. During the pulse "on" time, the sputter action removes various species from the cathode surface and the discharge current heats up the cathode body. During the pulse "off" time, both sputtering and cathode heating are stopped, resulting in a temporary cooling of the cathode upon whose surface water and other gas molecules are deposited. If the pulse "on" time is held constant and the "off" time is increased as illustrated in Figure 54, the pulse cycle with longer "off" time will result in more layers of gaseous impurities accumulated on the cathode surface during the same number of pulse cycles. In this sense, effects caused by heating and sputtering are enhanced when going from a slower pulse to a faster pulse; effects caused by surface deposition are promoted when going from a faster pulse to a slower pulse. As the "off" time is carefully controlled, a series of cathode surfaces with

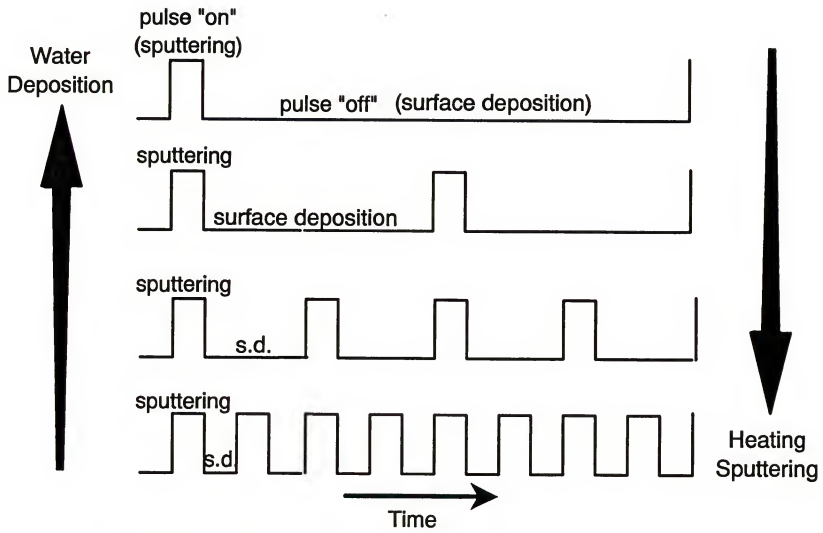

Figure 54 Schematic illustration of discharge processes on the cathode surface at various pulse "off" time.

controlled changes in their chemical compositions can be created for studying the corresponding behavior of the oxides.

Water Signal as a Function of Pulse Period

To test the concept postulated in Figure 54, experiments were carried out to monitor the water signal as a function of the pulse period. The pulse "on" time was held at a constant 5 ms and the "off" time was varied between 15 ms and 175 ms. The water signal was collected only through a 2 ms data gate placed in the middle of the pulse "on" time. The reason for this gating scheme will be explained in the later part of this section. Experiments were performed on both pin and compressed (Cu powder, Ag/La_2O_3 and Ta/La_2O_3) samples and the results are shown in Figure 55. The response of water signal to the increase of the pulse period can be classified into two groups among these samples. With cathodes in the first group, consisting of a Cu pin a the La_2O_3/Ta disk, the water signal increased with the pulse period. This observation was in agreement with the theory illustrated by Figure 54, i.e., the prolonged "off" time allowed extensive accumulation of water molecules on the cathode surface, causing a "burst" in the water concentration during the next discharge "on" time. Contrary to the first group, water signals observed in the second group, including the compressed Cu and La_2O_3/Ag cathodes, showed an increasing trend as the pulse period decreased. This means that more water was released into the discharge as cathode heating became more dominant due to longer "on" time rather than from the surface accumulation during the "off" time. One explanation could be that since these were compressed discs, the large amount of water molecules

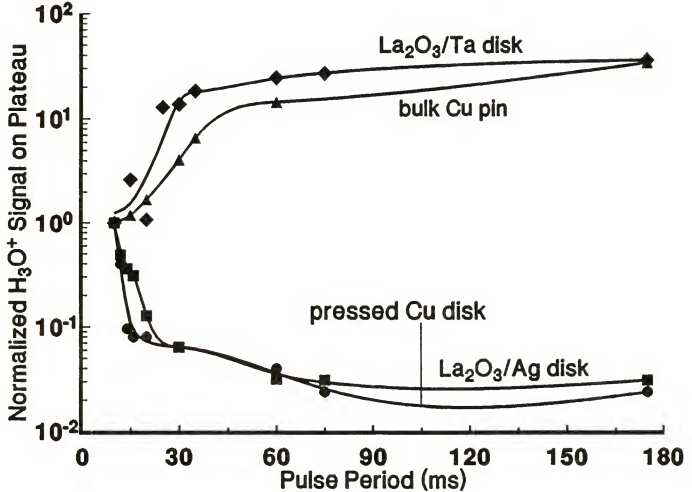

Figure 55 H_3O^+ signal as a function of pulse period for four types of samples: Cu pin, Compressed Cu disk, La_2O_3/Ag disk, and La_2O_3/Ta disk.

enveloped inside the cathode was more readily released when the cathode was heated than when it was cooled. Therefore, as the cathode was allowed to cool less (shorter "off" time), a larger amount of water was released into the discharge. Overall, the water signal behavior as a function of pulse period seemed to be determined by the origin of the water: whether in the discharge gas phase or inside the cathode body. An exception was in the case of a compressed Ta disk which deserves further discussion. Although the cathode was compress-formed, the changing trend of its water signal followed that of a pin cathode which did not have water trapped within. Here, increased heating did not seem to enhance the amount of water released from the cathode. This may be because the intensified heating of the cathode activated Ta's gettering ability [145], causing water molecules adsorbed on the granular Ta surfaces to diffuse into the granule bulk, thus preventing these water molecules from being vaporized into the discharge.

An additional evidence of the "two-origin-water" theory was demonstrated by a further experiment, in which both water origins were created in the same discharge and could be identified by the mass spectrometer. A Cu disk was used as the cathode and because it was compress-formed, it was expected to serve as the provider for the "internal" water. Copper was used because of its relatively low reactivity, avoiding "gettering" effect inside the cathode. Isotopically labeled water ($H_2{}^{18}O$) was bled into the Ar gas at five percent, serving as the "gas phase" water. The $H_3{}^{16}O^+$ signal was monitored and shown in Figure 56 as a function of the pulse period before adding $H_2{}^{18}O$ into the discharge. Thus with longer "off" time, the $H_3{}^{16}O^+$ signal of the "internal" water decreased due to less cathode

heating. Also shown in Figure 56 is the $H_3{}^{18}O^+$ signal as a function of the pulse period when present in the gas phase in a small percentage. The $H_3{}^{18}O^+$ signal increased, indicating further cathode deposition from the "gas phase" water. The distinct difference between the changing trends of the $H_3{}^{16}O^+$ and $H_3{}^{18}O^+$ signals suggest that water originating from the two different sources does respond differently to the pulse period change.

La^+/LaO^+ as a Function of Pulse Period

The purpose of studying the La^+/LaO^+ ratio as a function of the pulse period was to relate the La-LaO redox equilibria to chemical changes induced on the cathode surface. Two samples were used to represent the two "water origin" situations: Ag/La_2O_3 and Ta/La_2O_3 due to the different water signal behavior previously observed with both samples. Again, the pulse "on" time was held constant as the "off" time was varied.

The Ag/La_2O_3 sample was used mainly to demonstrate the effect of the "internal" water on the La^+/LaO^+ ratio. The water signal and the signal ratio of La^+/LaO^+ are plotted as functions of the pulse period in Figure 57. The decreasing trend of the water signal with the increasing "off" time has been explained in the previous section as a result of reduced cathode heating. For the pulse periods from 10 to 35 ms, the water signal decreased the fastest and the La^+/LaO^+ ratio showed an increase. The contrary changing trends of the water signal and the La^+/LaO^+ ratio was expected because according to the equilibrium theory, any increase in the oxidant concentration (such as water) would result in shifting the La-LaO equilibria to the formation of LaO. For the pulse periods

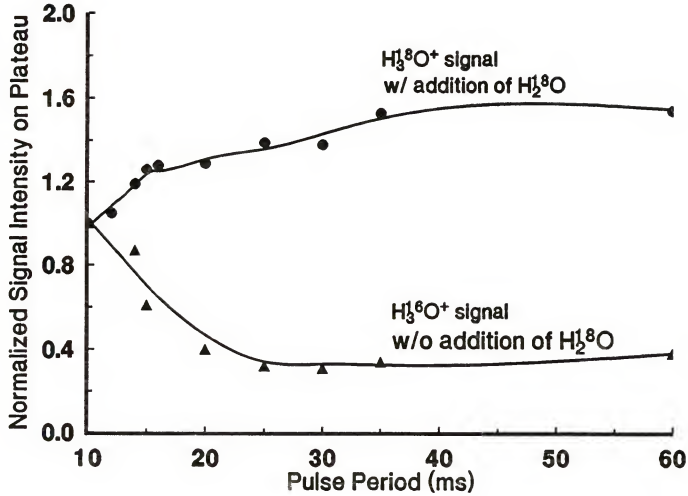

Figure 56 Normalized $H_3{}^{18}O^+$ and $H_3{}^{16}O^+$ signals (to their respective values at 10 ms period) as a function of pulse period with and without $H_2{}^{18}O$ addition.

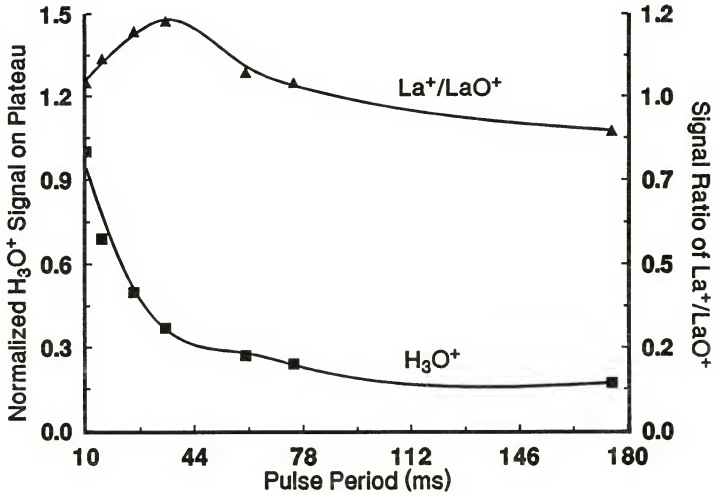

Figure 57 H_3O^+ signal and La^+/LaO^+ ratio as a function of pulse period. H_3O^+ signal is normalized to the value at 10 ms period.

between 35 ms and 175 ms, the La^+/LaO^+ ratio trailed off to a lower value. One possible explanation is that once the discharge voltage was shut off long enough to interrupt significant heat build-up in the cathode, water vapor coming from within the cathode was no longer the major oxidant contributor for the La-LaO equilibria. Instead, water accumulation on the cathode surface, a process that became more significant as the pulse was left off longer, was now a more important source of the oxidant involved in the La-LaO equilibria. At this point, oxidation of La by water happened primarily on the sample surface rather than in the gas phase. With the surface water concentration getting higher at longer periods, the La^+/LaO^+ ratio became smaller.

As observed earlier, water concentration in the discharge formed from a compressed Ta disk was not affected greatly by the heating effect. It was mainly influenced by deposition of the "gas phase" water on the cathode surface. Hence when using a La_2O_3/Ta sample, monitoring the La^+/LaO^+ ratio as a function of the pulse period should reveal information about how the La-LaO equilibria on the sample surface were affected by the deposition of water molecules originating in the gas phase. The water signal and the La^+/LaO^+ ratio obtained in these experiments are plotted as a function of the pulse period in Figure 58. Similar to that observed previously, increasing the pulse period ("off" time) allowed water molecules to build up on the cathode surface, resulting in a higher H_3O^+ signal during the next discharge "on" time. Water accumulating on the cathode surface acted as an "oxidation zone" for the cathode species. Part of the oxidation may occur through chemical bonding between the uppermost layer of the cathode

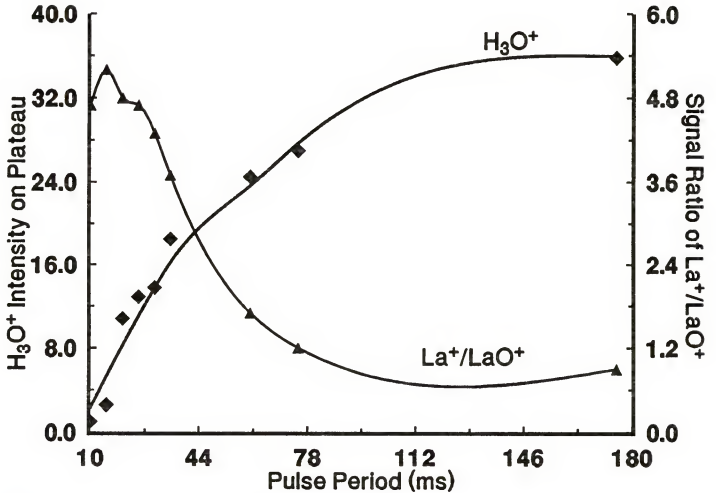

Figure 58 H_3O^+ signal and La^+/LaO^+ ratio as a function of pulse period for a La_2O_3/Ta sample. H_3O^+ signal is normalized to its value at 10 ms period.

atoms and the innermost layer of the water deposition. Another oxidation process may be considered as oxygen (from the water) attachment to the sputtered species, especially those that form stable monoxides (e.g., La), as they leave the cathode surface. As a result, the La-LaO equilibrium was shifted toward the formation of LaO, showing a decrease in the La^+/LaO^+ ratio (Figure 58).

To confirm the rationale developed with the compressed Ta sample, ^{18}O labeled water was again used to induce the formation of $La^{18}O$, which did not exist in the cathode disk. The process of forming $La^{18}O$ should happen only on the uppermost surface of the cathode or in the gas phase. While the gas phase mechanism has been mentioned in Chapter 3 and the discussion will be furthered in the next section, pulse studies allowed probing this process on the cathode surface. It was interesting to note that the residual amount of $H_2{}^{18}O$ mixed in the discharge gas responded in a similar fashion to the pulse period change as did $H_2{}^{16}O$ (Figure 59). Consequently, the $La^+/La^{18}O^+$ ratio also showed the same changing trend as did the $La^+/La^{16}O^+$ ratio responding to the pulse period change. Because the origin of $H_2{}^{18}O$ was only in the discharge gas phase, but not from within the cathode, the strong similarities between Figure 58 and Figure 59 suggest that water molecules of the two forms were functioning in a similar mechanism, that is, affecting the chemical composition on the cathode surface.

Plasma "Reagent" Introduction through Pulse Discharge

The effects that different metals, when used as a conducting binder, have on the oxide analyte have been explored in Chapter 3. Under DC discharge

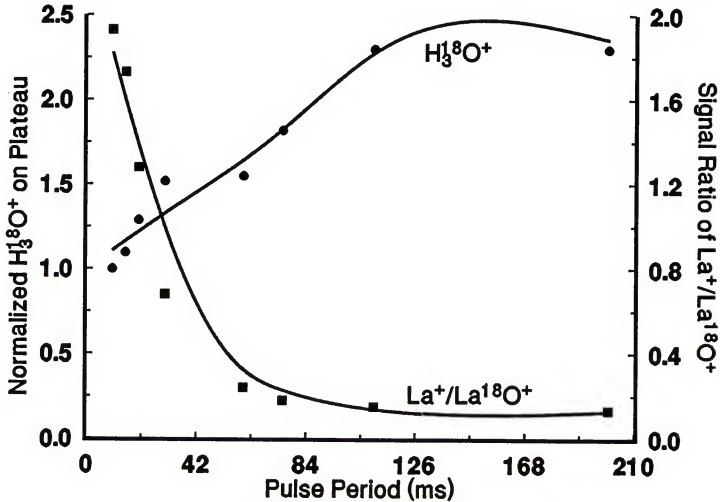

Figure 59 $H_3{}^{18}O^+$ signal and $La^+/La^{18}O^+$ ratio as a function of pulse period for a La_2O_3/Ta sample with addition of $H_2{}^{18}O$. $H_3{}^{18}O^+$ signal is normalized to its value at 10 ms period.

condition, the reducing effect demonstrated by getter reagents was considered mainly a manifestation of gas phase reactions. However, previous sections in this chapter have shown that the gettering of water molecules might also occur within a compressed getter cathode. This has led to a speculation that reactions between the getter atoms and the oxide molecules may also happen within the heated cathode body. The significance of the gas phase reaction mechanism was thus questioned. The following experiments were designed to further the investigation of effects that selected metals have on the La-LaO equilibria in the gas using a dual cathode configuration.

Instrumental Setup

To achieve the goal of confining induced reactions mainly to the gas phase, instead of mixing the reagents with the oxide analyte, they were sputtered into the discharge by means of a second electrode separate in space from the DC cathode containing the oxide analyte. The two-cathode arrangement in the ion source is shown in Figure 60. The DC discharge operation was identical to running a single DC discharge as described in Chapter 1. The power supply system for the secondary discharge (also called the "reagent" discharge) was similar to that used for a pulsed discharge that was described in the previous sections of this chapter. High purity silver was used as the hosting matrix for La_2O_3 in preparing the DC discharge cathode. Several high purity pins were used as cathodes for the "reagent" discharge: Ag, C, W, Ta, and Ta.

The first parameter to be determined was the optimum operational distance between the two cathodes. Because our system has limited flexibility in adjusting

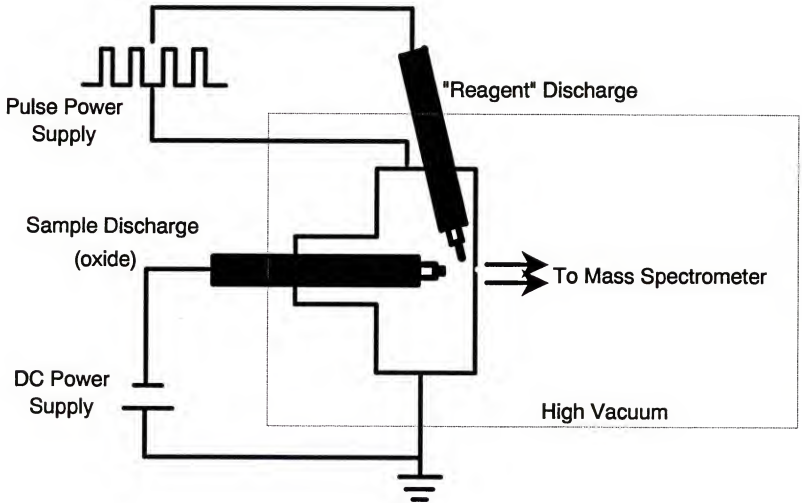

Figure 60 Schematic diagram of the dual discharge arrangement in the ion source.

the relative positions of the two probes, the main objective in optimizing the distance was to avoid losing the DC ion signal intensity while introducing the "reagent" cathode. In this experiment, a Ag pin served as the DC cathode and the Ag^+ signal was used for tuning the ion optics of the mass spectrometer. The "reagent" probe was originally separated from the DC cathode by 10 cm and was gradually brought closer to the DC cathode in 0.5 cm increments. Shown in Figure 61 is the effect of closing the cathodes on the Ag^+ signal intensity. When the distance between the cathodes was larger than 2 cm, the Ag^+ signal was not interfered by the physical intrusion of the "reagent" cathode. As the cathodes were brought closer than 2 cm, the Ag^+ signal started to decrease. The 2 cm between the cathodes was then determined to be the optimum distance for dual discharge operation.

The signal gating scheme for data acquisition was crucial in obtaining most relevant information about the gas phase reactions between the analyte species sputtered from the DC cathode and the "reagent" elements sputtered from the secondary cathode. The relationship between the signals from the two cathodes is shown in Figure 62. The DC signals should be steady lines with time once the discharge current was stabilized, while the pulse signals (from the secondary discharge) should follow the "on-off" pattern of the applied voltage. It has been shown that atoms sputtered from a pulsed cathode do not vanish immediately following the termination of the applied voltage. A time delay of a few milliseconds is usually required for the pulse-sputtered species to diffuse across the ion source space after the voltage is shut off [155]. This afterpeak zone was

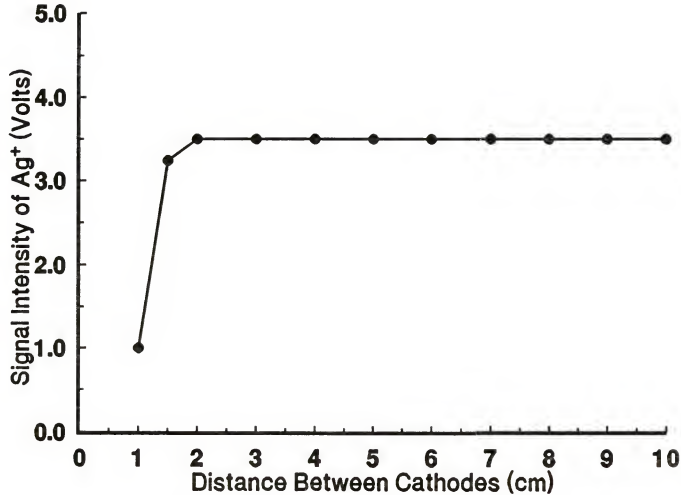

Figure 61 Signal intensity of Ag^+ as a function of the distance between the two cathodes.

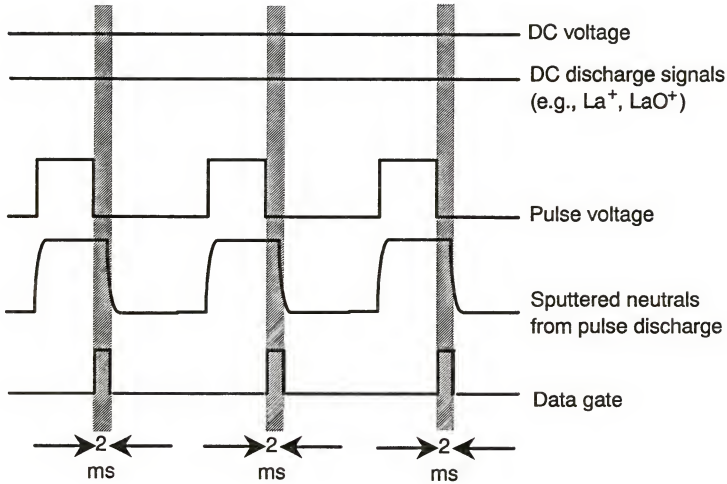

Figure 62 Illustration of the temporal relationships among dc signal profiles (La^+ and LaO^+), pulsed signal profiles, and the data acquisition window.

considered to be the best position for gating the DC signals under investigation because of several reasons: (1) during this time period, the plasma initiated by the "reagent" discharge has been extinguished, and hence should not impose electrical interferences on the DC plasma, and (2) at this point sputtered "reagent" atoms were still diffusing through the ion source, available for reactions with species sputtered from the DC discharge. Therefore, the La^+ and LaO^+ signals were collected only through the data gate shown in the shaded areas in Figure 62, where any change in the analyte signals observed could be attributed to chemical effects of the "reagent" material through gas phase reactions.

Reagent Provision

Because the two cathodes virtually shared the same plasma space, deposition of species sputtered from one cathode onto the other cathode was inevitable. The degree of the "reagent" deposition on the DC cathode needed to be examined and compared with the gas phase concentration of the "reagent", especially in the gated time period. To examine such deposition, an iron pin and a silver pin were used as the DC and the "reagent" cathodes respectively. The time profile of the Ag^+ signal was recorded while the Fe discharge was kept on and off in two separate experiments respectively. When the Fe discharge was kept off, the Ag^+ signal followed the voltage profile as shown in Figure 63a. With the Fe discharge kept on, the Ag^+ signal maintained its "on" time intensity for an additional 3 ms after the pulse voltage was terminated (Figure 63a). This Ag^+ signal extension was probably caused by Ag atoms, sputtered during the previous "on" time, continuing to be ionized in the plasma supported by the DC cathode.

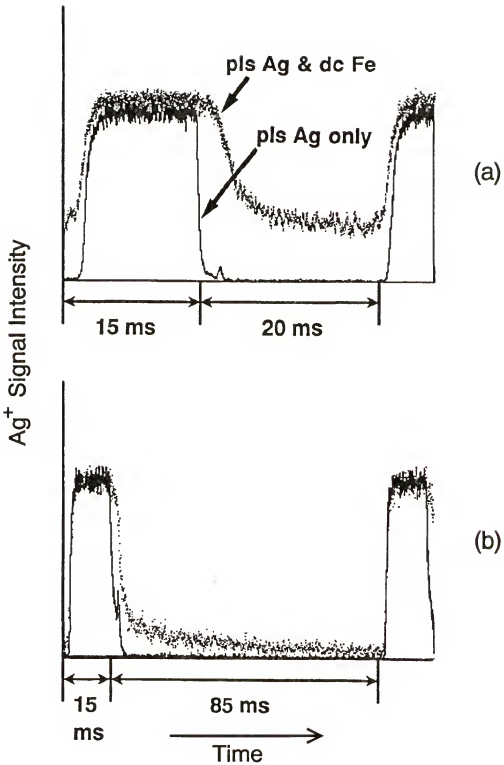

Figure 63 Comparison of the signal profiles of Ag^+ between running a pulsed Ag discharge only (solid lines) and running a pulsed Ag and a dc Fe discharges together (dotted lines). (a) pulse period is 35 ms; (b) pulse period is 100 ms.

Note that during the 20 ms "off" time, the Ag^+ signal leveled off at an intensity much higher than that obtained when the DC discharge was kept off. This "off" time Ag^+ signal was significantly high, which was a strong indication of Ag deposition on the DC cathode. It also suggested that a time period of 20 ms was not long enough for the DC discharge to sputter-remove the deposited Ag layers completely. However, when the pulse "off" time was increased to 85 ms (Figure 63b), Ag deposited on the DC cathode during the 15 ms "on" time was removed more completely during this longer "off" time. The fact that in Figure 63a-b, the Ag^+ signal has two decreasing slopes in the "off" time region suggests that different processes were responsible for the dissipation of Ag. The diffusion process was probably the governing factor in the first few milliseconds following the voltage termination, while sputter-cleaning the DC cathode may be in control for the remainder of the "off" time. Most importantly, these experiments have confirmed the delay of the "reagent" atoms in the gas phase during the first 2 ms following the pulse termination, i.e., the gated time period.

In order to induce reactions between the existing species and the added reagent in the plasma, sufficient reagent must be provided through sputtering of the secondary cathode. It has been reported by Klingler and Harrison that the ion signal behavior of a sputtered species in a pulsed discharge appears to be a function of the pulse period [158]. The same observations were also made in studies carried out here using three different cathode materials (Figure 64). The pulse "on" time was held at constant 10 ms while the pulse "off" time was varied between 5 ms and 165 ms. The ion signals of both Ti^+ and W^+ decreased with

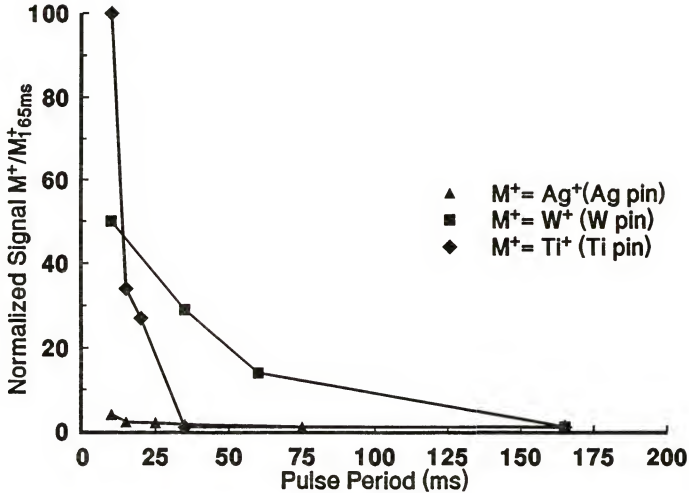

Figure 64 Normalized signals of Ag^+, W^+, and Ti^+ (to their respective values at 200 ms period) as a function of pulse period.

the increasing pulse period, or the increasing "off" time in essence, whereas the Ag^+ signal was affected little by the period change. One possible explanation relates this phenomenon with the effect that the length of the pulse "off" time has on the chemical composition on the cathode surface. As discussed in the previous section of this chapter, a long "off" time promotes the accumulation of water and other gaseous species on the sample surface. This gaseous deposition can decrease the sputter yield of the cathode in two ways: (1) it may physically block and de-energize the incoming Ar^+ ions, resulting in inefficient low energy sputtering, and (2) strong chemical bonding that is difficult to dissociate may develop among the adsorbed gas molecules and the cathode atoms, also causing low sputter yield. The second effect may be more pronounced with more reactive metals such as getter reagents. In Figure 64, the impact of changing the pulse period on Ag^+, W^+, and Ti^+ signals increased in the same order as their reactivity. Titanium, being the most reactive among the three, was most sensitive to the water deposition on its surface, and hence showed the most drastic decrease as the pulse "off" time was increased. Silver was the least reactive element among the three, and was not affected greatly by the period change. For the purpose of inducing gas phase reactions, it can be concluded from Figure 64 that the pulse must be operated at a period shorter than 50 ms to ensure sufficient "reagent" provision.

Effect on La^+/LaO^+

Because the amount of material introduced by the pulse discharge is a function of the pulse period, systematically changing the pulse period should

have a "titration" effect on other reactants (e.g., oxides from the DC discharge) already in the plasma. The effect of "titrating" the La-LaO equilibria with Ag, C, Ti, and Ta was studied by monitoring the La^+/LaO^+ ratio as the pulse period was varied. Results are presented as the enhancement of the La^+/LaO^+ ratio versus pulse period for the four added "reagents" in Figure 65, which resembles Figure 64 in appearance. It is clear that pulsing Ti, C, and Ta into the plasma increased the La^+/LaO^+ ratio, particularly at periods shorter than 50 ms. As the pulse was operated at longer periods, the La^+/LaO^+ ratio did not change significantly, possibly because the pulse cathode sputtering was not sufficient at these periods. The largest La^+/LaO^+ enhancement caused by each reagent was of the same order as observed when these reagents were mixed directly in the sample matrix, i.e., Ag < C < Ta = Ti (Chapter 3).

Further experiments were carried out to focus on the real time interaction between the getter reagent Ti and the oxide species in the gas phase. A comparison was made on signal profiles obtained when running the two discharges one at a time and simultaneously. When operated separately, the DC discharge signals of La^+ and LaO^+ were steady lines on the time scale; the pulse discharge signal of Ti^+ showed a square-wave appearance resembling the applied voltage (Figure 66a). As the two discharges were turned on at the same time and superimposed on one another, the Ti^+ signal maintained the square-wave shape with an elevated baseline during the "off" time (Figure 66b). The cause of the non-zero "off" time signal was attributed to the sputtering of Ti deposited on the DC cathode. It is interesting to note that the DC La^+ signal was increased, but

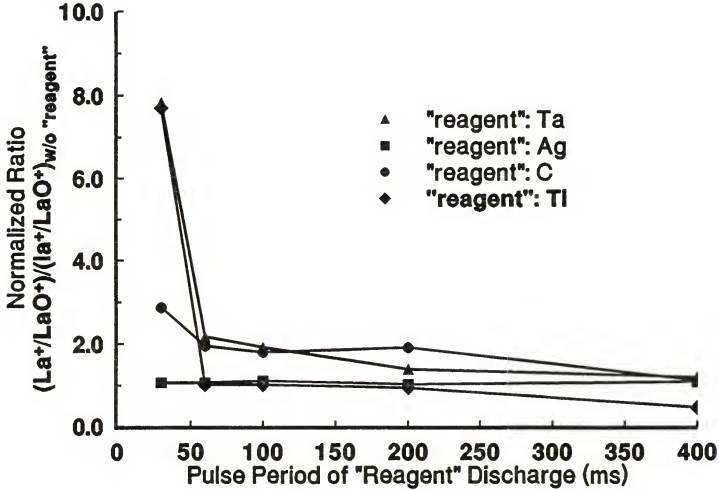

Figure 65 Effects of four plasma reagents (Ag, C, Ta, and Ti) on the La^+/LaO^+ ratio (normalized to its value obtained without the reagent discharge) at different pulse periods.

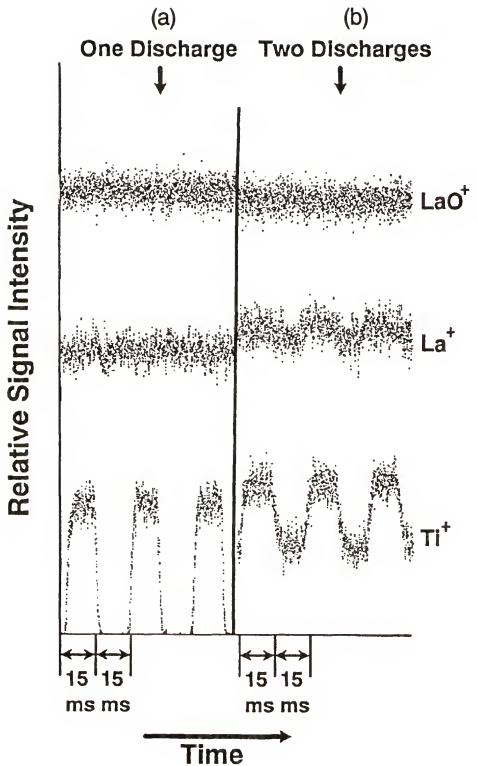

Figure 66 Comparison of La^+, LaO^+, and Ti^+ signal profiles. (a) signals were obtained by running the dc (La_2O_3/Ag) and pulsed (Ti) discharges separately. (b) signals were obtained by running the dc and pulsed discharges together.

no longer remained to be a steady line (Figure 66b). Instead, it showed a "pseudo-pulse" profile in synchronization with that of the Ti^+ signal. This phenomenon was strong evidence that Ti atoms sputtered into the plasma gas phase from the secondary cathode were directly responsible for the enhancement of the La^+ signal.

The dual discharge studies carried out in this section have provided an alternative way of investigating the gettering mechanism in the glow discharge. The majority of possible interactions between getter reagents and oxide analytes was confined to the gas phase. Results support the theory that gettering action in the gas phase contributes significantly to the overall reduction of the lanthanum oxide.

Plasma "Reagent" Introduction through Gas Injection

The previous section has focused on the effect of "reducing" reagents on the La-LaO equilibria when introduced in a transient mode. Experiments presented in this section were devoted to reversing the equilibria by transiently introducing various gaseous reagents (mostly oxidizing gases) into an already equilibrated plasma. The essence of the experiment is similar to that discussed in Chapter 3, the difference being the mode by which the gaseous reagents were introduced. Instead of bleeding the reacting gases into the Ar gas line at a constant pressure, a solenoid valve was used to pulse small portions of the reacting gas directly into the plasma volume. The pump system of the mass spectrometer provided a natural concentration gradient for the added gas

between pulses. Hence, the concentration of the added gas would undergo a systematic, yet controllable change in the plasma on a short time scale. By synchronizing the ion detection by the mass spectrometer with the injection pulses in a preset schematic, the chemical effects of the added gaseous reagents on the analyte species could be closely monitored.

In order to study the re-equilibration of the La-LaO system as a result of adding reactive gases, it is best that reactive species that were originally present in the discharge be eliminated before the addition of the intentional reagent. Such a condition, often accompanied by an optimized La^+/LaO^+ ratio, is achievable by using a getter reagent as the sample matrix and sputtering the cathode for an extended period of time. For this purpose, Ta was chosen to be the host matrix for La_2O_3 in the following experiments.

Experimental

The instrumental setup used in this study is illustrated in Figure 67. The glow discharge was maintained at a constant 1100 volts, and the Ar discharge gas pressure was 0.9 Torr. A Series 9 high speed solenoid valve (General Valve Corporation, Fairfield, NJ) was coupled onto the source tee perpendicular to the cathode probe. The injector "open" time could be varied from 0.16 ms to one second, and the operating pressure capable of being varied from 1×10^{-9} Torr to 85 atmospheres. An 8.5 cm long stainless steel capillary connected to the inside end of the injector directed the gas injection as close to the discharge volume as possible. In the controlling circuit, a custom designed pulse generator sent a series of one Hz pulses into a binary counter that delayed the pulse by a factor

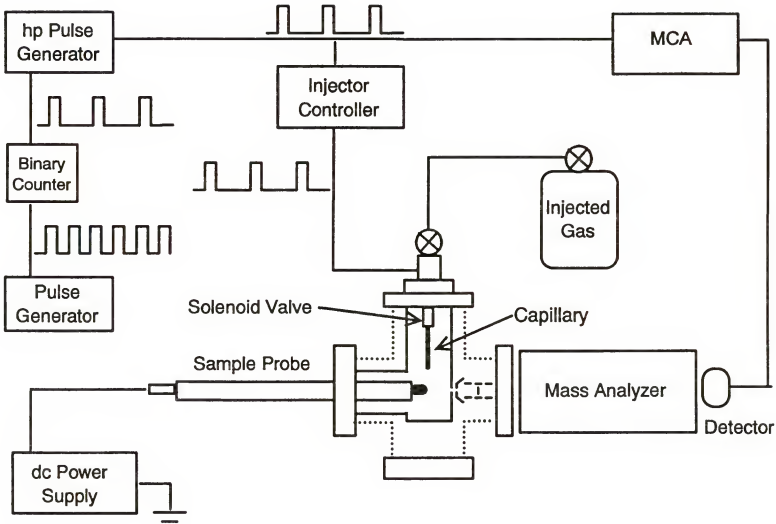

Figure 67 Schematic diagram of the pulse injection set-up with glow discharge operation.

of any nominal number between one and 255 preset by the operator. In most of the experiments carried out in this section, the pulse frequency was delayed by a factor of 60 before being sent into a Hewlett-Packard Model 8003A pulse generator used to trigger the injector controller. The injector controller was a +28 VDC power supply built by the chemistry department electronic shop at the University of Florida. The frequency at which the injector valve would open was controlled by the trigger signal coming from the HP pulse generator, whereas the valve open time was determined by adjusting the injector controller. Data acquisition was synchronized with the solenoid injection by the same trigger signal coming from the HP pulse generator.

The added gases in these experiments included Ar, H_2, $H_2{}^{16}O$, and $H_2{}^{18}O$. Ar was used primarily as a "blank" to determine the effect of physically disturbing the pressure, and hence the current of the plasma rather than to induce chemical reactions. Hydrogen, water vapor of $H_2{}^{16}O$, and water vapor of $H_2{}^{18}O$ were used to manipulate the La-LaO equilibria.

The concentration change of the injected gases with time was monitored by a millitorr range Teledyne-Hastings ion gauge without filling the ion source with the base Ar discharge gas. As shown in Figure 68, the pressures of all injected gases rose to a peak value and then slowly decreased. Overall, there was a 15-20 seconds delay between the opening of the injector valve and the peaking of the pressure, possibly caused by the time required for the injected gases to diffuse from the injection point to the ion gauge. The peaking magnitude of these gas pressures were different because the pressure behind the injector valve was

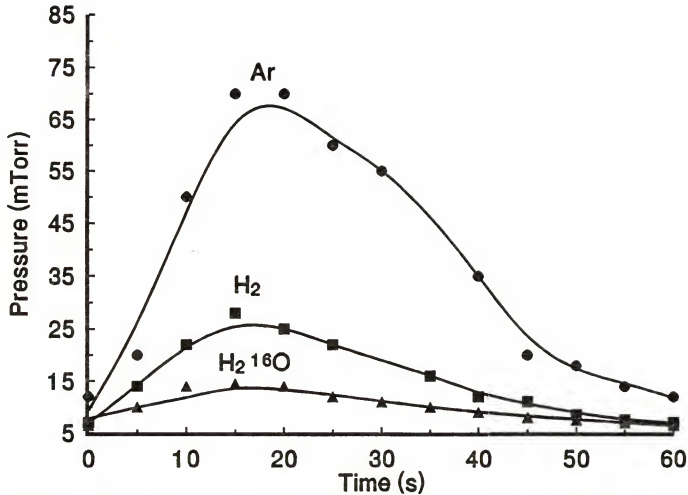

Figure 68 Concentration gradient (indicated by pressure) of Ar, H_2, and water with time as a result of pulse injection. Injection period is 60 s; solenoid valve open time is 3.6 ms for Ar and H_2, and 100 ms for water.

regulated at much higher values in the cases of Ar and H_2 than that of water. The 60-second repetition rate for injection has resulted in an apparent concentration gradient between the pulses, which provided the necessary conditions for studying the La-LaO equilibria in a "transient" chemical environment.

Ar Injection

The absolute signal intensities of the La^+, Ta^+, LaO^+, and H_2O^+ were recorded directly from an MCA both with and without the gas injection (Figure 69). If these species were classified in two categories according to their redox properties, La and Ta would be favored by a "reducing" environment and LaO and H_2O by an oxidizing one. As shown in Figure 69, the signal changing trends as a result of the Ar injection also broke down into the same two categories. The La^+ and Ta^+ signals were enhanced going from without injection (b) to with injection (a), which was most apparent during the first five seconds following the injection (a), whereas the H_2O^+ and LaO^+ signals were slightly repressed in the same process. Comparing the signal intensities obtained with Ar injection (Figure 69a) and those without the injection (Figure 69b), it is clear that the magnitudes of the relative signal enhancement/reduction were fairly small. Because Ar is believed not to participate in plasma redox reactions, the initial signal fluctuation observed here was probably caused by the changing discharge current in this time period, which went up to a maximum of 4.4 mA from the original 2.5 mA and recovered back at 2.5 mA after two to three minutes following the injection. This sudden increase in the discharge current may have caused a temporary boost in the plasma energy, which favored the bond dissociation of the oxide. This so

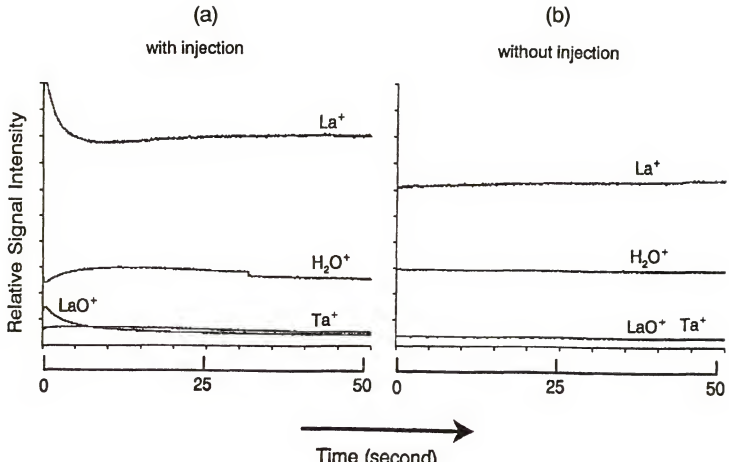

Figure 69 Effect of pulse injecting Ar gas on the signal profiles of La^+, LaO^+, H_2O^+, and Ta^+. The solenoid valve open time is 3.6 ms; injection period is 60 s. (a) Signal profiles with injection; (b) signal profiles without injection.

called "electrically" (rather than chemically) induced re-equilibration of the La-LaO system was of a minor degree, which may be understood better when compared with situations where more reactive gases were injected.

H_2 Injection

In the experiments discussed in Chapter 3, a small percentage of H_2 was bled into the discharge gas constantly in hope that its traditionally recognized reducing property might help dissociate oxide bonds. Surprisingly, the La-LaO equilibria not only did not re-equilibrate in favor of the La formation, but the La^+/LaO^+ ratio was actually decreased. The following hypothesis was given to account for this result: the H^+ and H_3^+ ions in the glow discharge, although present in a small percentage, may be carrying the majority of the current instead of Ar^+ to serve as the bombarding projectiles. This may result in an insufficient sputtering of the getter atoms as well as preferential sputtering of the oxygen atoms in the oxide [136]. Hence, the oxygen concentration relative to the metal species in the plasma is not reduced but maybe even enhanced. If and when hydrogen does react with free oxygen in the plasma, the direct products would be OH and H_2O molecules which can still act as oxygen donors for the La-LaO equilibria. The net result is that no net "reducing" force is provided by adding hydrogen into the discharge gas.

In the present studies, H_2 was pulse injected into the discharge instead of being constantly bled in. On a repeatable short time scale, the plasma changed from having no additional H_2 to having a surge of H_2 pulsed in and then recovering back to its original stage. The effect of the changing H_2 concentration

on the important species in the plasma (i.e., Ta^+, La^+, LaO^+, and H_2O^+) was the focus of this investigation.

Figure 70 shows the signal profiles of the aforementioned species with time zero synchronized to every injection pulse trigger. The injection has caused an overall increase in all four ions monitored, partially due to the rising current at the same time (Figure 70a). All four signals also returned to their original intensity levels shown in Figure 70b before the next injection cycle. It is interesting to note that the H_2O^+ signal was the most enhanced among all four signals. Whereas there might have been a certain amount of air impurity in the gas line, the much higher magnitude of the H_2O^+ signal than that of the other air components (e.g., N_2H^+) suggests that the sudden rise in the water signal was not due primarily to contamination in the injection line. A closer look at the relationship between H_3^+ and H_2O^+ on the same time scale (Figure 70c) revealed that the water signal peaked at the same time as a valley formed in the H_3^+ profile. Rakshit and Warnek have studied the gas phase reactions between ArH^+ and H_2, and believed that the reactions described in Equations IV-1 to IV-4 were responsible for the formation of H_3^+ [162]:

$$Ar^+ + H_2 = ArH^{+*} + H \qquad \text{(IV-1)}$$

$$ArH^{+*} + Ar = ArH^+ + Ar \qquad \text{(IV-2)}$$

$$ArH^{+*} + H_2 = H_3^+ + Ar \qquad \text{(IV-3)}$$

$$ArH^+ + H_2 = H_3^+ + Ar \qquad \text{(IV-4)}$$

Because in our discharge plasma, the concentration of O atoms was significantly high, which may have made the following reactions possible,

$$H_3^+ + O = HO^+ + H_2 \quad \text{(IV-5)}$$

$$H_3^+ + O = H_2O^+ + H \quad \text{(IV-6)}$$

The relationship observed between H_2O^+ and H_3^+ signals in Figure 70c suggests that these two species were involved in a reactant/product equilibrium, supporting the postulation depicted by Equation IV-5. When the hydrogen concentration reached a certain level in the discharge, it started to react with available oxygen to form water molecules (and/or ions); as the injected hydrogen was pumped away and became less concentrated in the ion source, the reaction reversed and water dissociated to release back hydrogen. Although the exact reaction mechanisms for this proposed explanation are not clear at this point, the possibility of forming water between hydrogen and oxygen during the sputtering step is in agreement with the reactive sputtering theory developed by other researchers [36].

The effect of the changing H_2-H_2O equilibrium on the La-LaO equilibria was again related to the redox properties of each species. Shown in Figure 70a, the maximum signal intensities of La^+ and Ta^+ (the "reducing" environment species) occurred at the same point in time, whereas the H_2O^+ and LaO^+ signals were optimized closer to each other in time. Again, it was not until the water concentration has decreased to a much lower level that the La^+ and Ta^+ signals started to reach their maxima. If the signal ratio of Ta^+/H_2O^+ is used to describe the relative strengths of the "reducing" force versus the "oxidizing" force, then influences of both forces on the La-LaO equilibria can be visualized by plotting the simultaneously obtained La^+/LaO^+ ratio and the Ta^+/H_2O^+ ratio on the same time

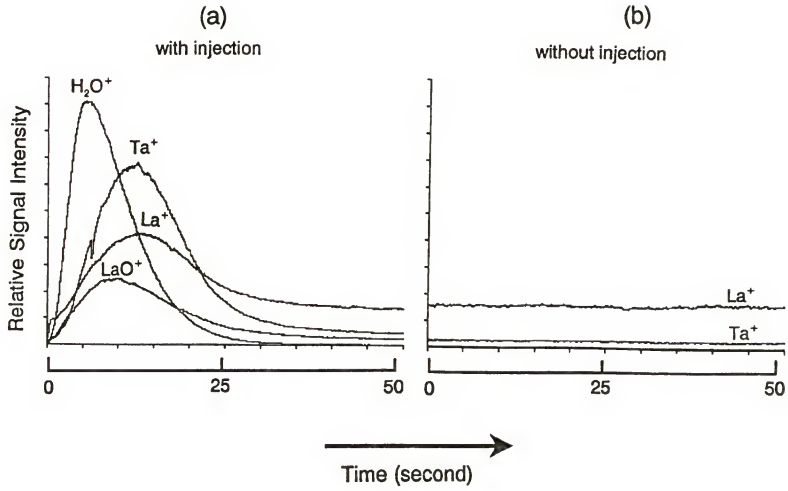

Figure 70 Effect of injecting H_2 on the signal profiles of La^+, LaO^+, H_2O^+, and Ta^+. The solenoid valve open time is 3.6 ms; pulse injection period is 60 s. (a) signal profiles with injection; (b) signal profiles without injection; (c) signal profiles of H_2O^+ and H_3^+ with injection.

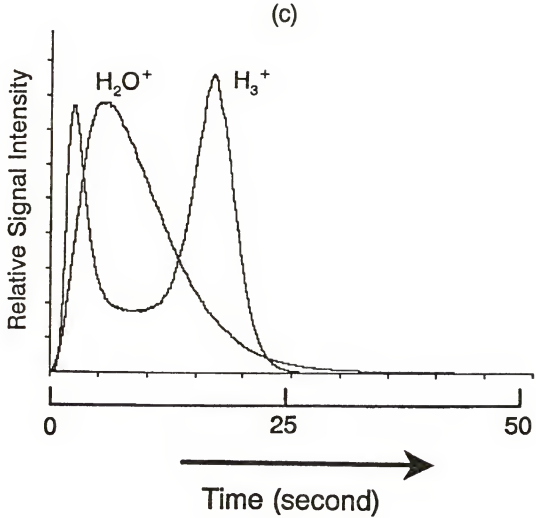

Figure 70--continued.

scale in Figure 71. The similarity between the two ratios following each hydrogen injection suggests that they virtually reflected the same processes of the plasma, that is, changing from being "oxidizing" to "reducing" in nature.

$H_2{}^{18}O$ Injection

Unlike the role of H_2, the function of water vapor used in these studies as a plasma reagent was more straight forward, that is, to provide additional oxygen carriers for the redox system under investigation. The steady state introduction of water vapor has been discussed in Chapter 3. In addition to providing time-resolved information about ions of interest, the pulsing mode addition conducted in this section would allow for much smaller amounts of water to be added, offering a chance to avoid oxidation of the cathode surface encountered in the steady addition mode.

While the repetition rate was set at the same value, two injector open times were used to allow different amounts of injection: 3.6 ms and 100 ms. In the former case (Figure 72a), following the opening of the valve, species that are favored by a high oxygen concentration (LaO^+ and H_2O^+) were enhanced to a peak value and then decreased back to their original intensities as the added water vapor was pumped away. At the same time, the Ta^+ and La^+ signals were quenched because of the presence of water and then slowly increased. While absolute signal intensity profiles plotted in Figure 72a show the direct response of the species involved in the La-LaO equilibria, how the equilibrium was affected by the injection of water was better illustrated by the LaO^+/La^+ ratio versus time plot shown in Figure 73a. When water was injected into the plasma, the

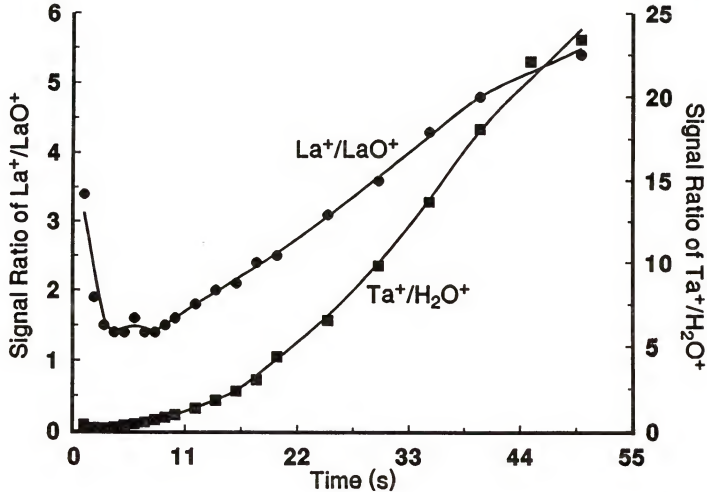

Figure 71 Signal ratios of La^+/LaO^+ and Ta^+/H_2O^+ as a function of time during the H_2 injection cycle. Injection period is 60 s; solenoid valve open time is 3.6 ms.

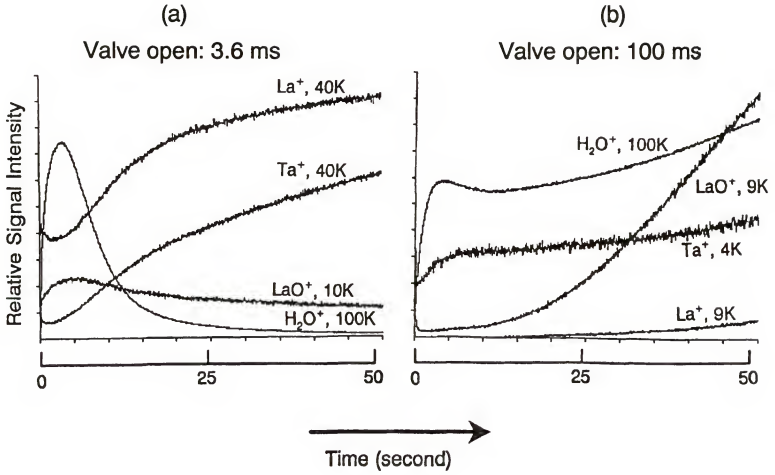

Figure 72 Effect of pulse injecting H_2O vapor on the signal profiles of La^+, LaO^+, H_2O^+, and Ti^+. Injection period is 60 s. (a) the solenoid valve open time is 3.6 ms; (b) the solenoid valve open time is 100 ms.

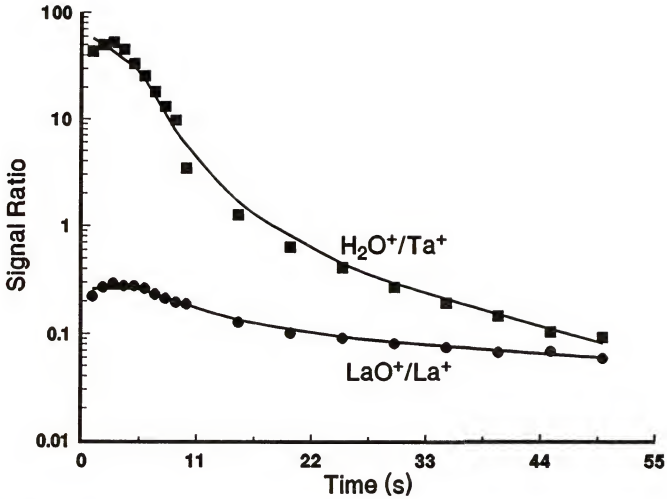

Figure 73 Signal ratios of H_2O^+/Ta^+ and La^+/LaO^+ as a function of time during the $H_2{}^{16}O$ injection cycle. Injection period is 60 s. (a) solenoid valve open time is 3.6 ms; (b) valve open time is 100 ms.

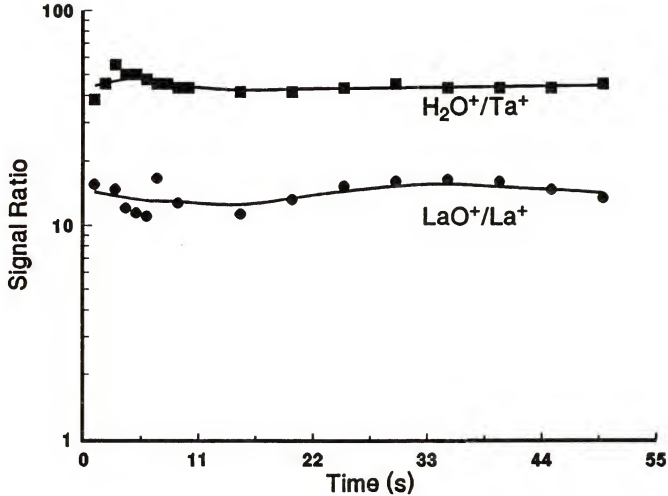

Figure 73--continued.

"oxidizing" force of the discharge immediately became much stronger than the "reducing" force ($H_2O^+/Ta^+ \approx 50$), which has brought up the LaO^+/La^+ ratio from 0.02 (the value before injection, not shown in the figure) to 0.3. Because the amount of water injected in the 3.6 ms open time was small, the majority of it was pumped away during the 60-second injection cycle. As a result, the H_2O^+/Ta^+ ratio was reduced by two orders of magnitudes at the end of the injection cycle. The LaO^+/La^+ ratio did not recover fully to the original value of 0.02, indicating that a residual amount of water vapor may still be present in the source at this point.

The same sets of data obtained with the 100 ms valve open time are also presented in Figures 72b (the absolute signal intensities) and 73b (the signal ratios). There are two apparent differences in Figure 72a from 72b: (1) the water and the LaO^+ signals did not drop throughout the entire injection cycle, and (2) the signal intensities of LaO^+ and H_2O^+ were higher than those of La^+ and Ta^+ respectively in Figure 72b (whereas La^+ and Ta^+ are higher than LaO^+ and H_2O^+ in Figure 72a). The probable cause of such differences is that the large amount of water injected during the 100 ms valve open time could not be pumped away in 60 seconds, resulting in a build-up of the water vapor pressure resembling the steady state mode of addition. The three sputtered species Ta^+, La^+, and LaO^+ all increased slowly with time, possibly a result of the recovering of the Penning ionization efficiency as the water concentration decreased. Although not easily seen in Figure 72b, the slowly increasing rates of all four signals are similar, resulting in the almost constant ratios of H_2O^+/Ta^+ and LaO^+/La^+ in Figure 78b.

Here, the LaO^+/La^+ ratio has increased from a 0.02 obtained before the injection (not shown in the figure) to a value larger than 10 in Figure 73b. The steadiness of both ratios with time resembled the case of introducing water in the constant mode.

$H_2{}^{18}O$ Injection

Injection into a DC discharge

By the same theory of bleeding ^{18}O labeled water into the discharge as discussed in Chapter 3, the purpose of pulse injecting $H_2{}^{18}O^+$ was to study the oxidation reaction processes by the gas phase synthesis of the new molecule $La^{18}O$. The advantage of conducting these experiments in the pulse injection mode was the ability to acquire information in a time-resolved fashion. Three valve open times were used in this study to increase the amount of water vapor introduced: 46 ms, 100 ms, and 146 ms. Time profiles of La^+, Ta^+, $La^{16}O^+$, $Ta^{16}O^+$, $La^{18}O^+$, $Ta^{18}O^+$, and $H_3{}^{18}O^+$ are only presented for the 46 ms open time in Figure 74, for they serve as a general representation of all three cases. The $H_3{}^{18}O^+$ signal profile provides an indication of how the water concentration gradient was formed with time, which showed a decreasing pattern. The only ion signals that closely followed the same pattern are $La^{18}O^+$ and $Ta^{18}O^+$, indicating that they were the products of oxidation reactions involving $H_2{}^{18}O$. A comparison was drawn between Figure 74a, in which the element of interest, La, was bound in its oxide when in the sample, and Figure 74b in which the element of interest, Ta, existed in its metallic form in the sample. Though original forms differed, their respective "synthesized" molecules $La^{18}O^+$ and $Ta^{18}O^+$ demonstrated similar time

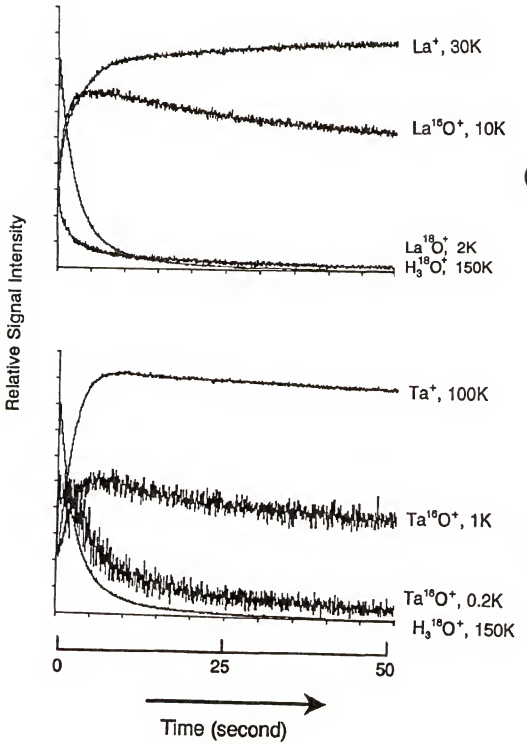

Figure 74 Signal profiles affected by pulse injecting $H_2{}^{18}O$ vapor into the discharge. The solenoid valve open time is 46 ms, and injection period is 60 s. (a) signals of $H_3{}^{18}O^+$ and the analyte species; (b) signals of $H_3{}^{18}O^+$ and the matrix species.

profiles following the injection of $H_2{}^{18}O$. This observation supports the belief that the reaction between sputtered La atoms and $H_2{}^{18}O$ molecules in the gas phase was a significant path for the formation of $La^{18}O$.

Further evidence of the reactant/product relationship between $H_2{}^{18}O$ and the ^{18}O containing oxides was provided by a series of signal ratio versus time plots shown in Figure 75. The only experimental difference among the three plots was the time length for which the injector valve remained open, and hence the amount of $H_2{}^{18}O$ injected in the plasma. In Figure 75a, because the amount of water injected was relatively small, La^+ was still the dominant ion among the three La containing species (La^+, $La^{16}O^+$, and $La^{18}O^+$), even with water injection. In Figure 75b where the valve open time was increased to 100 ms, although the La^+ intensity was still the highest among all three lanthanum species, the $La^{18}O^+/La^+$ ratio was now in the range of 0.01 - 0.1, five times larger than that in Figure 75a (0.002 - 0.02). The prolonged open time has also resulted in an overall increase in both $H_3{}^{18}O^+/Ta^+$ and $Ta^{18}O^+/Ta^+$ ratios by a factor of ten and five respectively. The proportionality in the signal enhancement of all the ^{18}O- containing molecules indicated that increasing the overall ^{18}O concentration in the plasma was the cause for the enhanced production of the ^{18}O-containing oxides. Again, the close resemblance in the changing patterns of the $La^{18}O^+/La^+$ and $Ta^{18}O^+/Ta^+$ ratios suggested that a similar reaction mechanism was responsible for the formation of both oxides in the glow discharge. Finally, it is worth pointing out that the $La^{16}O^+La^+$ ratio remained relatively stable through all three valve open time settings as well as within each injection cycle. When the injector open time was

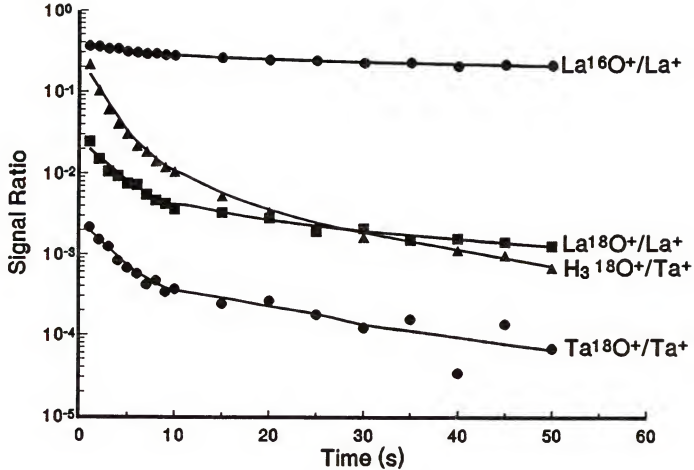

Figure 75 Signal ratios of $La^{16}O^+/La^+$, $La^{18}O^+/La^+$, $H_3{}^{18}O^+/Ta^+$, and $Ta^{18}O^+/Ta^+$ as a function of time during the $H_2{}^{18}O$ injection cycle. Injection period is 60 s. (a) solenoid valve open time is 46 ms; (b) valve open 100 ms; (c) valve open 150 ms.

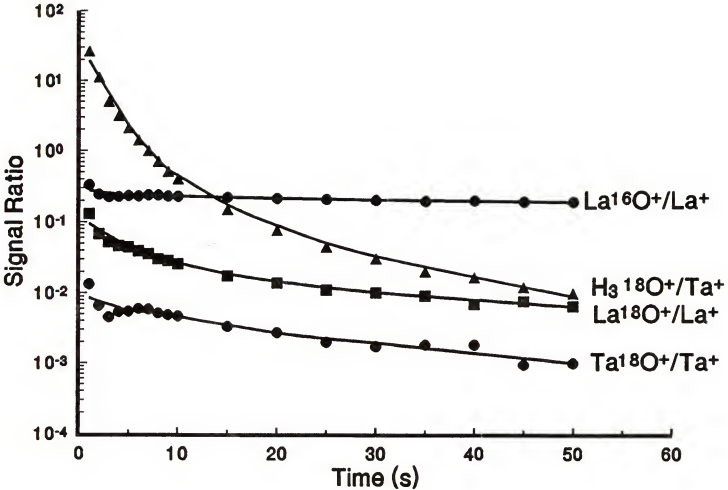

Figure 75--continued.

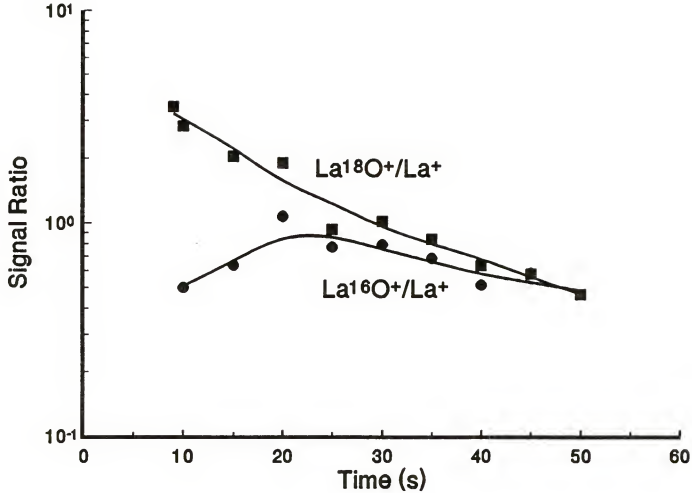

Figure 75--continued.

increased to 146 ms in Figure 75c, the $La^{16}O^+/La^+$ ratio (ranging from 0.9 to 0.5) was exceeded by the $La^{18}O^+/La^+$ ratio (ranging from 4 to 0.5), a result of the re-equilibration among the three lanthanum species caused by the significant increase in the $H_2{}^{18}O$ concentration.

Injection into a pulsed discharge

In this experiment, a pulsed power supply was used to support the discharge instead of the DC power supply, while the same solenoid injector was used as the reagent releaser. The instrumental arrangement is shown in Figure 76 which maintains the general layout as that described in Figure 67 with minor modifications. The discharge power supply was triggered by the same pulse signal used to drive the valve controller after being inverted. The MCA was synchronized with the discharge voltage pulse to record real time signal profiles. The temporal relationships among the time profiles of the discharge, injector, gas diffusion, and the data gate are illustrated in Figure 77. The gas injection was initiated at the same instant the discharge voltage was shut off. The discharge "on" time and the valve open time were set at a constant 100 ms and 150 ms respectively, while the discharge period (as well as the injector cycle) was varied between one and 100 seconds. The significance of this arrangement was that as the discharge "off" time was varied, two important events could happen to the injected gas in the discharge. As the "off" time increased, the injected gas was allowed a longer time to be pumped away from the ion source before the discharge was turned on for the next cycle. According to the surface deposition theory discussed in the previous section of this chapter, the lengthened "off" time

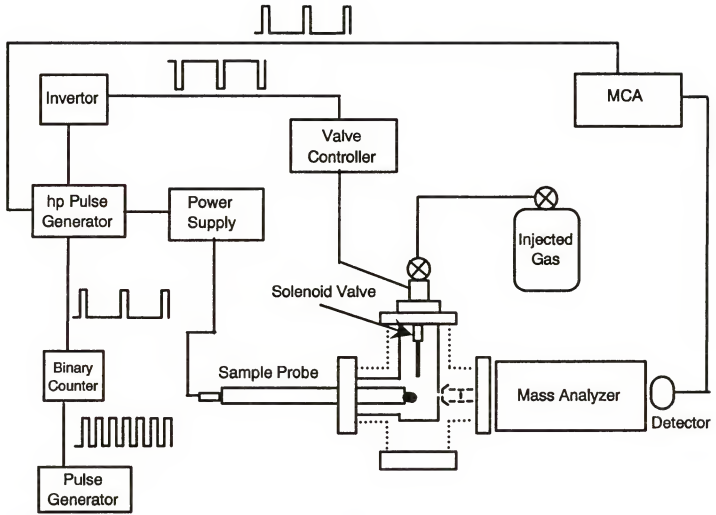

Figure 76 Illustration of the pulse injection scheme with the pulsed discharge operation. Opening of the solenoid valve is synchronized with the shutting off of the discharge.

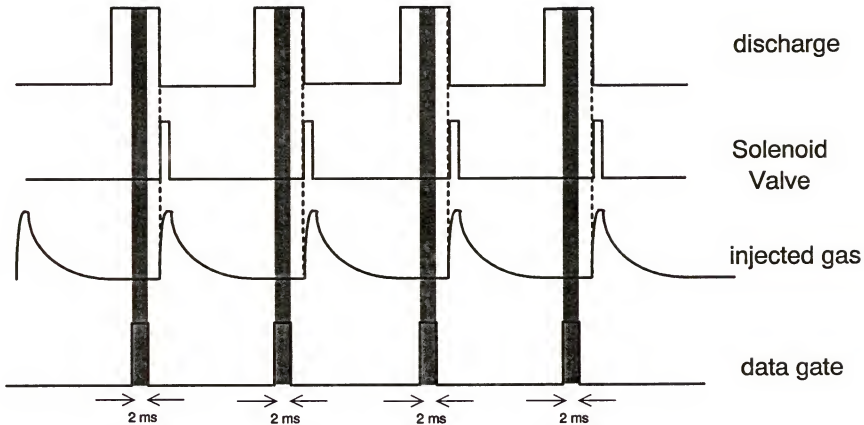

Figure 77 Illustration of temporal relationships among the pulsed discharge profile, injection profile, and the data acquisition gate.

also rendered the cathode surface a longer time to accumulate gaseous adsorption, including the injected gas molecules. As the "off" time was changed from a lower value to a higher one, the concentration dominance of the injected gas moved from in the gas phase to on the sample surface. Of interest was to study how the signal ratio of LaO^+/La^+ could be affected in this process.

The experiment was first carried out without the injection of water $H_2{}^{18}O$. The $La^{16}O^+/La$ ratio was recorded as a function of the discharge pulse period in Figure 78. The slowly increasing $La^{16}O^+/La^+$ ratio behaved in an expected manner, i.e., the water build-up on the cathode surface oxidized the analyte atom resulting in the slightly increasing $La^{16}O^+/La^+$. $H_2{}^{18}O^+$ vapor (may contain $H_2{}^{16}O^+$ due to gas line contamination) was later injected into the plasma at various pulse cycles. The $La^{16}O^+/La^+$ and $La^{18}O^+/La^+$ ratios are plotted against the discharge period (same as the injection period) in Figure 78. Both ratios were of much higher values in the low period region than that obtained without water injection. The high oxide content was attributed to the much higher water concentration in the gas phase at this point. Since most of the water vapor could be pumped out of the ion source when the injection period was set at 40 seconds or higher, both LaO^+/La^+ ratios started to decrease and eventually reached the same level of the $La^{16}O^+/La^+$ ratio as obtained without water injection. The total decrease of the LaO^+/La^+ ratio was about two orders of magnitude throughout the entire injection cycle, whereas the $H_3{}^{18}O^+$ signal was only reduced by a factor of 70% over the same time range. This suggests that the La-LaO equilibria were more subject to water present in the gas phase than that on the sample surface.

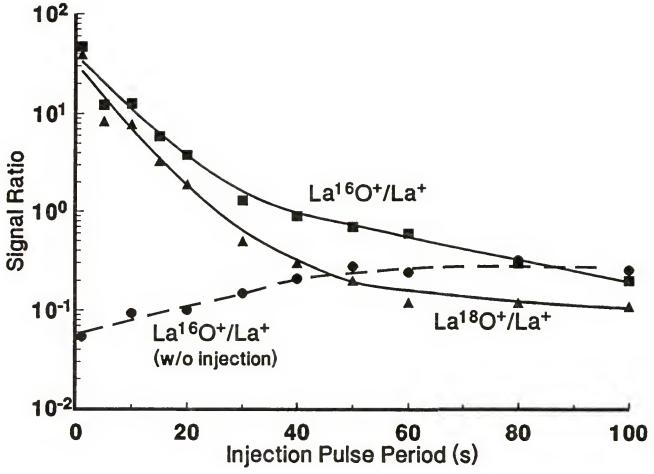

Figure 78 Comparison of Signal ratios $La^{16}O^+/La^+$ and $La^{18}O^+/La^+$ obtained with $H_2{}^{18}O$ injection (solid lines) and $La^{16}O^+/La^+$ obtained without $H_2{}^{18}O$ addition (dashed line) at different pulse and injection periods. The discharge is operated in pulsing mode with a La_2O_3/Ta sample.

Conclusions

Some fundamental processes of lanthanum oxide redox equilibria in the glow discharge have been investigated by means of transient plasma perturbations. Studies using pulsed discharges have shown that the redox equilibria between La and LaO also exist on the sample surface, where the La-LaO equilibration is dependent on the chemical composition on the cathode. Water molecules deposited on the cathode tend to oxidize the sputtered atoms as they leave the cathode surface, causing the La-LaO equilibria to shift toward forming the LaO molecules. A clean cathode surface created by getter matrices is favorable for preventing La atoms from water oxidation.

Plasma modification studies were also carried out by adding selected "reagent" atoms or gas molecules into the La-LaO equilibria established in the discharge. Reagent addition was confined mainly to the gas phase, making it possible to distinguish between reactions occurring on the cathode surface and reactions happening in the gas phase. Results have shown that interactions between getter atoms and the La-LaO equilibria do exist in the gas phase, causing enhancement of the La^+ signal. Oxidation reactions between La and water molecules in the gas phase have also been verified by detection of the synthesized $La^{18}O^+$ ions.

CHAPTER 5
CONCLUSIONS AND FUTURE STUDIES

Research presented in this dissertation has explored some of the practical and fundamental aspects of using glow discharge mass spectrometry to analyze geological samples, particularly the rare earth materials. It can be concluded that the redox equilibria between REE-REO controls the analytical sensitivity of GDMS in this type of application. To improve the analytical results, plasma impurities serving as oxidants for the REE-REO equilibria must be eliminated, which can be accomplished by means of both cryogenic cooling and getter materials. Plasma manipulation studies have shown that the redox equilibration, though established both on the sample surface and in the gas phase, is governed predominantly by gas phase reactions.

However, it needs to be pointed out that since the majority of the studies has been conducted with only one oxide sample, i.e., lanthanum oxide, some of the conclusions deduced from the experimental results may not be applicable to all of the rare earths. Using the knowledge attained with lanthanum oxide as a model case, further studies may be carried out to improve our understanding of the many chemical processes that occur in the glow discharge plasma involving nonconductors such as geologicals. In this chapter, suggestions for future studies are given from two directions: objects of study and experimental approach.

Objects of Study

Despite the strong physical and chemical similarities of the REE as recognized by the traditional macro-scale chemistry, the rare earth oxides do possess different crystal structures and bond strengths, which lends the possibility of significantly different behavior in the atomic-scale glow discharge environment. To achieve a full understanding of the REE chemistry in the glow discharge, Experiments must be performed with samples other than lanthanum oxide. Because the dissociation of the oxide bond is often the core of the REE plasma processes, a good selection of samples should include rare earth oxides with M-O bond energies ranging from relatively weak (4-5 eV) to strong (above 8 eV) (e.g., europium oxide, gadolinium oxide, and cerium oxide).

The ionization mechanisms of the rare earth samples in the glow discharge are still poorly understood. Because some of the REE can remain in their ionic bonds even through the sputtering step (e.g., sputtered as MO molecules), their ionization processes are expected to be more complex than those responsible for metallic samples. Under certain discharge conditions, a small but not negligible fraction of the REE are present as doubly charged ions, a phenomenon that has been shown to create problems for ICPMS when used for REE analysis. Further studies on factors that influence the formation of doubly charged REE ions in various discharge gases may reveal insight to the ionization processes of species that do not have a metallic origin in the glow discharge.

The use of getter reagents has been shown to be effective in enhancing the analytical sensitivity of REE in GDMS. From the practical standpoint, the success of this method may be limited to samples upon which the getter matrix itself will not create spectral interferences. But from the fundamental standpoint, the concept of using reactive species such as getter reagents as plasma modifiers introduces all kinds of possibilities for affecting and probing the plasma chemistry of the glow discharge. Results presented in this dissertation have already shown that certain species can be synthesized in the glow discharge from selected reagents. Based on this observation, more emphasis may be given to the monitoring of reaction products in the plasma. These products may be a result of reactions between gaseous impurities and various getter reagents, or between intentionally added gas reactants and the analytes of interest. Coupling of a cryogenic cooling device (hopefully with further mechanical improvement) with such reaction monitoring should also help us understand better the factors controlling the chemical environment in the glow discharge.

Experimental Strategies

While the traditional DC discharge operation is fairly straight forward and should still be used for establishing foundational parameters, more precise and exclusive information concerning the glow discharge processes will possibly be gained by using time-resolved operations for plasma modification studies.

In the work presented in this dissertation, plasma reagent introduction by means of an additional pulsed discharge has been successful in terms of

identifying regions of reactions, i.e., in the gas phase or on the cathode surface. Here, the discharge that contained the analyte oxide was operated only in the DC mode. The capability of running two pulsed discharges (dual pulsed discharge) has been developed in our laboratory, which should allow time resolved operation of both the analyte and the reagent discharges. By adjusting the pulsing schemes of the two discharges with respect to each other, a better control can be obtained, both in time and amount, for the addition of the analyte and reagent materials. The effect of selected reagents on the oxide analyte signals can therefore be studied through reactions induced at better controlled time and space.

By the same principle, reactive gas injections by means of a solenoid valve may be coupled with analyte discharges operated in either DC or time-resolved fashion. It has already been shown that by adjusting the trigger point for the solenoid valve to open with respect to the pulsing scheme of the discharge, gaseous reactants can be added either with or without the discharge being "on". The significant of doing so is that it provides a means of differentiating between how the added gases affect the chemistry of the analyte, whether on the sample surface and or in the gas phase. At the present time, a pumping time of at least 60 seconds is needed between the injection cycles to ensure a sufficient concentration gradient of the added gases in the ion source. Although this makes the entire experiment seem time-consuming, an advantage would be that on this time scale, atomic absorption experiments can be carried out *in situ* to monitor the behavior of the neutral species in the reaction processes without the need for

fast signal recording devices. Multifaceted information including reaction products, reaction origins, ion signal profiles, and atomic population profiles may be obtained through these experiments.

REFERENCES

1. Howatson, A.M. *An Introduction to Gaseous Discharges,* 2nd ed.; Pergamon: New York, 1976.

2. Cobine, J.D. *Gaseous Conductors, Theory and Engineering Applications*; Dover: New York, 1958.

3. Chapman, B. *Glow Discharge Processes*; Wiley: New York, 1980.

4. Westwood, W.D., *Prog. Surf. Sci.*; 7, 71 (1976).

5. Pillow, M.E., *Spectrochim. Acta*; 36B, 821 (1981).

6. Boumans, P.W.J.M., *Anal. Chem.*; 44, 1219 (1972).

7. Guentherschulze, A. *Vacuum*; 111, 360 (1953).

8. Wehner, G.K. and Anderson, G.S. in *Handbook of Thin Film Technology*; Maissel, L.I. and Glang, R., Eds.; McGraw-Hill Book Co.: New York, 1981.

9. Wehner, G.K. in *Methods and Phenomena: Their Applications in Science and Technology*, Vol. 1, Wolsky, S.P. and Czanderna, A.W., Eds., Elsevier Scientific: New York, Chapter 1, 1975.

10. Stuart, R.V. and Wehner, G.K., *J. Appl. Phys. ;*35, 1819 (1964).

11. Gough, D.S., Hannaford, P., and Walsh, A., *Spectrochim. Acta*; 28B, 197 (1973).

12. *Sputtering by Particle Bombardment I*, Behrisch, R., ed., Springer Topics in Applied Physics Vol. 47, Springer-Verlag, Berlin, 1981.

13. Oechsner, H., *Appl. Phys.*; 8, 185 (1975).

14. Bay, H.L., Roth, J. and Bohdansky, J., *J. Appl. Phys.*; 48, 4722 (1977).

15. Barshick, C.M., Ph.D. Dissertation; University of Virginia (1990).

16. Laegreid, N. and Wehner, G.K., *J. Appl. Phys.*; 32, 365 (1961).

17. Rosenberg, D. and Wehner, G.K., *J. Appl. Phys.*; 33, 1842 (1962).

18. Davis, W.D. and Vanderslice, T.A., *Phys. Rev.*; 131, 219 (1963).

19. Abril, I., Gras-Marti, A. and Valles-Abarca, J.A.; *Phy. Rev.*; 28A, 3677 (1983).

20. Little, P.L. and van Engle, A., *Prog. Roy. Soc. London*; 224A, 209 (1954).

21. Dahlgren, S.D. and MacClanahan, E.D., *J. Appl. Phys.*; 43, 1514 (1972).

22. Betz, G., *Surf. Sci.*; 92, 283 (1989).

23. Shimizu, R. and Saeki, N., *Surf. Sci.*; 62, 751 (1977).

24. Coburn, J.W., *J. Vac. Sci. Technol.*; 13, 1037 (1976).

25. Jensen, K. and Ceje, E., *Z. Physic.*; 269, 293 (1974).

26. White, C.W. and Simms, D.L., *Science*; 177, 481 (1972).

27. Stirling A.J. and Westwood, W.D, *J. Appl. Phys.*; 41, 742 (1970).

28. Stirling A.J. and Westwood, W.D, *J. Phys. D.*; 4, 246 (1971).

29. Stirling A.J. and Westwood, W.D, *Thin Solid Films*; 7, 1 (1971).

30. Stirling A.J. and Westwood, W.D, *Thin Solid Films*; 8, 199 (1971).

31. Oechsner, H. and Gerhard, W., *Surf. Sci.*; 44, 408 (1974).

32. Gerhard, W. and Oechsner, H., *Z. Physik B*; 22, 41 (1975).

33. Oechsner, H., *Inter. J. Mass Spec. Ion Proc.*; 103, 31 (1990).

34. Wurz, P., Husinky, W. and Betz, G., *Appl. Phys.*; 52A, 213 (1991).

35. McHugh, J.A. and Sheffield, J.C., *J. Appl. Phys.*; 35, 512 (1964).

36. *Sputtering by Particle Bombardment II*, Behrisch, R., ed., Springer Topics in Applied Physics Vol. 52, Springer-Verlag: Berlin, 1983, p.109.

37. Hofer, W.O. and Liebl, H.: In *Ion Beam Surface Layer Analysis*, eds. Meyer, O., Linker, G. and Kappeler, F., Plenum Press, New York, 1976, p.659.

38. Hofer, W.O., Bay, H.L. and Martin, P.J., *Nucl. Mater.*; 76/77, 156 (1987).

39. Wach, W. and Wittmack, K., *Nucl. Instrum. Methods*; 149, 259 (1978).

40. Brundy, M.M. and Seidel, W., *Ber. Bunsenges Phys. Chem.*; 95, 42 (1991).

41. Harrison, W.W., Hess, K.R., Marcus, R.K. and King, F.L., *Anal. Chem.*; 58, 341 A (1986).

42. King, F.L. and Harrison, W.W., *Mass Spectrom. Reviews.*; 9, 285 (1990).

43. Brown, S.C. *Introduction to Electrical Discharges in Gases*, John Wiley and Sons: New York, 1966, Chap. 5.

44. Coburn, J.W. and Kay, E., *Appl. Phys. Lett.*; 18, 435 (1971).

45. Coburn, J.W. and Kay, E., *Appl. Phys. Lett.*; 19, 350 (1971).

46. Coburn, J.W. and Kay, E., *J. Appl. Phys.*; 43, 4965(1972).

47. Coburn, J.W., Taglauer, E. and Kay E.; *J. Appl. Phys.*, 45, 1779 (1975).

48. Eckstein E.W., Coburn, J.W. and Kay, E.; *J. Mass Spectrom. Ion Phys.*, 17, 129 (1975).

49. Smyth, K.C., Bentz, B.L., Bruhn, C.G. and Harrison, W.W., *J. Am. Chem. Soc.*; 101, 797 (1975).

50. Hess, K.R. and Harrison, W.W., *Anal. Chem.*; 60, 691 (1988).

51. Smith, R.L., Serxner, D. and Hess, K.R., *Anal. Chem.*; 61, 1103 (1989).

52. Harrison, W.W. and Bentz, B.L., *Pro. Analyst. Spectrosc.*; 11, 53 (1988).

53. Mitchell, D.G. and Johnson A., *Spectrochim. Acta.*; 25B, 175 (1969).

54. Lowe, R.M., *Spectrochim. Acta*; 26B, 201 (1970).

55. Perreira, N.P., Strauss J.A. and Human, H.G.C., *Spectrochim Acta*; 38B, 899 (1983).

56. Fang, D.C. and Marcus, R.K., *J. Anal. Atom. Spectrosc.*; 3, 873 (1988).

57. Caroli, S., Senofonte, O., Violate, N. and Astrologo, R., *J. Anal. Atom. Spectrom.*; 3, 887 (1988).

58. Nickel, H., Gunter, D., Mazurkiewicz, M. and Naoumidis, A., *Spectrochim. Acta*; 46B, 125 (1991).

60. Hess, K.R. and Marcus, R.K., *Spectroscopy*; 2:9, 24 (1987).

61. Broekaert, J.A.C. and Tolg, G., *Fresenius Z. Anal. Chem.*; 326, 495 (1987).

62. Harrison, W.W., *J. Anal. Atom. Spectrosc.*; 3, 867 (1988).

63. Hieftje, G.M. and Vickers, G.H., *Anal. Chem. Acta*; 216, 1 (1989).

64. Adams, F. and Vertes, A., *Fresenius J. Anal. Chem.*; 337, 638 (1990).

65. Stuewer, D., *Fresenius J. Anal. Chem.*; 337, 737 (1990).

66. Harrison, W.W., Barshick, C.M., Klingler, J.A., Ratliff, P.H. and Mei, Y., *Anal. Chem.*; 62, 943A (1990).

67. Harrison, W.W., *J. Anal. Atom. Spectrosc.*; in press.

68. Horlick, G., *Spectrosc.*; 7, 22 (1992).

69. Robinson, K. and Hall, F.H., *J. Metals*; 39, 14 (1987).

70. Sanderson, N.E., Hall, N.E., Clark, J., Charalambous, P. and Hall, D., *Mikrochim Acta*; 1, 275 (1987).

71. Jakubowski, R., Stuewer, D. and Vieth, W., *Anal. Chem.*; 59, 1825 (1987).

72. Jakubowski, R., Stuewer, D. and Toelg, G., *Spectrochim. Acta B*; 46, 155 (1991).

73. Vassamillet, L.F., *J. Anal. Atom. Spectrosc.*; 4, 451 (1989).

74. Mykytiuk, A.P., Semeniuk, P., and Berman, S., *Spectrochim. Acta Rev.*; 13, 1 (1990).

75. Hall, D.J. and Sanderson, N.E., *Surf. Interface Anal.*; 9, 285 (1988).

76. Jakubowski, N., Steuwer, D. and Veith, W., *Fresenius Z. Anal. Chem.*; 331, 145 (1988).

77. Hamilton, E.I. and Minski, M.J., *Int. J. Mass Spectrom. Ion Phys.*; 10, 77 (1972/73).

78. Donohue, D.L. and Harrison, W.W., *Anal. Chem.*; 47, 1528 (1975).

79. Bruhn, C.G., Bentz, B.L. and Harrison, W.W., *Anal. Chem.*; 51, 673 (1979).

80. Huneke, J.C., *J. Res. National Bureau Standards*; 93, 392 (1988).

81. Veith, W. and Huneke, J.C., *Spectrochim. Acta B*; 46, 137 (1991).

82. Bentz, B.L., Bruhn, C.G. and Harrison, W.W., *Int. J. Mass Spectrom. Ion Phys.*; 28, 409 (1978).

83. King, F.L. *Ph.D. Dissertation*; University of Virginia, January, 1989.

84. Peter, G. and Hofler, K., *J. Vac. Sci. Technol. A*; 5, 2285 (1987).

85. Russell, B.J. and Walsh, A. *Spectrochim. Acta*; 15, 883 (1959).

86. Gough, D.S., *Anal. Chem.*; 48, 1926 (1976).

87. Chakrabarti, C., Headrick, K.L., Bertels, P. and Back, M.H., *J. Anal. Atom. Spectrom.*; 3, 713 (1988).

88. Gough, D.S., Hannaford, P. and Lowe, R.M., *Anal. Chem.*; 61, 1652 (1989).

89. Loving, T.J. and Harrison, W.W., *Anal. Chem.*; 54, 1523 (1983).

90. Klingler, J.A., *Ph.D. Dissertation*, University of Florida, 1991.

91. Jarvis, K.E., *J. Anal. Atom. Spectrom.*; 4, 563 (1989).

92. Kantipuly, C.J. and Westland, A.D., *Talanta*; 35, 1 (1988).

93. Smith, A.D., Gillis, K.M. and Ludden, J.N., *Chem. Geol.*; 81, 17 (1990).

94. Germani, M.S., Gokmen, I., Sigleo, A.C., Kowalczyk, G.S., Olmez, I., Small, A.M., Anderson, D.L., Falley, M.P., Gulovail, M.C., Choquette, C.E., Lepel, G.E., Gordon, G.E. and Zoller, W.H., *Anal. Chem.*; 52, 240 (1980).

95. Czamanske, G.K., Hower, J. and Millard, R.C., *Geochim. Cosmochim. Acta*; 30, 745 (1966).

96. Norrish, K. and Hutton, J.T., *Geochim. Cosmochim. Acta*; 33, 431 (1969).

97. Roelandts, I., *Anal. Chem.*; 53, 676 (1981).

98. Sholkovitz, E.R., *Chem. Geol.*; 88, 333 (1990).

99. Nakamura, N., Yamamoto, S.N., Noda, S., Nishikawa, Y., Komi, H. and Nakayama, T., *Anal. Chem.*; 61, 755 (1989).

100. Hebeda, E.H. and Schijf, J., *Int. J. Mass Spectro. Ion Proc.*; 104, 227 (1991).

101. Nicholls, G.D., Graham, A.L., Williams, E. and Wood, M., *Anal. Chem.*; 39, 584 (1967).

102. McLennan, S.M. and Taylor, S.R., *Chem. Geol.*; 29, 333 (1980).

103. Roychowdhury, P., Roy, N.K., Das, D.K. and Das, A.K., *Talanta*; 12, 1183 (1989).

104. Weiss, D., Pauker, T. and Rubeska, I., *J. Anal. Atom. Spectrom.*; 5, 371 (1990).

105. Rathi, M.S., Khanna, P.P. and Mukherjee, P.K., *Talanta*; 3, 329 (1991).

106. Borsier, M., *Spectrochim. Acta Rev.*; 14, 79 (1991).

107. Date, A.R. and Grey, A.L., *Spetrochim. Acta*; 40B, 115 (1985).

108. Lichte, F.E., Meier, A.L. and Crook, J.G., *Anal. Chem.*, 59, 1150 (1987).

109. Hall, G.E.M. and Pelchat, J.C., *J. Ana;. Atom. Spectrom.*; 5, 339 (1990).

110. Shibata, N., Fudagawa, N. and Kubota, M., *Anal. Chem.*; 63, 636 (1991).

111. Date, A.R., *Spectrochim. Acta Rev.*; 14, 3 (1991).

112. Taylor, S.R., *Geochim. Cosmochim. Acta*; 29, 1243 (1965).

113. *Handbook on the Physics and Chemistry of Rare Earths*; Schneider, K.A. and Eying, L. (eds.), Vol#.4, p.359, North-Holland, New York, 1979.

114. Schnetzler, C.C., Thomas, H.H. and Philpotts, J.A., *Anal. Chem.*; 39, 14 (1967).

115. Date, A.R. and Hutchison, D., *Spectrochim. Acta*; 41B, 175 (1986).

116. Brenner, I.B., Watson, A.E., Russell, G.M. and Goncalves, M., *Chem. Geol.*; 28, 321 (1980).

117. Horvath, Z., Lasztity, A. and Barnes, R.M., *Spectrochim. Acta Rev.*; 14, 45 (1991).

118. Halicz, L. and Brenner, I.B., *Spectrochim. Acta*; 42B, 207 (1987).

119. Jarvis, K.E. and Williams, J.G., *Chem. Geol.*; 78 (1989).

120. Imai, N., *Analytica Chemica Acta*; 235, 381 (1990).

121. ElAlfy, S., Laqua, K. and Massmann, H., *Z. Anal. Chem.*; 263, 1 (1973).

122. Brenner, I.B., Laqua, K. and Dvorachek M., *J. Anal. Chem. Spectrom.*; 2, 623 (1987).

123. Winchester, M.R. and Marcus, R.K., *Appl. Spectrosc.*; 42, 941 (1988).

124. Winchester, M.R., Hayes, S.M. and Marcus, R.K., *Spectrochim. Acta*; 5, 615 (1991).

125. Ehrlich, G., Stahlberg, U. and Hoffmann, V., *Spectrochim. Acta*; 2, 115 (1991).

126. Winchester, M.R. and Marcus, R.K., *J. Anal. Atom. Spectrom.*; 5, 575 (1990).

127. Winchester, M.R., Lazik, C. and Marcus, R.K., *Spectrochim. Acta*; 46B, 483 (1991).

128. Robinson, K. and Hall, E.F.H., *Testing and Analysis*, VG Instruments technical papers.

129. Marcus, R.K. and Harrison, W.W., *Anal. Chem.*; 59, 2369 (1987).

130. King, F.L., McCormack, A.L. and Harrison W.W., *J. Anal. Atom. Spectrom.*; 3, 883 (1988).

131. Coburn, J.W., Taglauer, E. and Kay, E., *Japan. J. Appl. Phys. Suppl. 2, Pt. 1*; 501 (1974).

132. Grasserbauer, M., *Mikrochim. Acta*; I, 291 (1987).

133. Oechsner, H., Schoof, H. and Stumpe, E., *Surf. Sci.*; 76, 343 (1978).

134. Oechsner, H., Ruhe, W. and Stumpe, E., *Surf. Sci.*; 85, 289 (1979).

135. Gerhard, W., *Z. Physik*; B22, 31 (1975).

136. Taglauer, E. and Heiland, W., *Appl. Phys. Lett.*; 33, 950 (1978).

137. Taglauer, E., Heiland, W. and MacDonald, R.J., *Surf. Sci.*; 90, 661 (1979).

138. Umezawa, Y. and Reilley, C.N., *Anal. Chem.*; 50, 1290 (1978).

139. Baretzky, B., Moller, W. and Taglauer, E., *Nucl. Inst. and Meth. in Phys. Research*; B18, 496 (1987).

140. Malherbe, J.B., Hofmann, S. and Sanz, J.M., *Appl. Surf. Sci.*; 27, 355 (1986).

141. King, F.L. and Harrison, W.W., *Int. J. Mass Spectrom. Ion Proc.*; 89, 172 (1989).

142. Loving, T.J and Harrison, W.W., *Anal. Chem.*; 54, 1526 (1983).

143. VG Technical Bulletin, VG Isotopes, Manchester, England.

144. Yarwood, J.; *High Vacuum Technique: Theory, Practice and Properties of Materials*, 4th Ed. Chapman & Hall, London (1976).

145. Giorgi, T.A.; *Japan. Phys. Suppl.*, 2, 53 (1974).

146. Holland, L. and Cox, R.E.; *Vacuum*, 24, 107 (1974).

147. Radzig, A.A. and Smirov, B.M.; *Reference Data on Atoms, Molecules and Ions*, Springer, New York (1985).

148. Tong, S.L. and Harrison, W.W.; unpublished results.

149. Wagatsuma, K. and Hirokawa, K.; *J. Anal. Atom. Spectrom.*, 4, 525 (1989).

150. Jakubowski, N. and Stuewer, D.; *Fresenius. Z. Anal. Chem.*, 335, 680 (1989).

151. Stern, E. and Caswell, H.L.; *J. Vacuum Sci. Tech.*, 128 (1966).

152. Powell, M.J., Boomer, M.J. and McVickers, R.J.; *Anal. Chem.*, 58, 2867 (1986).

153. Lindinger, W., *Phys. Rev.*; 7, 328 (1973).

154. Velazco, J.C., Knolts, J.H. and Setser, J.W.; *J. Chem. Phy.*, 69, 4357 (1978).

155. Ratliff, P.H. and Harrison, W.W.; unpublished results.

156. Smith, B.W., Omenatto, N. and Winefordner, J.D.; *Spectrochim. Acta*, 37B, 759 (1982).

157. Glish, M., Smith. B.W. and Winefordner, J.D.; *Anal. Chem.*, 62, 157 (1990).

158. De Jong, G.J. and Piepmeier, E.H.; *Spectrochim. Acta*, 29B, 159 (1974).

159. Savickas, P.J.; Ph.D. Dissertation, University of Virginia (1984).

160. Klingler, J.A., Savickas, P.J., and Harrison, W.W., *J. Am Soc. Mass Spectrom.*, 1, 138 (1990).

161. Klingler, J.A., Barshick, C.M. and Harrison, W.W., *Anal. Chem.*, 63, 2571 (1991).

162. Rakshit, A.B. and Warneck, P., *J. Chem. Phys.*, 74, 2853 (1981).

BIOGRAPHICAL SKETCH

Yuan Mei was born in Beijing, China in 1964. She attended Peking University and graduated with her Bachelor of Science degree in July, 1987. In the same year, her graduate career began at the University of Virginia under the supervision of Dr. Willard W. Harrison in the field of analytical chemistry. With the relocation of Dr. Harrison's research group, she transferred to the Chemistry Department at the University of Florida in 1989. She completed her graduate studies and received a Doctor of Philosophy degree in May, 1992.

I certify that I have read this study and that in my opinion it conforms to acceptable standards of scholarly presentation and is fully adequate, in scope and quality, as a dissertation for the degree of Doctor of Philosophy.

Willard W. Harrison, Chairman
Professor of Chemistry

I certify that I have read this study and that in my opinion it conforms to acceptable standards of scholarly presentation and is fully adequate, in scope and quality, as a dissertation for the degree of Doctor of Philosophy.

Richard A. Yost
Professor of Chemistry

I certify that I have read this study and that in my opinion it conforms to acceptable standards of scholarly presentation and is fully adequate, in scope and quality, as a dissertation for the degree of Doctor of Philosophy.

Vaneica Y. Young
Associate Professor of Chemistry

I certify that I have read this study and that in my opinion it conforms to acceptable standards of scholarly presentation and is fully adequate, in scope and quality, as a dissertation for the degree of Doctor of Philosophy.

Robert J. Hanrahan
Professor of Chemistry

I certify that I have read this study and that in my opinion it conforms to acceptable standards of scholarly presentation and is fully adequate, in scope and quality, as a dissertation for the degree of Doctor of Philosophy.

Paul A. Mueller
Professor of Geology

This dissertation was presented to the Graduate Faculty of the Department of Chemistry in the College of Liberal Arts and Sciences and to the Graduate School and was accepted as partial fulfillment of the requirements for the degree of Doctor of Philosophy.

May 1992

Dean, Graduate School